NASA CR-72672
PSI 70-2

DROPLET VAPORIZATION WITH LIQUID HEAT CONDUCTION

by

V. D. Agosta and S. S. Hammer

PROPULSION SCIENCES, INC.

prepared for

NATIONAL AERONAUTICS AND SPACE ADMINISTRATION

NASA Lewis Research Center
Contract NAS 3-12030
Richard J. Priem, Project Manager

NOTICE

This report was prepared as an account of Government-sponsored work. Neither the United States, nor the National Aeronautics and Space Administration (NASA), nor any person acting on behalf of NASA:

A.) Makes any warranty or representation, expressed or implied, with respect to the accuracy, completeness, or usefulness of the information contained in this report, or that the use of any information, apparatus, method, or process disclosed in this report may not infringe privately-owned rights; or

B.) Assumes any liabilities with respect to the use of, or for damages resulting from the use of, any information, apparatus, method or process disclosed in this report.

As used above, "person acting on behalf of NASA" includes any employee or contractor of NASA, or employee of such contractor, to the extent that such employee or contractor of NASA or employee of such contractor prepares, disseminates, or provides access to any information pursuant to his employment or contract with NASA, or his employment with such contractor.

Requests for copies of this report should be referred to

National Aeronautics and Space Administration
Scientific and Technical Information Facility
P.O. Box 33
College Park, Md. 20740

NASA CR-72672
PSI 70-2

FINAL REPORT

DROPLET VAPORIZATION WITH LIQUID HEAT CONDUCTION

by

V. D. Agosta and S. S. Hammer

PROPULSION SCIENCES, INC.
P. O. Box 814
Melville, New York 11746

prepared for

NATIONAL AERONAUTICS AND SPACE ADMINISTRATION

February 10, 1970

CONTRACT NAS3-12030

NASA Lewis Research Center
Cleveland, Ohio
Richard J. Priem, Project Manager
Chemical Rockets Division

ABSTRACT

An analytical solution for droplet evaporation is presented. The governing differential equation includes finite liquid thermal conductivity within the droplet interior. The boundary conditions are a heat balance at the droplet surface, and finite temperatures at the droplet center. The effect of initial droplet size and temperature, droplet thermal conductivity and environmental gas pressure on temperature and vaporization rate histories are investigated. It is found that for the larger droplets, a dynamic equilibrium state is approached; i.e., the droplet surface regression rate parameter and the surface temperature approach common values.

TABLE OF CONTENTS

LIST OF FIGURES

LIST OF FIGURES (Contd)

Figure

LIST OF FIGURES (Contd)

Figure

DROPLET VAPORIZATION WITH LIQUID HEAT CONDUCTION

By V. D. Agosta and S. S. Hammer

SUMMARY

The scope of this study is to explore the effect of liquid thermal conductivity on the behavior of an evaporating droplet. An analytical solution of the governing differential equation for heat conduction within the droplet interior is presented. The boundary conditions are finite temperature at the droplet center and a heat balance at the droplet surface. The effect of initial droplet size and temperature, droplet thermal conductivity and environmental gas pressure on temperature and evaporation rate histories are investigated.

It is found that for larger droplets, a common dynamic equilibrium state asymptotically is approached. The effect of thermal conductivity is to vary the time required for the droplet surface temperature to reach the asymptotic value. The time to vaporize ten percent of the initial droplet mass was not influenced by the thermal conductivity. The droplet equilibrium surface regression rate and temperature increases with environmental gas pressure. The droplet surface temperature reaches the critical value at an environmental gas pressure that is dependent on the volatility of the fluid. Finally, for droplets equal or greater than 100 microns diameter and with realistic thermal conductivities, the temperature gradients attained at 10^{-4} sec. are contained in the outer ten percent of the droplet radius.

INTRODUCTION

The burning rate for small fuel droplets is usually based on the quasi-steady envelope flame model (Refs. 1-4). Essentially, this model assumes that heat is transferred back from the flame envelope such that vaporization is sustained, and that the burning rate is equal to the flow of fuel from the interior of a droplet through a sphere of the same size and located in the same environment. It is further assumed that either the temperature at the droplet surface is near the boiling point or is uniform throughout the droplet. The quasi-steady droplet evaporation model appears to break down near the propellant critical point (Ref. 5).

The primary objective of the analysis presented herein is to determine the behavior of vaporizing droplets in which heat conduction in the liquid droplet is included in the model. This is accomplished by analyzing the droplet interior and employing the environment as boundary conditions. Since the droplet is the mass source, then it is argued that its behavior must be analyzed subject to the constraints of its environment. An additional bonus that becomes apparent is that the model presented herein can serve as one for the evaporation behavior of droplets near the droplet critical conditions.

It is our pleasure to acknowledge Dr. Gino Moretti, who developed the computer program for this study.

THEORY

Initially, a droplet with uniform temperature is introduced into a hot atmosphere which is essentially at the adiabatic flame temperature. Droplet heating and vaporization occur simultaneously from the initial conditions and approach asymptotically a dynamic equilibrium state. The droplet vapors diffuse, mix and react chemically with the hot gases. Thus the physical structure of the model consists of a spherical droplet surrounded by a film of reacting vapor-gas mixture. The thickness of the film is defined as that distance where the reaction is in equilibrium for the local or given $^{O}/F$ ratio. Heat transfer, q_T, is assumed to occur backward toward the droplet which goes: (1) toward heating up the diffusing vapors, q_{sh}, (2) supplying the heat of vaporization, q_λ, and (3) heating up the droplet, q_ℓ, Fig. 1.

The governing differential equation for heat conduction in a spherical liquid droplet is given by

$$T_t = \alpha\left(T_{rr} + \frac{2}{r} T_r\right) \qquad 0 \le r \le r_s \qquad t \ge 0 \tag{1}$$

where

T is the temperature,
r radius, r_s surface radius,
t time, and
α liquid thermal diffusivity.

The subscripts r and t represent differentiation with respect to

radius and time, respectively. For small droplets the assumption of spherical geometry is usually accepted. It is recognized that where drag exists, droplets deform; however, in this analysis the deformation is neglected. The initial condition assumes that the droplet is at uniform temperature T_o,

$$T(r,0) = T_o \qquad 0 \leq r \leq r_s \qquad t = 0 \tag{2}$$

The boundary conditions are

$$T(0,t) \text{ is finite} \qquad r = 0 \qquad t \geq 0 \tag{3}$$

and

$$h(T_f - T_s) = \varkappa T_r + \frac{\dot{w}}{A_d}[\lambda + (\overline{c_p})_v (T_f - T_s)] \qquad r = r_s \qquad 0 \leq t \leq \infty \tag{4}$$

where

h	is the heat transfer coefficient,
T_f	ambient (adiabatic flame) temperature,
T_s	droplet surface temperature,
$\varkappa$	thermal conductivity of droplet,
λ	heat of vaporization,
$(\overline{c_p})_v$	vapor specific heat,
$\dot{w}$	mass evporation rate,
A_d	droplet surface area.

It is assumed that the film thickness surrounding the droplet is small compared to the droplet diameter.

The problem is still not completely defined because the mass evaporation rate is unknown. Thus, a constitutive equation is required and is

$$\rho_\ell \dot{r}_s = \frac{\dot{w}}{A_d} = K_g p \ln \frac{p}{p - p_v}, \quad r = r_s \tag{5}$$

where

$\dot{r}_s$ is the droplet surface regression rate,
ρ_ℓ the liquid density,
K_g mass transfer coefficient,
p total gas pressure,
p_v vapor pressure corresponding to the droplet temperature surface.

It is assumed that the Clausius-Clapeyron equation relates the droplet surface temperature to the vapor pressure. A general relationship for this purpose is

$$\ln p_v = a + \frac{b}{T} + cT \tag{6}$$

where a, b, and c are constants to be determined from thermodynamic data. The above Eq. (6) is also used for interpolation purposes. The heat of vaporization is a function of the droplet surface temperature and is given by

$$\lambda \left[1 - \frac{T_s}{T_c} \right]^{\gamma} \tag{7}$$

wjere λ_o and γ are constants and T_c the critical temperature. The average vapor specific heat, $(\overline{c_p})_v$, is either given by suitable equations, e.g.,

$$(\overline{c_p})_v = \frac{\int_{T_s}^{T_f} (\overline{c_p})_v dT}{T_f - T_s} \tag{8}$$

or from tables. The heat and mass transfer coefficients h and K_g, respectively, are obtained from the Nusselt correlations,

$$\frac{2r_s h}{K_m} = 2 + 0.6(Pr)^{1/3}(Re)^{1/2} \tag{9}$$

and

$$\frac{2r_s R_o T K_g}{M_v D} = 2 + 0.6(Sc)^{1/3}(Re)^{1/2} \qquad (10)$$

where

K_m is the vapor-gas mixture thermal conductivity,
R_o universal gas constant,
M_v vapor molecular weight,
D molecular diffusion coefficient,
$\bar{T}$ arithmetic mean temperature, $\frac{T_f+T_s}{2}$
Pr Prandtl number $(c_p\mu/\kappa)_m$,
Sc Schmidt number $(\mu/D\rho)_m$.
Re Reynolds number $2r_s(u-v)(\frac{\rho}{\mu})_m$,
μ vapor-gas mixture viscosity,
ρ vapor-gas mixture density,
u gas velocity,
v droplet velocity.

It is recognized that most of the thermodynamic properties are functions of droplet surface temperature. However, to include such functional relationships at this time is impractical from a computational point-of-view.

A Laplace transform procedure was used to obtain a solution for the temperature profile in the liquid droplet employing the additional assumption that

$$\dot{r}_s \Delta t \ll r_s \ . \qquad (11)$$

The solution is given below (see Appendix A for derivation):

$$T=T_o - \left[\frac{T_o(1+Ar_s)+B}{Ar}\right]\cdot\left\{\operatorname{erfc}\frac{1-R}{2\sqrt{\tau}} - \operatorname{erfc}\frac{1+R}{2\sqrt{\tau}} - \right.$$

$$\exp(Ar_s(1-R)+A^2r_s^2\tau)\cdot\operatorname{erfc}\left(\frac{1-R}{2\sqrt{\tau}} + Ar_s\sqrt{\tau}\right) +$$

$$\left.\exp(Ar_s(1+R)+A^2r_s^2\tau)\cdot\operatorname{erfc}\left(\frac{1+R}{2\sqrt{\tau}} + Ar_s\sqrt{\tau}\right)\right\} \qquad (12)$$

where $R = \dfrac{r}{r_s}$

$$\tau = \frac{\alpha t}{r_s^2}$$

$$A = \left[\frac{h}{\varkappa} - \frac{1}{r_s} - \frac{(\overline{c_p})_v}{\varkappa} K_g p \ln\frac{p}{p-p_v}\right]$$

and

$$B=r_s\left[\left(\frac{\lambda}{\varkappa} + \frac{(\overline{c_p})_v T_f}{\varkappa}\right)K_g p \ln\frac{p}{p-p_v} - \frac{hT_f}{\varkappa}\right] .$$

The analysis of droplet evaporation in a gas stream, as formulated, is developed into a computer program. Once the initial conditions are specified at time t=0 (e.g., the initial droplet radius, the initial uniform droplet temperature and the ambient conditions), one obtains a formula for the surface temperature of the droplet at any successive time, t_1. A number of coefficients in that equation depend on mean values of physical parameters over the entire span $t=0,t_1$ (physical properties used in this study are given in Appendix B). Therefore, the computation has to be performed stepwise, in order to provide averaged intermediate values of the physical parameters between t=0 and $t=t_1$ (see Appendix C for calculation procedure and computer program).

The program is as follows: Time is increased by steps. At each step, the surface temperature and the droplet radius are averaged from the initial values to the values pertinent to that step. The mean physical properties are computed, according to

the formulae given. Then the new surface temperature is computed from the Laplace transform solution and the rate of decrease of droplet radius is evaluated. This allows the new droplet radius at the next step to be determined. Since some of the yet unknown new values have to be used in making the averages, one has to start each step with a suitable guess on the surface temperature and then find the right value by a trial-and-error technique.

The program is written in such a way that different gases and different liquids can be considered, by changing some of the data cards.

A computer run is terminated when ten percent of the initial droplet mass is evaporated, or when the droplet surface temperature reaches the propellant critical temperature. The regression rates and times are normalized by using steady state droplet evaporation rates and lifetimes. It is assumed a priori that for various droplet diameters, the droplet surface temperatures approach a common value during evaporation (i.e., a wet-bulb temperature) (Ref. 6). Thus, considering the equation for mass transfer from the droplet surface, Eq. (5),

$$\frac{\dot{w}}{A_d} = \dot{r}_s \rho_\ell = K_g p \ln \frac{p}{p-p_v} \tag{5}$$

the chamber pressure, p, and the liquid density, ρ_ℓ, are given constants. The propellant vapor pressure, p_v, is constant because of the aforementioned assumption. Therefore, Eq. (5) reduces to

$$\dot{r}_s = C_1 K_g \tag{13}$$

where C_1 is determined from the constant terms in Eq. (5). Nusselt's relation for mass transfer, Eq. (10) is given as

$$\frac{2 r_s R_o \bar{T} K_g}{M_v D} = 2 + 0.6 (Sc)^{1/3} (Re)^{1/2} \tag{10}$$

where r_s is the droplet radius.

Assuming that for high speed flow ,

$$0.6(Sc)^{1/2}(Re)^{1/2} > 2 \tag{14}$$

gives

$$K_g \propto r_s^{-1/2} \tag{15}$$

Combining Eqs. (13) and (15) gives

$$\dot{r}_s r_s^{1/2} \simeq \text{constant} \tag{16}$$

If the decrease in droplet radius during the initial stages of evaporation is neglected,

$$r_s \simeq r_o \tag{17}$$

Thus,

$$\dot{r}_s r_o^{1/2} = \text{constant} , \tag{18}$$

where r_o is the initial droplet radius.

This variable is used as the normalized surface regression rate. Integrating Eq. (16) between the limits $0 \leq r_s \leq r_o$ and $0 \leq t \leq t_d$, where t_d is the droplet lifetime, gives

$$t_d \propto r_o^{3/2} \tag{19}$$

Thus, the nondimensional time is defined as

$$\frac{t}{t_d} \equiv C_2 \frac{t}{r_o^{3/2}} . \tag{20}$$

RESULTS

The results for droplet evaporation for four propellant combinations are given. The parameters varied are: the initial droplet radius, the initial droplet temperature, the thermal conductivity, and the chamber pressure. The reference case for all propellants is an initial droplet diameter of 100 microns, initial temperature of the normal boiling point, and the chamber pressure equal to that of the evaporating propellant critical pressure.

A. Variation in Droplet Histories with Initial Droplet Radius

In Fig. 2, the droplet surface regression rate parameter $\dot{r}_s\sqrt{r_o}$ is plotted against the nondimensional time for the following propellant combinations:

Fig. 2a	50/50 aerozine with NTO
Fig. 2b	NTO with 50/50 aerozine
Fig. 2c	oxygen with gaseous hydrogen
Fig. 2d	n-heptane with gaseous oxygen.

The propellants are at their normal boiling points and the ambient pressure is that of the propellant critical pressure.

Several general statements can be made for all these propellant combinations: (1) The surface regression rate parameter curves for all the droplet sizes do not coalesce during the heating up period, indicating different histories; (2) As time increases, the surface regression rate parameters approach a common value for the larger droplets. The surface regression rates for the smaller droplets (e.g., 25μ droplet in particular) continue to increase, indicating that "steady state" behavior is not approached; (3) It is noticed that the curves for the surface regression rate parameter cross, and that the value of the nondimensional time at which crossover occurs decreases as the propellant becomes more volatile. This result suggests that the heating up period decreases with propellant volatility; (4) As the propellant becomes more volatile, the asymptotic value of the burning rate parameter increases.

In Fig. 3, the droplet surface temperature history is plotted against the nondimensional time. It is observed that in all cases,

a common surface temperature is approached asymptotically for each propellant. The reduced surface temperature, i.e., T_s/T_c, where T_c is the critical temperature of the droplet propellant, varies from 0.77 for n-heptane to 0.97 for nitrogen tetroxide. From these results, it is seen that the reduced surface temperature increases as the volatility of the propellant becomes greater.

Fig. 4 shows the droplet temperature distribution with radius at 10^{-4} sec. We observe two trends, namely: (1) for each propellant and for all droplet sizes, the surface temperatures approach a common value; and (2) steep positive temperature gradients occur in approximately the outer ten percent of the droplet radius. In one case, i.e., the 25 micron diameter droplet of n-heptane, the temperature gradient is broadened and extends to 30% of the droplet radius. However, if instead of plotting the droplet temperature distribution at the end of 10^{-4} sec., the nondimensional time at the crossover point is used, then for the case of the 25 micron droplet of n-heptane, the surface temperature gradient is contained in the outer ten percent of the droplet radius.

B. Variation in Droplet Histories with Initial Droplet Temperature

In the following series of computer tests, the initial droplet temperature was varied. In these cases the initial droplet diameter was assumed to be 100 microns, and the gas pressure that of the droplet propellant critical pressure. Three runs were made with the droplet initially at: (1) the propellant normal boiling point, (2) the temperature $[T_{nbp}+5/6T_c]/2$, and (3) the temperature $5/6T_c$. The results of these tests are plotted in Figs. 5, 6 and 7. In Fig. 5, the surface regression rate parameter is plotted against the reduced time. It is seen that with 50/50 aerozine and n-heptane, the surface regression rate parameter approaches an asymptotic value independent of initial propellant temperature. With NTO and oxygen, the curves do not appear to cross within the real time of 10^{-4} sec. Certainly the crossover point, if any, has translated to larger values of time. Similar behavior is observed for the surface temperatures versus time, Fig. 6; namely, it is seen that a common value of surface temperature is approached asymptotically for each propellant.

In Fig. 7, the temperature distribution within the droplet is shown for the time 10^{-4} sec. Again it is seen that the surface temperatures approach a common value for each propellant, and that the temperature gradient is located in the outer ten percent of the droplet radius. One significant departure is observed for n-heptane with an initial temperature of 810°R. The temperature gradient at the surface is negative. In this case the initial droplet temperature was above the equilibrium surface temperature. The dynamic balance of heat and mass transfer, Eq. (4), requires that part of the droplet internal energy be used to supply the heat of vaporization.

C. Variation in Droplet Histories with Droplet Thermal Conductivity

In the following computer test runs, the effect of liquid thermal conductivity on the droplet evaporation behavior and temperature distribution was considered. The results of this study are plotted in Figs. 8, 9 and 10. In all these tests, the data extends to where ten percent of the droplet mass has evaporated. The liquid thermal conductivity was varied between 10^{-5} and 10^{-1} BTU ft.$^{-1}$sec^{-1}°R^{-1}. Values lower than 10^{-5} or greater than 10^{-1} caused computational procedure errors due to the form of the equations.

In Fig. 8, the surface regression rate parameter is plotted versus the nondimensional time. For 50/50 Aerozine and n-heptane, steady state evaporation is not approached for the cases where the larger thermal conductivities are used. This observation is based on the fact that the latter curves do not level off and approach common asymptotic values of the surface regression rate by the time ten percent of the mass is vaporized. The more volatile propellants are less sensitive to the value of thermal conductivity and level off toward common values of regression rate, thus attaining equilibrium values sooner. For all cases it is noticed that for smaller values of thermal conductivity, the surface regression rate parameter increases faster. The same general remarks can be made based on the surface temperature data given in Fig. 9. In Fig. 10, the droplet temperature distribution is shown. The results agree with intuition in that the greater the liquid thermal conductivity, the more uniform is the droplet temperature.

In passing it is noted that the time required for a 100 micron droplet to reach the ninety percent mass point was about the same, i.e., $5 \times 10^{-5} \leq t_{90\%} \leq 10^{-4}$ sec., regardless of the thermal conductivity. This behavior is due to the fact that only a small fraction of heat transfer, q_T, goes toward heating up the droplet, q_ℓ. However, the behavior of these heated droplets in a time dependent environment could be vastly different.

D. Variation in Droplet Histories with Environment Gas Pressure

In this series of computer tests, the environmental gas pressure was increased from the propellant critical pressure to that where the droplet surface temperature reached the propellant critical temperature. In the data no evidence is seen of an approach to an asymptotic value of surface temperature. This behavior appears to be in agreement with that observed by Faeth (Ref. 7).

In Fig. 11, the droplet surface temperatures are plotted versus the reduced gas pressure, p_r, for 100 micron droplets initially at normal boiling point temperature. As the pressure increases, the surface temperature increases. The values plotted represent the droplet surface temperature at a time when ten percent of the droplet mass has evaporated. For this ninety percent mass point, the reduced pressure at which the critical temperature is reached at the surface is:

n-heptane	:	$p_r = 8.3$
50/50 Aerozine	:	$p_r = 4.1$
NTO	:	$p_r = 1.37$
O_2	:	$p_r = 1.26$

It is observed that as the propellant volatility increases, the reduced pressure decreases.

In Fig. 12, the surface regression rate is shown as a function of chamber pressure. It is seen that the surface regression rate increases as the chamber pressure increases. The trend, therefore, is for the droplet lifetime to decrease as the chamber pressure increases. This is in agreement with the work of Faeth (Ref. 7).

SUMMARY OF RESULTS

The evaporative behavior of a liquid propellant droplet has been determined from a solution to a system of equations which include heat transfer within the droplet. In general, for droplets larger than 100 microns in diameter, the droplet heats up within 10^{-4} sec and approaches a steady state of evaporation. Smaller droplets, e.g., 25 micron diameter droplets, do not approach a steady state behavior. The evaporative behavior of droplets with diameter larger than 100 microns is correlated by the surface regression rate parameter, $\dot{r}_s\sqrt{r_o}$ and the nondimensional time, t/t_b after steady state have been achieved.

Analytical results obtained from the solution are:

(1) Regardless of the droplet initial temperature or radius, a common value of the droplet surface temperature is asymptotically approached. Therefore, where the droplet is heat transfer limited, or where the droplet initial temperature is greater than the steady state surface temperature, the droplet internal energy can contribute to the heat of vaporization.

(2) The effect of thermal conductivity is to vary the time required for the droplet surface temperature to reach the asymptotic value. The time required to evaporate ten percent of the droplet mass was not influenced by the value of the liquid thermal conductivity.

(3) The droplet equilibrium surface regression rate and temperature increases with environmental gas pressure. The droplet surface temperature reaches the critical value at an environmental gas pressure that is dependent on the volatility of the fluid.

(4) For droplets equal to or greater than 100 microns diameter and with realistic thermal conductivities, the temperature gradients attained at 10^{-4} sec are contained in the outer ten percent of the droplet radius.

APPENDIX A

ANALYTIC SOLUTION FOR TEMPERATURE DISTRIBUTION

A short time solution for the temperature distribution in a liquid sphere where evaporation occurs at the surface is obtained by utilizing Laplace transformations. Eq. (1) can be transformed to a more convenient form by the substitution

$$U = Tr \tag{A-1}$$

which gives

$$U_t = \alpha U_{rr} \qquad 0 \leq r \leq r_s \quad t \geq 0 \tag{A-2}$$

The initial condition expressed in Eq. (2) is

$$U(r,0) = rT_o \qquad 0 \leq r \leq r_s \quad t=0 \tag{A-3}$$

and the boundary conditions corresponding to Eqs. (3a) and (3b) are

$$U(0,t) = 0 \qquad r=0 \quad t \geq 0 \tag{A-4a}$$

$$U_r = U\left[\frac{1}{r_s} - \frac{h}{\kappa} + \frac{(\overline{c_p})_v}{\kappa} \dot{r}_s \rho_\ell\right] - \dot{r}_s \rho_\ell \frac{r_s}{\kappa}\left[\lambda + (\overline{c_p})_v T_f\right] + \frac{r_s h}{\kappa} T_f$$

$$r=r_s \quad t \geq 0 \tag{A-4b}$$

It is assumed that $\dot{r}_s \Delta t << r_s$, and that λ and p_v are constants over the time interval Δt.

The Laplace transform is taken of Eq. (A-2),

$$\int_o^\infty e^{-pt} U_{rr} dt - \frac{1}{\alpha} \int_o^\infty e^{-pt} U_t dt = 0 \tag{A-5a}$$

Expanding and including the initial condition of Eq. (A-3) gives

$$\bar{U}_{rr} - q^2\bar{U} = -\frac{r}{\alpha}T_o \qquad \text{(A-5b)}$$

where $q^2 \equiv \frac{p}{\alpha}$. (A-5c)

The boundary conditions of Eqs. (A-4a) and (A-4b) becomes

$$\bar{U}(0,t) = 0 \qquad r=0,\ t\geq 0 \qquad \text{(A-6a)}$$

$$\bar{U}_r + A\bar{u} + \frac{B}{p} = 0 \qquad r=r_s,\ t\geq 0 \qquad \text{(A-6b)}$$

where

$$A \equiv \left[\frac{h}{\kappa} - \frac{1}{r_s} - \frac{(\overline{c_p})_v K_g p}{\kappa} \ln\frac{p}{p-p_v}\right] \qquad \text{(A-7a)}$$

and

$$B \equiv r_s\left[\left(\frac{\lambda}{\kappa} + \frac{(\overline{c_p})_v T_f}{\kappa}\right) K_g p \ln\frac{p}{p-p_v} - \frac{hT_f}{\kappa}\right] \qquad \text{(A-7b)}$$

The general solution to Eq. (A-5b) is

$$\bar{U} = C_1 e^{qr} + C_2 e^{-qr} + \frac{T_o r}{q^2\alpha} \qquad \text{(A-8)}$$

Substitution into boundary condition (A-6a) gives

$$C_2 = -C_1 \qquad \text{(A-9a)}$$

and into Eq. (A-6b) gives

$$C_1 = -\frac{\frac{T_o}{q^2\alpha}[1+Ar_s] + \frac{B}{p}}{(A+q)e^{qr_s} - (B-q)e^{-qr_s}} \qquad \text{(A-9b)}$$

Thus the solution becomes

$$\bar{U} = \frac{T_o r}{p} - \left[\frac{T_o(Ar_s+1)+B}{p}\right] \cdot$$

$$\cdot \sum_{n=0}^{\infty} (-1)^n \frac{(q-A)^n}{(q+B)^{n+1}} \left[e^{-q(2n+1)(r_s-r)} - e^{-q(2n+1)(r_s+r)}\right] \qquad \text{(A-10)}$$

For a solution valid over a short interval of time, the series can be truncated after the n=0 term. This was verified by extending the series and testing for convergence. The inverse transform of Eq. (A-10) is

$$T = T_o - \left[\frac{T_o(1+Ar_s)+B}{Ar}\right] \cdot \left\{\text{erfc}\ \frac{1-R}{2\sqrt{\tau}} - \text{erfc}\ \frac{1+R}{2\sqrt{\tau}} - \right.$$

$$\exp(Ar_s(1-R)+A^2 r_s 2\tau) \cdot \text{erfc}\left(\frac{1-R}{2\sqrt{\tau}} + Ar_s\sqrt{\tau}\right) +$$

$$\left. \exp(Ar_s(1+R)+A^2 r_s{}^2 \tau) \cdot \text{erfc}\left(\frac{1+R}{2\sqrt{\tau}} + Ar_s\sqrt{\tau}\right)\right\} \qquad \text{(A-11)}$$

A qualitative discussion of the solution is now given. If we refer to Eq. (A-11), we find that it is made up of two parts. The first is, T_o, and it is recognized as the droplet initial temperature. The second is the product of

$$\left[\frac{T_o(1+Ar_s)+B}{Ar}\right] \cdot \quad F(r,t)$$

and is the droplet heatup and vaporization due to the backward heat transfer from the hot environment, i.e., for the case where the environment is considered steady in temperature. Therefore, the two parts make up the solution to the heat and mass transfer

to a burning droplet in a constant temperature environment. From summary slide rule calculations it is found that for hydrazine-type and hydrocarbon-type fuels, droplet heatup times are about 10^{-4} sec. In addition, steep temperature gradients occur at the droplet surface, the interior apparently not affected in the absence of radiation and convection. Thus the transient behavior of such a droplet is different from one with infinite thermal conductivity (i.e., a constant temperature droplet) due to decreased thermal inertia.

APPENDIX B

THERMODYNAMIC CONSTITUTIVE EQUATIONS

The thermodynamic properties for the propellant combinations employed in this study are given below. Where mixtures are considered, then Gibbs-Dalton's Law is used:

$$\text{pressure} , \quad p = \sum_i p_i \tag{B-1}$$

$$\text{enthalpy} , \quad h = \sum_i y_i h_i \tag{B-2}$$

$$\text{entropy} , \quad s = \sum_i y_i s_i \tag{B-3}$$

where y_i is the mass fraction, and for transport properties,

$$\theta = \sum_i \frac{x_i \theta_i}{\sum x_j \varphi_{ij}} \tag{B-4}$$

where

$$\varphi_{ij} = \frac{1}{\sqrt{8}} \left(1+ \frac{M_i}{M_j}\right)^{-\frac{1}{2}} \left[1+\left(\frac{\theta_i}{\theta_j}\right)^{\frac{1}{2}} \left(\frac{M_i}{M_j}\right)^{\frac{1}{4}}\right]^2 \qquad \text{(B-5)}$$

and θ is the transport property,
M the molecular weight,
x the mole fraction.

For the propellant combinations, 50/50 Aerozine with nitrogen tetroxide, oxygen with gaseous hydrogen, and nitrogen tetroxide with 50/50 Aerozine, the following constitutive equations are used:

Diffusion coefficient equation,

$$D_r = \frac{2.33 \times 10^{-6} \left(P_{CA} P_{CB}\right)^{1/3}}{\sqrt{\frac{M_A M_B}{M_A + M_B}}} \cdot \frac{\left(T_{CA} T_{CB}\right)^{0.416}}{p} \left(\frac{\bar{T}}{\sqrt{T_{CA} T_{CB}}}\right)^{1.823} \qquad \text{(B-6)}$$

Vapor pressure - Temperature relationship,

$$p_v = \exp\left(a + \frac{b}{T} + cT\right) \qquad \text{(B-7)}$$

Heat of vaporization relationship,

$$\lambda = \lambda_o \left[1+ \frac{T_s}{T_c}\right]^{\gamma} \qquad \text{(B-8)}$$

where p_c is the critical pressure; T_c the critical temperature;

$\bar{T}$ the arithmetic mean temperature; p_v the vapor pressure; a,b,c constants; λ, λ_o heats of vaporization; and T_s the droplet surface temperature. The subscript A refers to the propellant under investigation, the subscript B to the remaining mixture under investigation. Thermodynamic equilibrium is assumed for the mixture B in the film surrounding the droplet at a mean temperature $\bar{T} = [T_f+T_s]/2$. Dissociation energies are included in the determination of the thermal and transport properties. Average values are determined for the following properties and assumed constant: liquid thermal conductivity, liquid density, liquid specific heat, vapor molecular weight, vapor specific heat, gas mixture apparent molecular weight, gas mixture viscosity, gas mixture thermal conductivity, gas mixture specific heat.

For the case of n-heptane with gaseous oxygen, the thermodynamic properties used are those given in Ref. 18. The thermodynamic properties used in this study are given below:

50/50 Aerozine with NTO

α	1.805×10^{-6} ft^{2}sec^{-1}
ρ	56.5 lbm.ft^{-3}
P_{CA}	2.44×10^5 lbf ft^{-2}
P_{CB}	2.37×10^5 lbf ft^{-2}
T_{CA}	1094^oR
T_{CB}	629^oR
M_A	45.0
M_b	22.5
μ	4.30×10^{-5} lbm ft^{-1}sec^{-1}
Pr	0.70306
κ_B	3.54×10^{-5} Btu ft^{-1}sec$^{-1}{}^oR^{-1}$
$(\bar{c_p})_v$	1.100 Btu lbm$^{-1}{}^oR^{-1}$
κ	4.20×10^{-5} Btu ft^{-1}sec$^{-1}{}^oR^{-1}$
a	17.167
b	6381.9

c	0.0010199
λ_o	538.0 Btu lbm^{-1}

NTO with 50/50 Aerozine

α	1.0378×10^{-6} $ft^2 sec^{-1}$
ρ	89.34 lbm ft^{-3}
P_{CA}	2.06×10^5 lbf ft^{-2}
P_{CB}	2.37×10^5 lbf ft^{-2}
T_{CA}	$776^{\circ}R$
T_{CB}	$629^{\circ}R$
M_A	46.0 (NO_2 diffuses in film B)
M_B	22.5
μ	4.30×10^{-5} lbm $ft^{-1} sec^{-1}$
Pr	0.70306
K_B	3.54×10^{-5} Btu $ft^{-1} sec^{-1} {}^{o}R^{-1}$
$\overline{(c_p)}_v$	2.900 Btu $lbm^{-1} {}^{o}R^{-1}$
$\varkappa$	2.16×10^{-5} Btu $ft^{-1} sec^{-1} {}^{o}R^{-1}$
a	17.844
b	6300.0
c	0.0032450
λ_o	268.0

Oxygen with gaseous Hydrogen

α	7.5677×10^{-7} $ft^2 sec^{-1}$
ρ	72.0 lbm ft^{-3}
P_{CA}	1.06×10^5 lbf ft^{-2}
P_{CB}	4.10×10^5 lbf ft^{-2}
T_{CA}	$278.16 {}^{o}R$
T_{CB}	$1160^{\circ}R$
M_A	32.0
M_B	18.0

μ	4.20×10^{-5} lbm $ft^{-1} sec^{-1}$
Pr	0.71213
K_B	4.04×10^{-5} Btu $ft^{-1} sec^{-1} {}^{o}R^{-1}$
$\overline{(c_p)}_v$	2.210×10^{-5} Btu $ft^{-1} sec^{-1} {}^{o}R^{-1}$
a	16.928
b	1476.50
c	0

Heptane with Gaseous Oxygen

α	5.391×10^{-7} $ft^2 sec^{-1}$
ρ	67.80 lbm ft^{-3}
P_{CA}	5.67×10^{4} lbf ft^{-2}
T_{CA}	$972^{o}R$
M_A	100.2
M_B	31.0
μ	5.43×10^{-5} lbm $ft^{-1} sec^{-1}$
Pr	2.0499
K_B	1.29×10^{-5} Btu $ft^{-1} sec^{-1} {}^{o}R^{-1}$
$\overline{(c_p)}_v$	1.085 Btu $lbm^{-1} {}^{o}R^{-1}$
ν	2.21×10^{-5} Btu $ft^{-1} sec^{-1} {}^{o}R^{-1}$

APPENDIX C

CALCULATION PROCEDURE

Method

The procedure used in calculating the droplet evaporation histories and temperature distributions is illustrated by the flow diagram. The droplet surface temperature is given by Eq. (A-11), which requires a knowledge of time averaged thermodynamic amd transport properties which in turn are functions of the droplet surface temperature history. At each succeeding time step the

surface temperature is first assumed constant, thermodynamic and transport properties are calculated and the surface temperature at the end of the time step is determined from Eq. (A-11). The thermodynamic properties are reevaluated with the calculated surface temperature and Eq. (A-11) is solved. The procedure continues until the assumed surface temperature and calculated surface temperature differ by less than 10^{-4}. The surface regression rate, mass evaporation rate, droplet radius, and droplet temperature distribution are then determined. The time is incremented and the procedure continues.

Flow Diagram

Step 1. Load into the machine the following boundary conditions, initial conditions, and computational parameters:

Card 1. (I5) KOUNTA - Number of test cases to be analyzed.
Card 2. (18A4) TITLE - Title or description of test case.
Card 3. (7I5) NRUN - Number of test case.
MONTH - Month
MDAY - Day
MYEAR - Year
KA - Maximum number of time steps to be calculated.
JA - Frequency at which the temperature distribution is calculated and printed, i.e., if JA=10 the temperature distribution is calculated on every 10th step.
NP - Controls frequency of printing droplet radius, regression rate, surface temperature, etc.
NP=+1 Print the first 100 steps and every JA step thereafter.
NP=-1 Print every step.
Card 4. (8E10.4)
P - Chamber pressure (lbf/ft^2)
TF - Flame temperature (^oR)
RS - Initial drop radius (ft)
TO - Initial drop temperature (^oR)
U - Gas velocity (ft/sec)
V - Drop velocity (ft/sec)
DT - Time increment (sec.)
TEND - Droplet lifetime at which calculations end (sec)

Card 5. (8E10.4)

CPL - Specific heat-liquid (Btu/lbm^{o}R)
RHOL - Liquid density (lbm/ft^3)
AKL - Liquid thermal conductivity (Btu/ft sec^{o}R)
CPV - Propellant vapor specific heat (Btu/lbm^{o}R)
EMV - Propellant vapor molecular weight
VIS - Combustion gas viscosity (ft-sec/lbm)
CPB - Combustion gas specific heat (Btu/lbm^{o}R)
AKB - Combustion gas thermal conductivity (Btu/ft-sec^{o}R)

Card 6. (8E10.4)

PCA - Critical pressure-propellant (.bf/ft^2)
PCB - Critical pressure-combustion gases (lbf/ft^2)
TCA - Critical temperature-propellant (^{o}R)
TCB - Critical temperature-combustion gases (^{o}R)
EMA - Molecular weight-propellant
EMB - Molecular weight-combustion gases

Card 7. (4E10.4)

PVA, PVB, PVC, PVD - Values of constants A,B,C,D in equation for propellant vapor pressure

$$P_v(T) = \exp\left(A - \frac{B}{T-C} + DT\right)$$

Card 8. (4E10.4)

SLA, SLB, SLC, SN1 - The first three are values of constants A,B,C in equation for latent heat of vaporization. SN1 determines which of two general equation forms is used.

$$SN1 = 1 \qquad \lambda(T) = A\left(1 - \frac{T}{B}\right)^{C}$$

$$SN1 = 0 \qquad \lambda(T) = A+BT-CT^2$$

Card 9. (4E10.4)

DVA, DVB, DVC, DN1 - The first three are values of constants A,B,C in equation for diffusivity. DN1 determines which of two general equation forms is used.

$$DN1=1 \quad D_V = \frac{2.33(10^{-6})(P_{CA}\cdot P_{CB})^{1/3}}{\sqrt{\frac{M_A\cdot M_B}{M_A+M_B}}} \quad \frac{(T_{CA}\cdot T_{CB})^{.416}}{\left(\frac{\bar{T}}{\sqrt{T_{CA}\cdot T_B}}\right)^{1.823}}$$

$$DN1=0 \quad D_V=(A+BT+CT^2)\left(\frac{300}{P}\right)$$

Step 2. Calculate the initial drop mass, droplet surface regression rate and evaporation rate based upon initial conditions.

Step 3. Increment time and assume droplet surface temperature equal to that calculated at last time increment.

Step 4-5-6. Calculate the following time averaged properties: r_s, T_s, T_{film}, P_v. A time averaged property is determined summing the product of the property and time increment over all of the increments and dividing by the total elapsed time. The heat transfer coefficient, mass transfer coefficient and heat of vaporization are then evaluated using the time averaged properties. Equation (A-11) is then solved for surface temperature.

Step 7,8. The calculated value of surface temperature is compared with the assumed value. If the difference exceeds .0001 the last calculated surface temperature is assumed (Step 8) and steps 4,5,6 are repeated until convergence is obtained.

Step 9. The mass transfer coefficient is recalculated based upon the present values of surface temperature, film temperature, droplet radius and vapor pressure. The instantaneous regression rate

$$\dot{r}_s = -Kg \frac{P}{\rho_L} \ln\left(1 - \frac{P_v(T_s)}{P}\right)$$

and evaporation rate

$$\dot{m} = \rho_L 4\pi r_s^2 \dot{r}_s$$

are calculated.

Step 10. The temperature distribution (T as a function of r/r_s) in the drop is calculated by solving Eq. (A-11) at $R=r/r_s=.1,.2,.3.....1.0$ using time averaged properties.

Step 11. The calculation results for the last time increment are printed. These include: temperature distribution, step number, time, drop radius, radius regression rate, mass evaporation rate, surface temperature, mass transfer coefficient, heat transfer coefficient, Schmidt number, Reynolds number, diffusivity and the ratio of the present drop mass to the initial mass.

Step 12. Several tests are made to determine if calculations should continue, i.e., should control transfer to step 3 for an additional time increment. If the number of steps already completed is greater than some input number (KA), or if the time is greater than some predetermined quantity (TEND), or if the ratio of present mass to initial mass is less than .9, the calculations on the present test case will terminate and the next set of boundary conditions will be read.

In addition to the above described tests, there are additional checks built into the program. If the solution for surface temperature requires more than 20 iterations, the calculations terminate, a diagnostic message is printed and the next case is read. The calculations will also terminate with an appropriate

message if:

a) drop vapor pressure is greater than chamber pressure,
b) drop temperature is greater than critical temperature,
c) drop radius becomes negative.

The program contains a built-in variation in time increment. The input value of DT (time increment) is used until the time equals 100DT. At that time the time increment is increased by a factor of 10. The time increment is increased whenever the total elapsed time equals 100 times the present time increment.

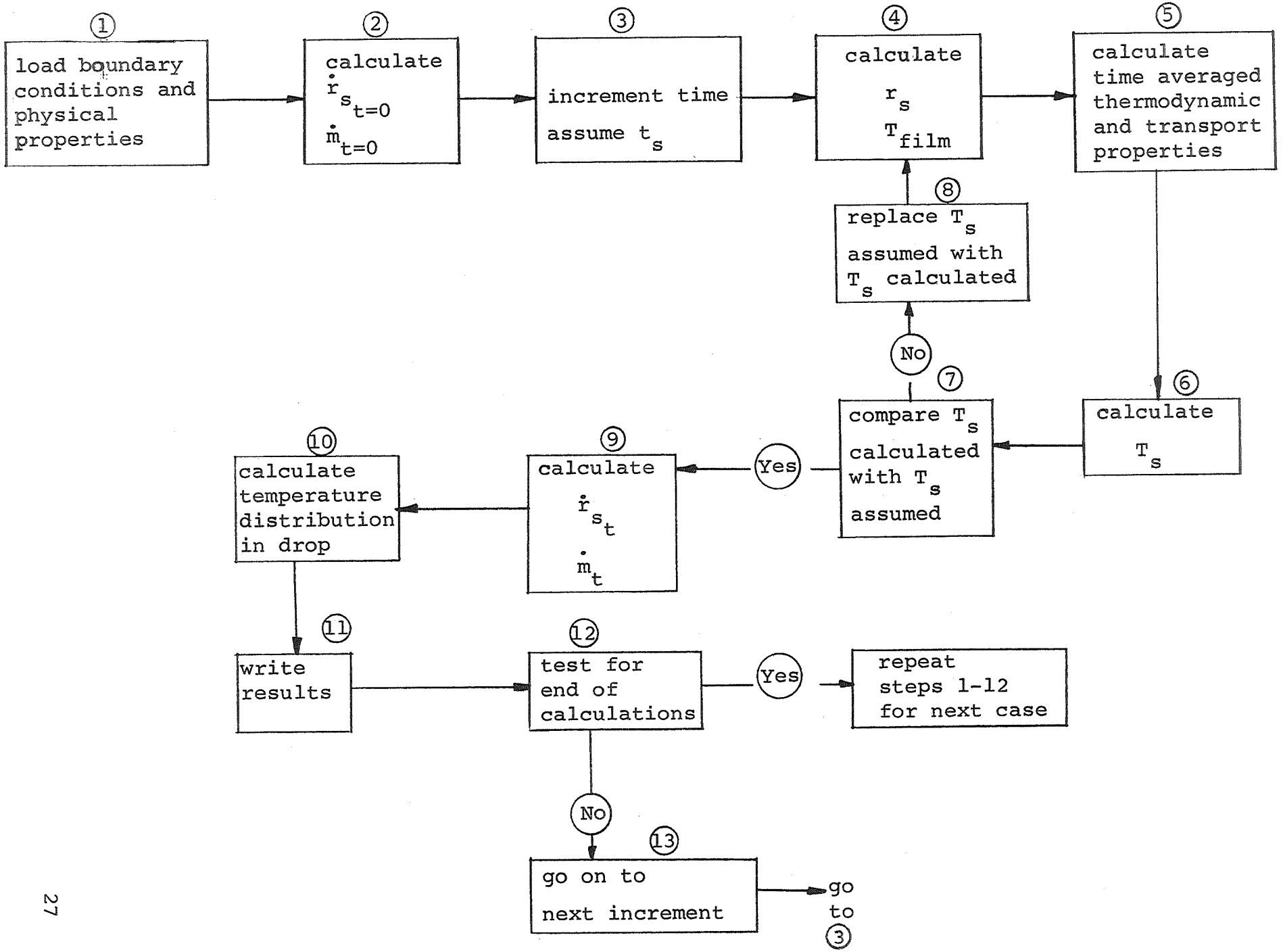

FIG. 13. FLOW DIAGRAM FOR COMPUTER PROGRAM

```
      PROGRAM DROPS(INPUT,OUTPUT,TAPE5=INPUT,TAPE6=OUTPUT)
C     PROGRAM DROPS, MAIN
C
000003      DIMENSION TS1(2),ERR(2),TITLE(18)
C
000003  100 FORMAT(14I5)
000003  101 FORMAT(8E10.4)
000003  102 FORMAT(1H0,11H RUN NUMBERI5,5X,2HONI3,1H/I2,1H/I2//11H STOP AFTERI
           16,18H STEPS OR AT TIME= E12.4/13H OUTPUT EVERYI6,6H STEPS//14H GAS
           2 PRESSURE=  E13.5,7H LB/FT2/17H GAS TEMPERATURE=  E13.5,8H RANKINE
           3/24H DROPLET INITIAL RADIUS=  E13.5,3H FT/21H DROPLET TEMPERATURE=
           4 E13.5,8H RANKINE/14H GAS VELOCITY=  E13.5,7H FT/SEC/18H DROPLET V
           ELOCITY=  E13.5,7H FT/SEC/15H TIME STEPSIZE=  E13.5,4H SEC)
000003  103 FORMAT(9H0   ALPHA,7X,4HRHOL,6X,12HGAS CONSTANT,3X,3HPCA,9X,3HPCB,
           19X,3HTCA,9X,3HTCB/  7E12.4//4X,2HMA,10X,2HMB,10X,2HMV,11X,1HA,11X,
          21HB,9X,3HVIS,9X,2HPR/  7E12.4//4X,2HKB,8X,5H(CP)V,7X,5HKAPPA/  3E12
           2.4)
000003  104 FORMAT(11H0PV(T)=EXP(F7.3,1H-F8.3,4H/(T-F7.3,2H)+F10.7,3H*T))
000003  105 FORMAT(16H0ITERATION FAILS)
000003  106 FORMAT(I7,  7E13.5,  3E9.2,  F6.3)
000003  107 FORMAT(1H0,5X,1HK,5X,4HTIME,10X,2HRS,10X,5HRSDOT,9X,4HWDOT,10X,2HT
           1S,10X,2HKG,11X,1HH,8X,3HSCH,8X,3HREY,8X,2HDV,3X,4HM/MI/1H0)
000003  108 FORMAT(F35.1,  E15.5)
000003  109 FORMAT(1H0///17X,47HTEMPERATURE DISTRIBUTION IN THE DROPLET AT STE
           1PI6//30X,4HR/RS,12X,1HT)
000003  110 FORMAT(1H1,30X,25HPROPULSION SCIENCES, INC./36X,12HP.O. BOX 814/
           133X,18HMELVILLE, NEW YORK//22X,45HWORK PERFORMED UNDER NASA CONTRA
           2CT NAS3-12030   )
000003  111 FORMAT(1H0///17X,52HDROP VAPOR PRESSURE IS GREATER THAN CHAMBER PR
           1ESSURE   )
000003  112 FORMAT(18A4)
000003  113 FORMAT(1H0//20X,18A4)
000003  114 FORMAT(11H0LAMBDA(T)=F7.2,1H+F8.4,3H*T-F10.7,5H*T**2)
000003  115 FORMAT(11H0LAMBDA(T)=F7.2,6H(1.-T/F7.2,3H)**F7.4)
000003  116 FORMAT(83H0D(P,T)=(PCA*PCB)**.33/SQRT(MA*MB/(MA+MB))*(TCA*TCB)**5/
           112/P*A*(T/SQRT(TCA*TCB))**B)
000003  117 FORMAT(9H0D(P,T)=(E13.5,1H+E13.5,3H*T+E13.5,13H*T**2)*300./P)
000003  118 FORMAT(34H0DROP RADIUS IS NEGATIVE AT TIME =E13.5)
000003  119 FORMAT(55H0DROP TEMPERATURE CAUSING VAPOR PRESSURE FCN TO BLOW UP)
000003  120 FORMAT(47H0MASS REMAINING IS LESS THAN .9 OF INITIAL MASS)
C
000003      PV(X)=EXP(PVA-PVB/(X-PVC)+PVD*X)
000017      D1(X,Y)=(PCA*PCB)**.333333/SQRT(EMA*EMB/(EMA+EMB))*(TCA*TCB)**.416
           1667/X*AA*(Y/SQRT(TCA*TCB))**BB
000056      D2(X,Y)=(DVA+DVB*Y+DVC*Y**2.)*300./X
000072      SL1(X)=SLA*(1.-X/SLB)**SLC
000103      SL2(X)=SLA+SLB*X-SLC*X**2.
000115      D(X,Y)=DN1*D1(X,Y)+ABS(DN1-1.)*D2(X,Y)
000135      RR=1545.
000136      AA=2.33E-6
000140      BB=1.823
C
000141      KOUNT=0
000143      READ(5,100)KOUNTA
000150    1 KOUNT=KOUNT+1
000152      IF(KOUNT.GT.KOUNTA)CALL EXIT
000155      READ(5,112)TITLE
```

```
000163          READ(5,100)NRUN,MONTH,MDAY,MYEAR,KA,JA,NP
000205          READ(5,101)P,TF,RS,T0,U,V,DT,TEND,CPL,RHOL,AK,CPV,EMV,VIS,CPM,AKB
               1,PCA,PCB,TCA,TCB,EMA,EMB
000265          READ(5,101)PVA,PVB,PVC,PVD
000301          READ(5,101)SLA,SLB,SLC,SN1
000315          READ(5,101)DVA,DVB,DVC,DN1
000331          ALPHA=AK/(RHOL*CPL)
000333          PR=CPM*VIS/AKB
000336          WRITE(6,110)
000342          WRITE(6,113)(TITLE(I),I=1,18)
000354          WRITE(6,102)NRUN,MONTH,MDAY,MYEAR,KA,TEND,JA,P,TF,RS,T0,U,V,DT
000414          WRITE(6,103)ALPHA,RHOL,RR,PCA,PCB,TCA,TCB,EMA,EMB,EMV,AA,BB,VIS,PR
               1,AKB,CPV,AK
000462          WRITE(6,104)PVA,PVB,PVC,PVD
000476          IF(SN1.LT..5)WRITE(6,114)SLA,SLB,SLC
000512          IF(SN1.GT..5)WRITE(6,115)SLA,SLB,SLC
000526          IF(DN1.GT..5)WRITE(6,116)
000534          IF(DN1.LT..5)WRITE(6,117)DVA,DVB,DVC
000550          TCRIT=100.*DT
000552          SSAMI=4.*3.14159*RS**3.*RHOL/3.
          C
000560          DUM8=12.5663704*RHOL
000562          DUM2=.6*PR **.333333
000566          DUM3=2.*ABS(U-V)
000572          DUM4=EMV/2./RR
000575          K=0
000576          J=0
000577          TIME=0.
000577          TS=T0
000601          TSSUM=TS
000602          TAVSUM=(TF+T0)*.5
000604          RSSUM=RS
000606          ROBAR=P*EMB/(RR*TAVSUM)
000611          VORSUM=VIS/ROBAR
000613          SCH=VORSUM/D(P,TAVSUM)
000617          DUM1=.6*SCH**.333333
000623          PVSUM=PV(T0)
000626          DUM=1.-PVSUM/P
000631          IF(DUM.LE.1.E-10)GO TO 11
000634          AKG=(2.+DUM1*SQRT(RS*DUM3/VORSUM))*D(P,T0)*DUM4/RS/TAVSUM
000652          RSDOT= AKG*P*ALOG(1.-PVSUM/P)/RHOL
000663          WDOT=DUM8*RS**2*RSDOT
000667          WRITE(6,107)
000672          WRITE(6,106)K,TIME,RS,RSDOT,WDOT,TS
000712          RSINT=0.
000713          VORINT=0.
000713          TAVINT=0.
000714          PVINT=0.
000715          TSINT=0.
          C
000717        2 K=K+1
000721          J=J+1
000722          TIME=TIME+DT
000724          KIP=1
000724          ME=1
000725          TS1(1)=TS
000727          TS1(2)=0.9*TS
000731        3 TAV=(TF+TS1(ME))*.5
```

```
000734          DD=D(P,TAV)
000740          ROAV=P*EMB/(RR*TAV)
000744          VOR=VIS/ROAV
000745          RS1=RS+RSDOT*DT
000751          IF(RS1.LE.0.0) GO TO 12
000753          RSBAR=(RSINT+RS1*DT)/TIME
000755          VORBAR=(VORINT+VOR*DT)/TIME
000760          IF(ABS(PVA-PVB/(TS1(ME)-PVC)+PVD*TS1(ME)).GT.300.) GO TO 13
000773          PVBAR=(PVINT+PV(TS1(ME))*DT)/TIME
001001          TAVBAR=(TAVINT+TS1(ME)*DT)/TIME
001004          TSBAR=(TSINT+TS1(ME)*DT)/TIME
001010          H=AKB/2./RSBAR*(2.+DUM2*SQRT(DUM3*RSBAR/VORBAR))
001021          DUM1=.6*(VORBAR/D(P,TAVBAR))**.333333
001031          AKGBAR=(2.+DUM1*SQRT(RSBAR*DUM3/VORBAR))*D(P,TAVBAR)*DUM4/RSBAR/TA
               1VBAR
001050          DUM=1.-PVBAR/P
001054          IF(DUM.LE.1.E-10)GO TO 11
001057          DUM=(AKGBAR*P*ALOG(DUM))/AK
001063          C=H/AK+CPV*DUM
001067          IF(SN1.LT..5)HEVAP=SL2(TSBAR)
001074          IF(SN1.GT..5)HEVAP=SL1(TSBAR)
001101          B=-HEVAP*DUM-C*TF
001105          A=C-1./RSBAR
001107          DUM5=SQRT(ALPHA*TIME)/RSBAR
001114          DUM6=DUM5*A*RSBAR
001116          DUM7=DUM6**2
001117          DUM9=EXP(DUM7)
001121          TSA=T0+(T0+(B+T0/RSBAR)/A)*(ERFC(1./DUM5)-ERFC(0.)+DUM9*(ERFC(DUM6
               1)-EXP(2.*A*RSBAR)*ERFC(1./DUM5+DUM6)))
001161          ERR(ME)=TSA-TS1(ME)
001164          IF(ABS(ERR(ME)).LE.1.E-4)GO TO 4
001170          IF(ME.EQ.2)GO TO 5
001172          ME=2
001173          GO TO 3
001173        5 TSAA=TS1(1)-ERR(1)*(TS1(2)-TS1(1))/(ERR(2)-ERR(1))
001202          ERR(1)=ERR(2)
001203          TS1(1)=TS1(2)
001204          TS1(2)=TSAA
001206          KIP=KIP+1
001207          IF(KIP.LE.20)GO TO 3
001212          WRITE(6,105)
001215          GO TO 1
          C
001216        4 RS=RS1
001217          RSINT=RSINT+RS*DT
001222          TS=TS1(ME)
001224          DUM1=.6*(VOR/DD)**.333333
001231          AKG=(2.+DUM1*SQRT(RS*DUM3/VOR))*DD*DUM4/RS/TAV
001244          IF(ABS(PVA-PVB/(TS-PVC)+PVD*TS).GT.300.) GO TO 13
001256          DUM=1.-PV(TS)/P
001262          IF(DUM.LE.1.E-10)GO TO 11
001265          RSDOT=AKG*P*ALOG(DUM)/RHOL
001271          TAVINT=TAVINT+TAV*DT
001275          VORINT=VORINT+VOR*DT
001277          TSINT=TSINT+TS*DT
001302          PVINT=PVINT+PV(TS)*DT
001306          WDOT=DUM8*RS**2*RSDOT
001310          SCH=VOR/DD
```

```
001312            REY=2.*RS*ABS(U-V)/VOR
001320            SSAM=4.*3.14159*RS**3.*RHOL/3.
001325            RAT=SSAM/SSAMI
001327            IF(TIME.GT.TCRIT.AND.NP.GT.0)GO TO 10
001341            WRITE(6,106)K,TIME,RS,RSDOT,WDOT,TS,AKG,H,SCH,REY,DD,RAT
001374         10 IF(RS.LE.0.)TEND=TIME
001400            IF(J.LT.JA.AND.TIME.LT.TEND)GO TO 6
                C
001412          8 J=0
001413            TT=TIME/DT+.5
001416            IF(TT.GT.100.)DT=10.*DT
001422            WRITE(6,109)K
001430            DO 7 N=1,10
001432            R=.1*FLOAT(N)
001435            DOM1=(1.+R)/2./DUM5
001440            DOM2=(1.-R)/2./DUM5
001442            T=T0+(T0+(B+T0/RSBAR)/A)/R*(ERFC(DOM1)-ERFC(DOM2)+DUM9*(EXP(A*RSBA
                 1R*(1.-R))*ERFC(DOM2+DUM6)-EXP(A*RSBAR*(1.+R))*ERFC(DOM1+DUM6)))
001512          7 WRITE(6,108)R,T
001524            WRITE(6,107)
001530            IF(NP.LT.0) GO TO 6
001532            WRITE(6,106)K,TIME,RS,RSDOT,WDOT,TS,AKG,H,SCH,REY,DD,RAT
001565            IF(RAT.LT..9) GO TO 14
001570          6 IF(K.GT.KA.OR.TIME.GE.TEND)GO TO 1
001603            GO TO 2
001603         11 WRITE(6,111)
001607            GO TO 1
001610         12 WRITE(6,118)TIME
001616            GO TO 1
001617         13 WRITE(6,119)
001623            GO TO 1
001624         14 WRITE(6,120)
001630            GO TO 1
                C
001631            END
```

APPENDIX D

SYMBOLS

A	factor, Eq. (12)
A_d	droplet surface area
B	film thickness factor, Eq. (12), Eq. (A-7a)
a,b,c	constants, Eq. (6)
C	constant, Eq.(13), (A-9a)
$(\overline{c_p})_v$	average droplet vapor specific heat
D	molecular diffusion coefficient, factor, Eq. (A-7b), diameter
h	film heat transfer coefficient, enthalpy
K	evaporative constant, Eq. (20)
Kg	mass transfer coefficient
Km	thermal conductivity of vapor-gas mixture
M	molecular weight
Pr	Prandtl number
p	pressure; transform variable
q	defined in Eq. (A-5c), heat transfer
R	ratio r/r_s
Re	Reynolds number
R_o	universal gas constant
r	droplet radius
$\dot{r}_s$	regression rate of droplet surface
s	entropy
Sc	Schmidt number
T	temperature
$\overline{T}$	average temperature $[T_f+T_s]/2$
t	time
U	function defined in Eq. (A-1)
u	gas velocity
v	droplet velocity
$\dot{w}$	mass evaporation rate
x	mole fraction
y	mass fraction
α	thermal diffusivity
γ	exponent, Eq. (7)
ρ	gas density
$\varkappa$	droplet thermal conductivity
λ	heat of vaporization

λ_o constant, Eq. (7)
μ viscosity
ρ density
τ $\alpha t/r_s^2$
θ transport property
φ Eq. (B-5)

Subscripts

m mixture
sh superheat
λ evaporation
ℓ liquid
T total
s surface
o initial, reference
f flame
v vapor
c critical, chamber
r radius, differentiation with respect to radius
t time, differentiation with respect to time
i,j specie index

REFERENCES

1. Williams, F.A.: "On the Assumptions Underlying Droplet Vaporization and Combustion Theories". J. Chem. Phys., Vol. 33, p.133, 1960.

2. Spalding, D.B.: "The Theory of Burning of Solid and Liquid Propellants". Aeronautical Research Council, A.R.C. 21, 358, C.F. 299, R. 485, London, February 1959.

3. Wise, H. and Agoston, G.A.: "Burning of a Liquid Droplet". Advances in Chemistry, American Chemical Society, N.Y., 1958, Sec. 20, pp. 116-135.

4. Wood, B.J., Rosser, W.A. Jr., and Wise, H.: "Combustion of Fuel Drops". AIAA J., 1, pp. 1076-1081, 1963.

5. Rosner, D.E.: "On Liquid Droplet Combustion at High Pressures". AIAA J., 5, pp. 163-166, January 1967.

6. Priem, R.J. and Heidmann, M.F.: "Propellant Vaporization as a Design Criterion for Rocket-Engine Combustion Chambers". NASA TR R-67, p. 21, 1960.

7. Faeth, G., Dominicis, D.P. and Olson, D.R.: "An Investigation of Near Critical and Supercritical Burning of Fuel Droplets". NASA CR-72314, Pennsylvania State Univ., 1967.

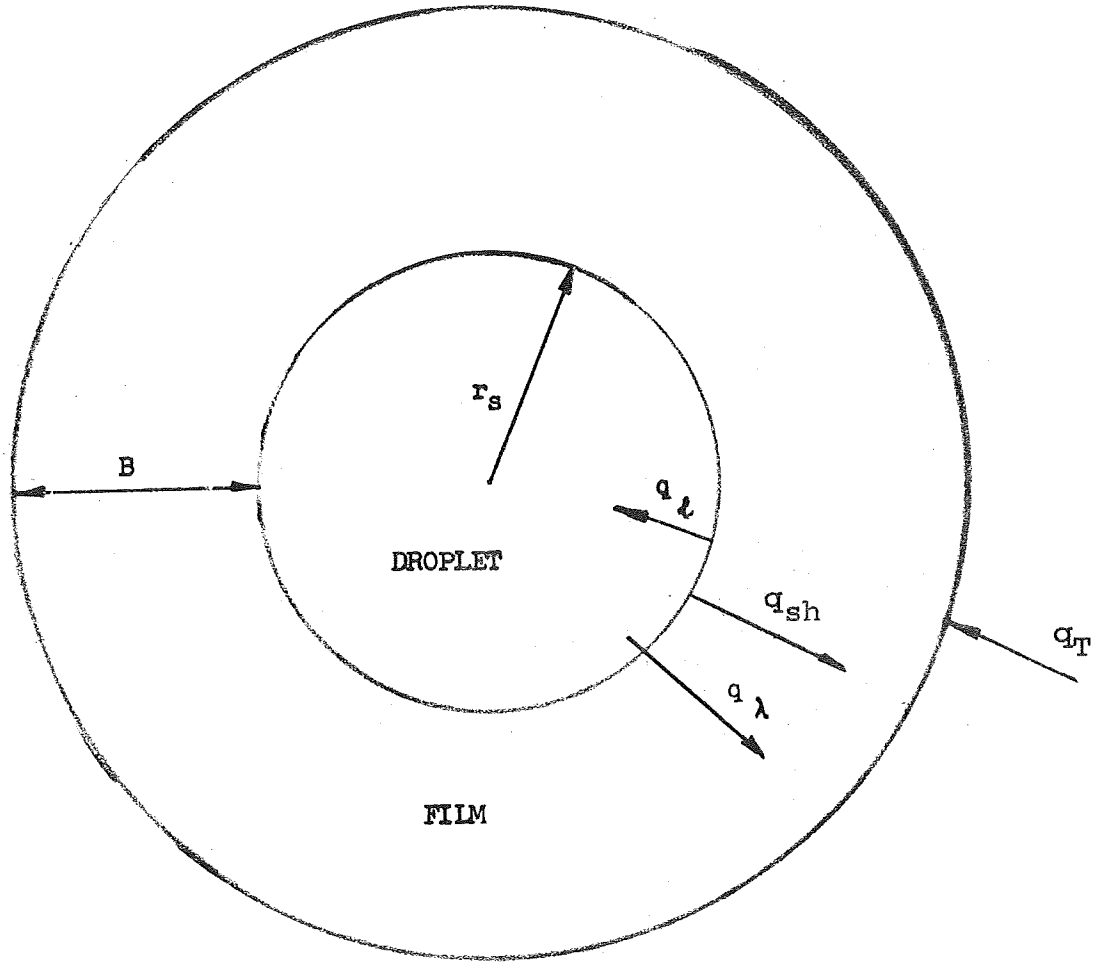

FIG. 1. SCHEMATIC DIAGRAM OF HEAT TRANSFER TO VAPOR FILM AND LIQUID DROPLET

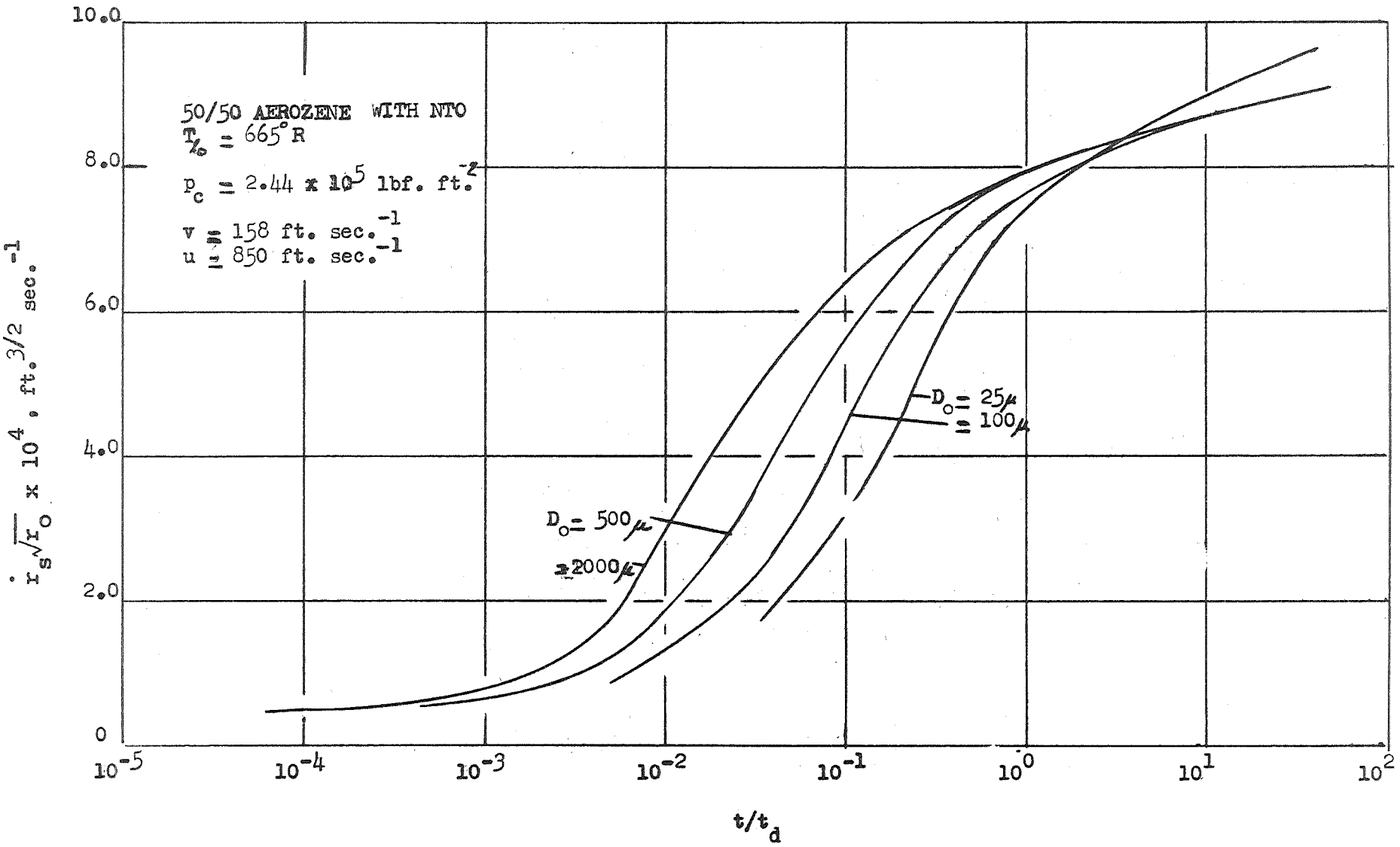

FIG. 2a. SURFACE REGRESSION RATE VS. TIME FOR VARIATION IN INITIAL DROPLET RADIUS, 50/50 AEROZINE WITH NTO

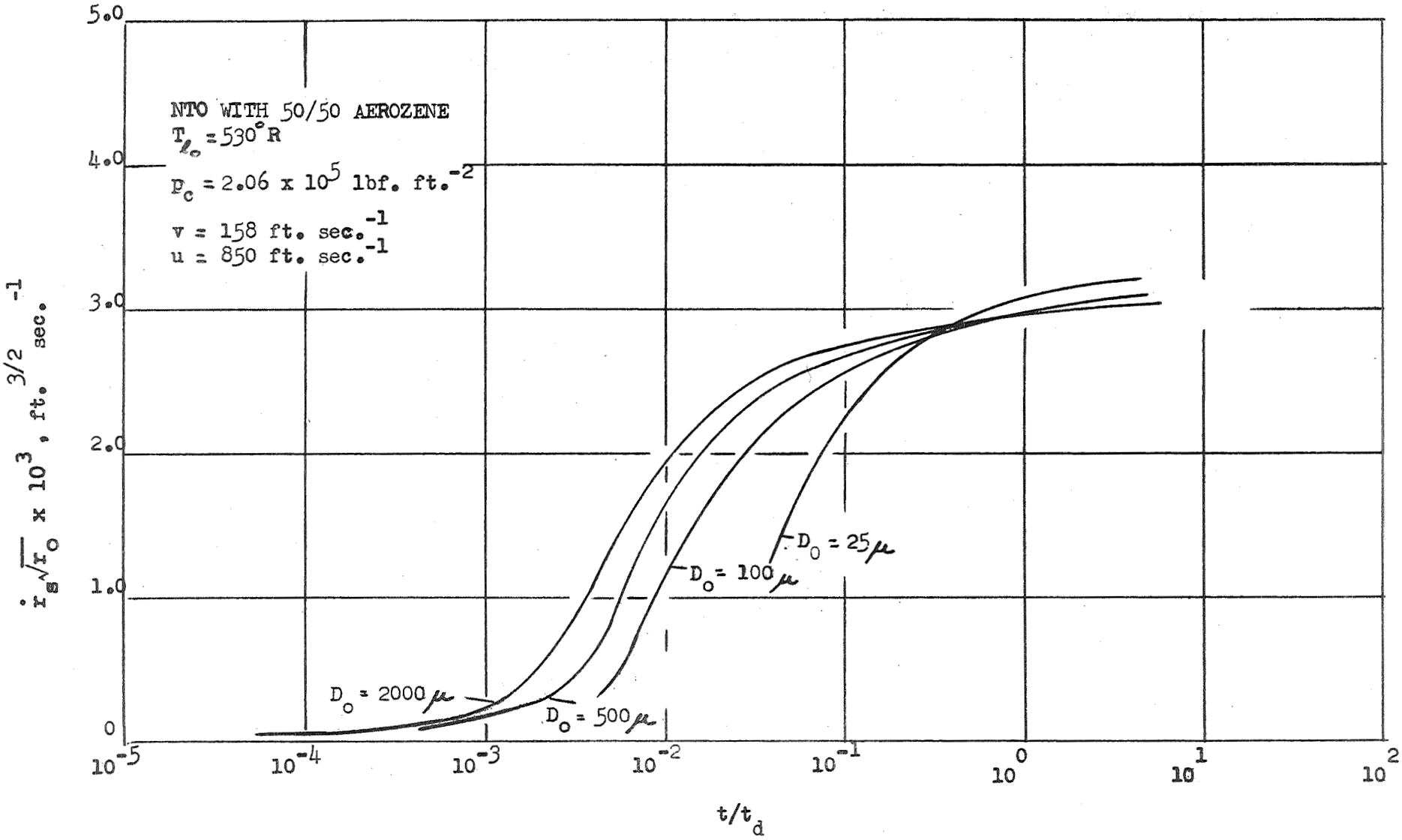

FIG. 2b. SURFACE REGRESSION RATE VS. TIME FOR VARIATION IN INITIAL DROPLET RADIUS, NTO WITH 50/50 AEROZINE

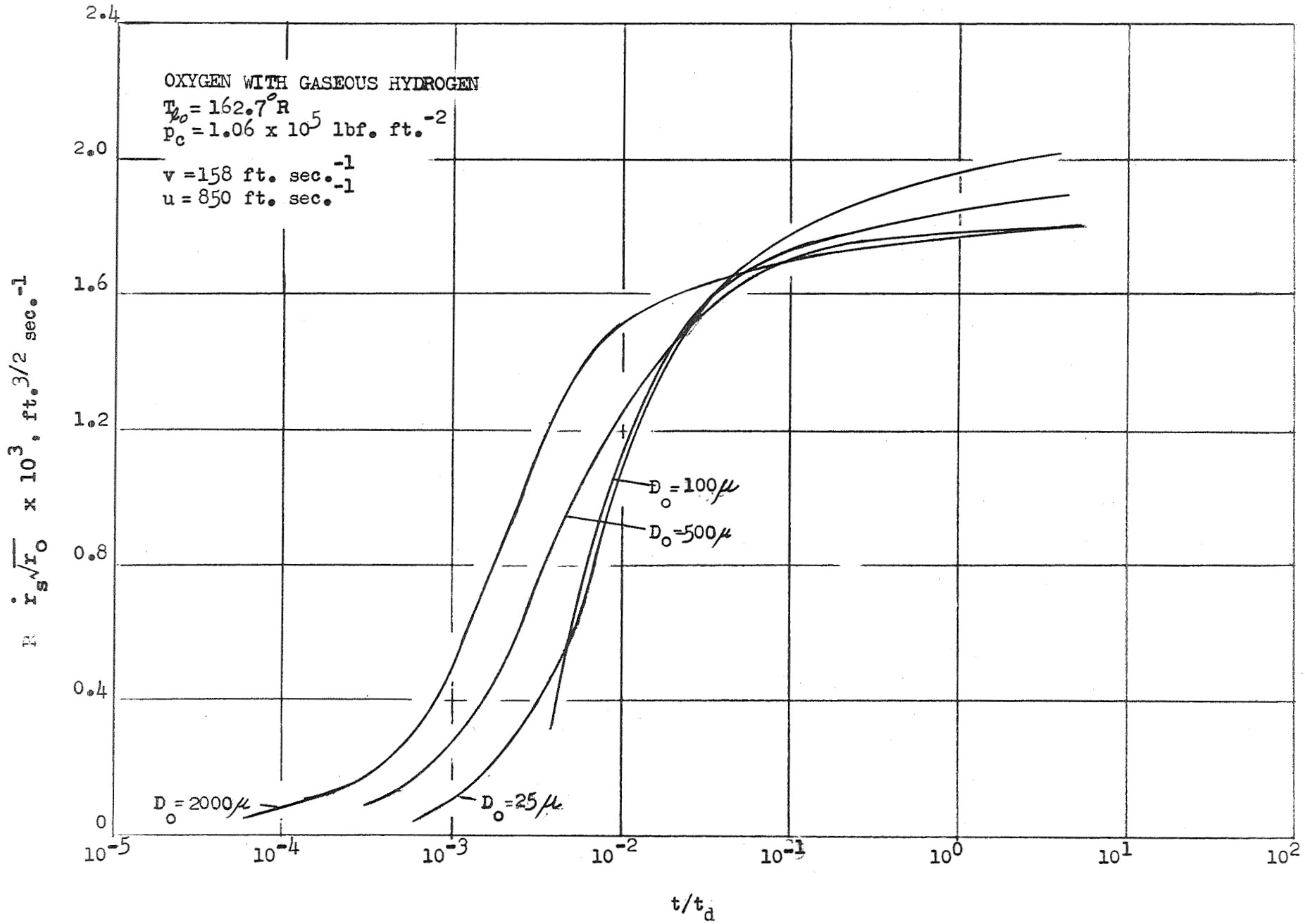

FIG. 2c. SURFACE REGRESSION RATE VS. TIME FOR VARIATION IN INITIAL DROPLET RADIUS, OXYGEN WITH GASEOUS HYDROGEN

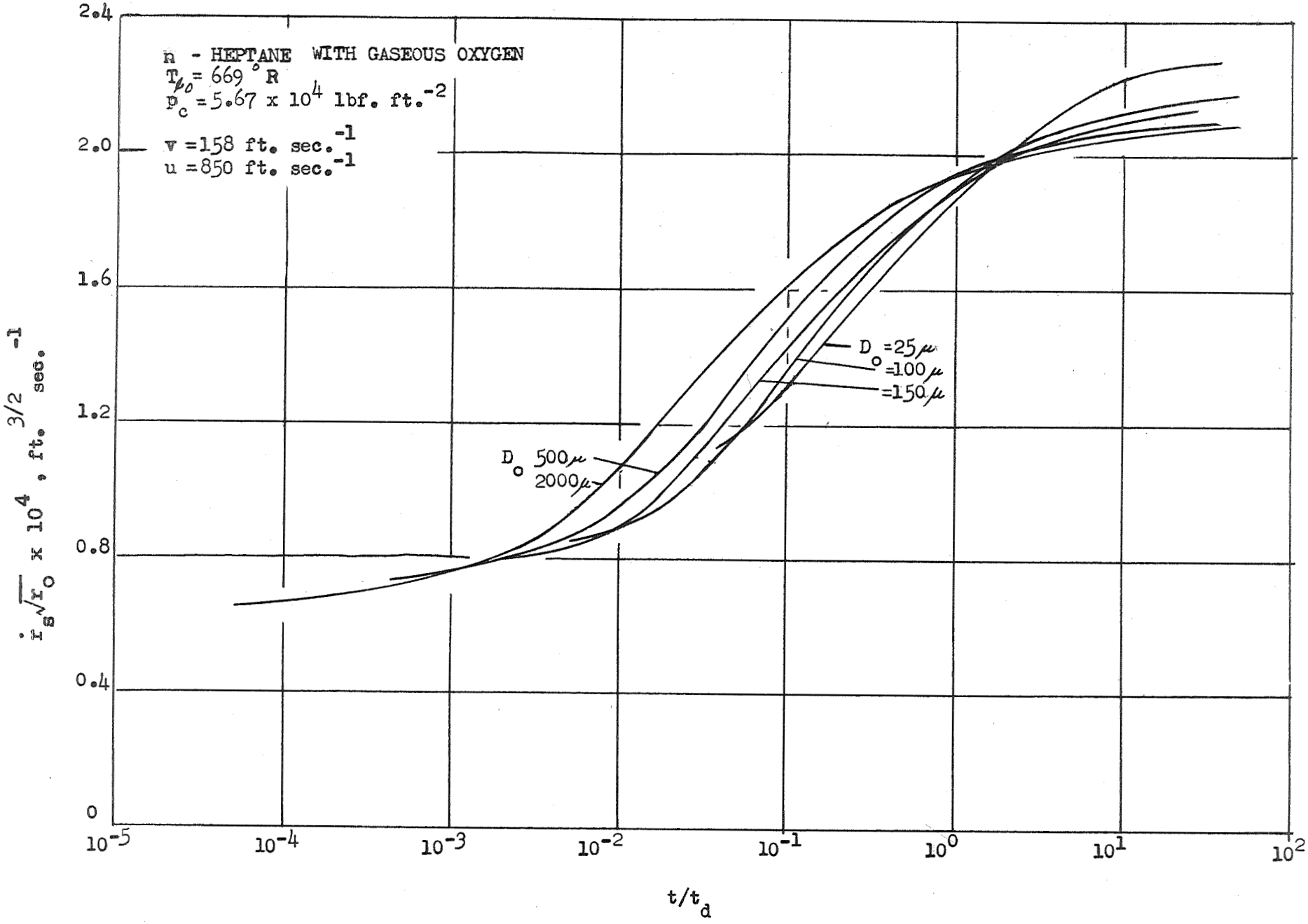

FIG. 2d. SURFACE REGRESSION RATE VS. TIME FOR VARIATION IN INITIAL DROPLET RADIUS, n-HEPTANE WITH GASEOUS OXYGEN

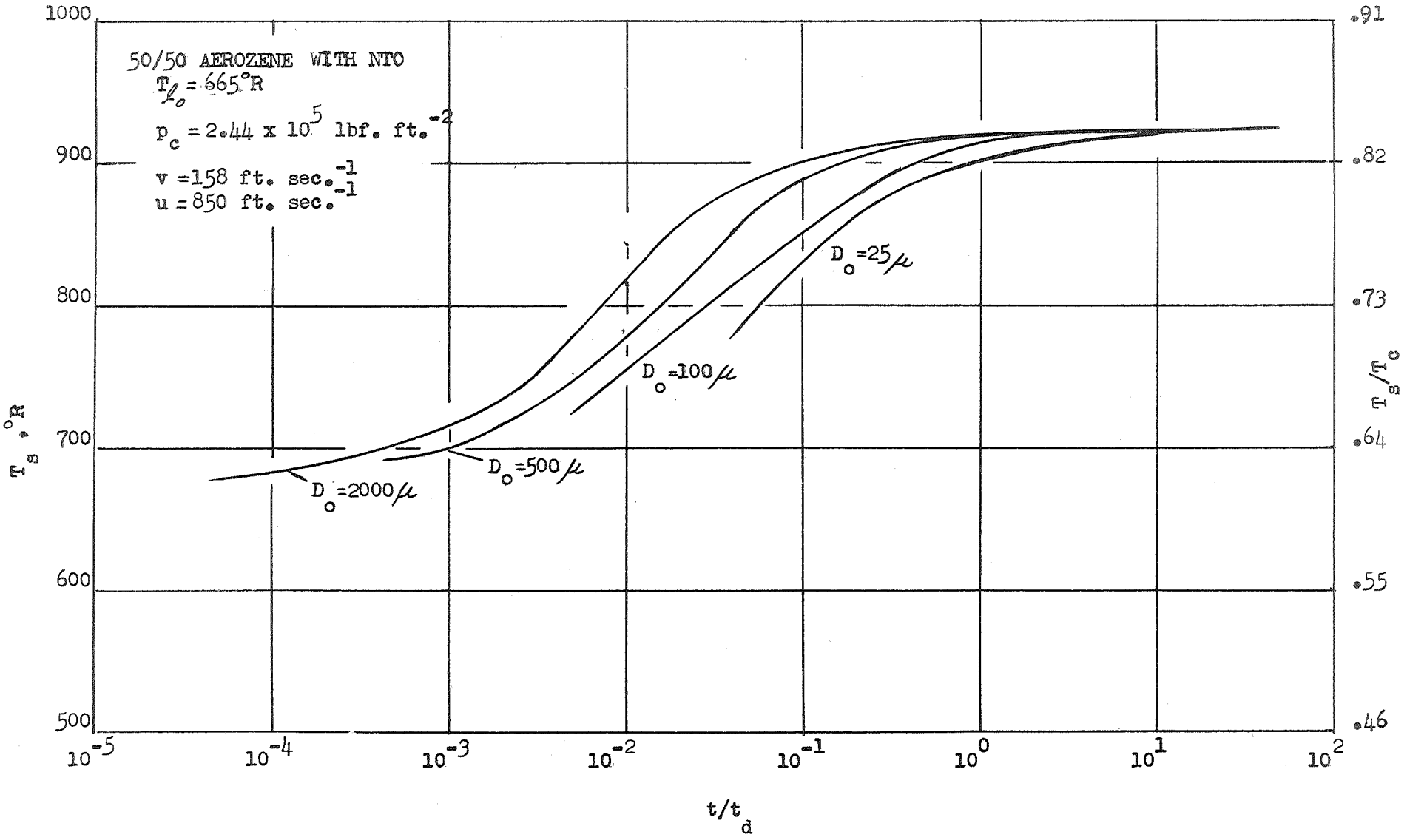

FIG. 3a. SURFACE TEMPERATURE VS. TIME FOR VARIATION IN INITIAL DROPLET RADIUS, 50/50 AEROZINE WITH NTO

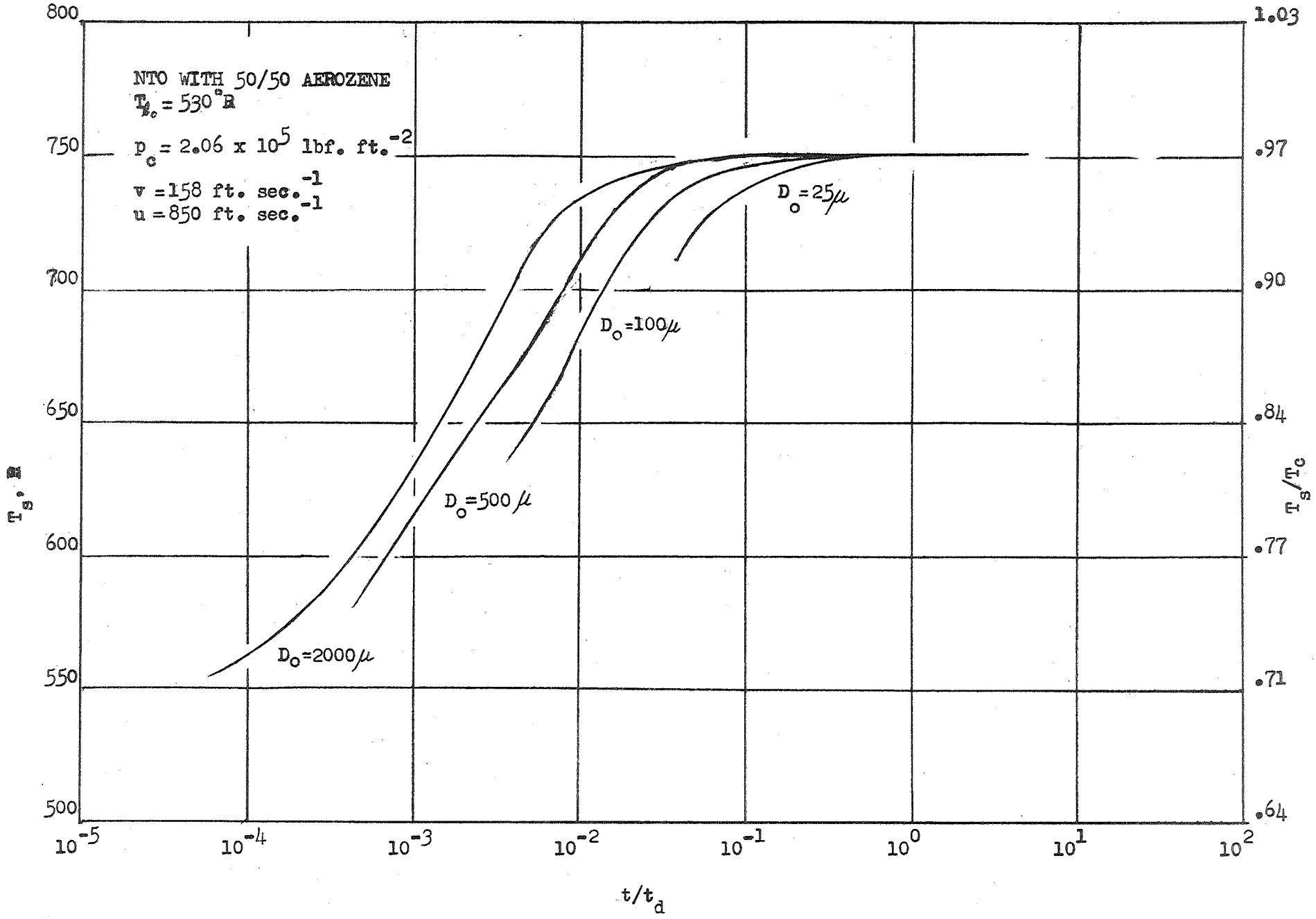

FIG. 3b. SURFACE TEMPERATURE VS. TIME FOR VARIATION IN INITIAL DROPLET RADIUS, NTO WITH 50/50 AEROZINE

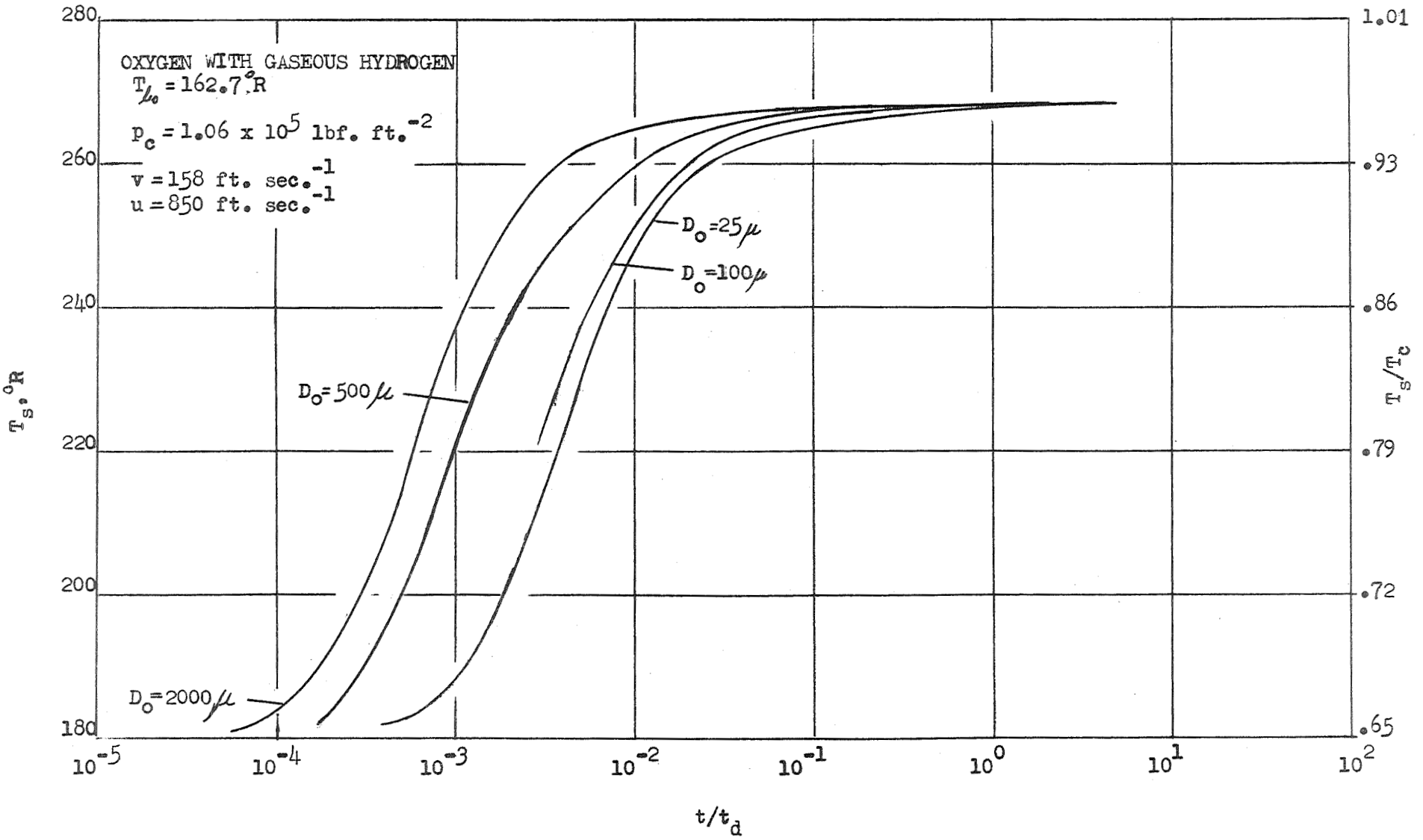

FIG. 3c. SURFACE TEMPERATURE VS. TIME FOR VARIATION IN INITIAL DROPLET RADIUS, OXYGEN WITH GASEOUS HYDROGEN

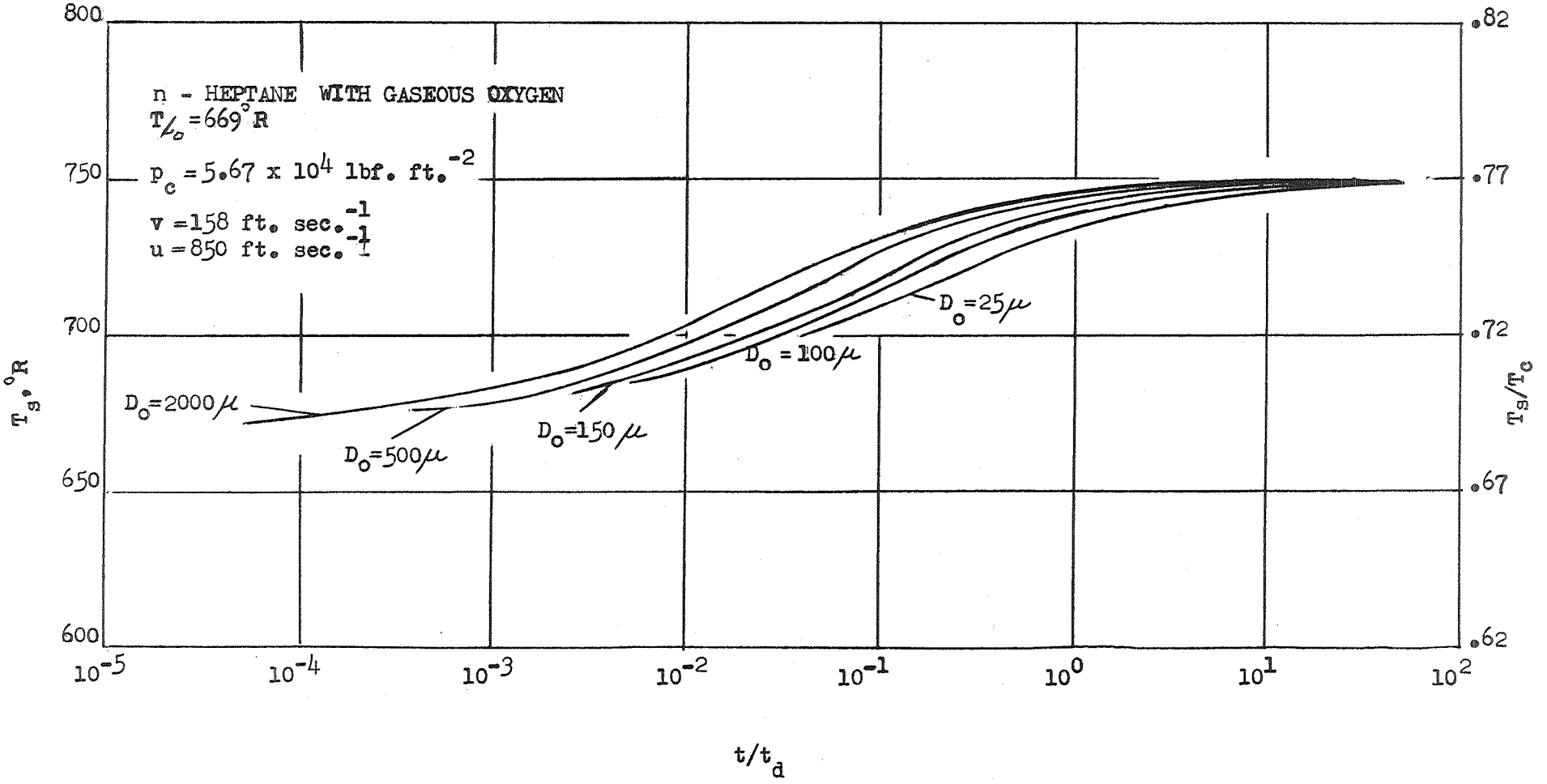

FIG. 3d. SURFACE TEMPERATURE VS. TIME FOR VARIATION IN INITIAL DROPLET RADIUS, n-HEPTANE WITH GASEOUS OXYGEN

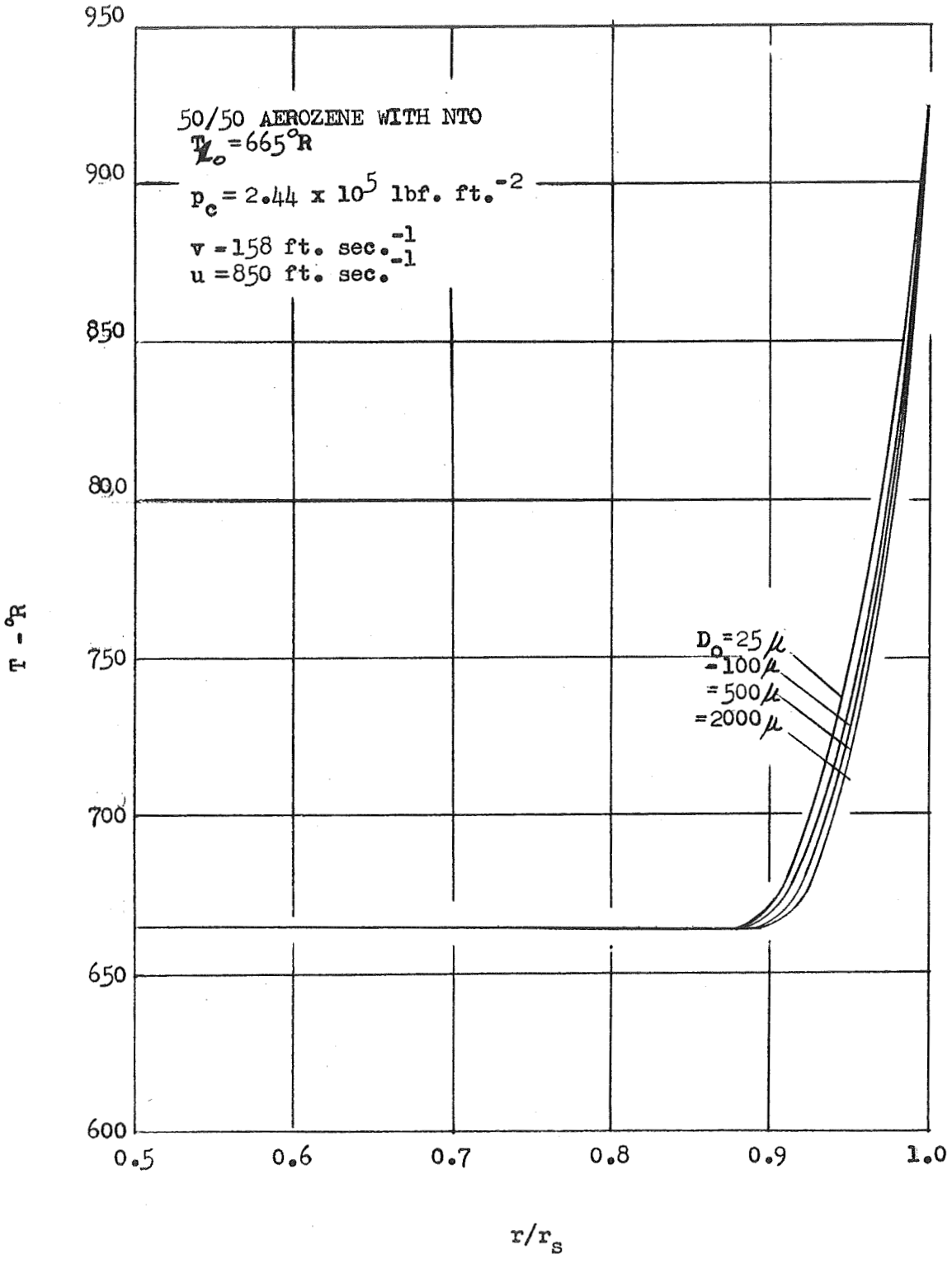

FIG. 4a. DROPLET TEMPERATURE DISTRIBUTION FOR VARIATION IN INITIAL DROPLET RADIUS, AT A TIME 10^{-4} SECOND, 50/50 AEROZINE WITH NTO

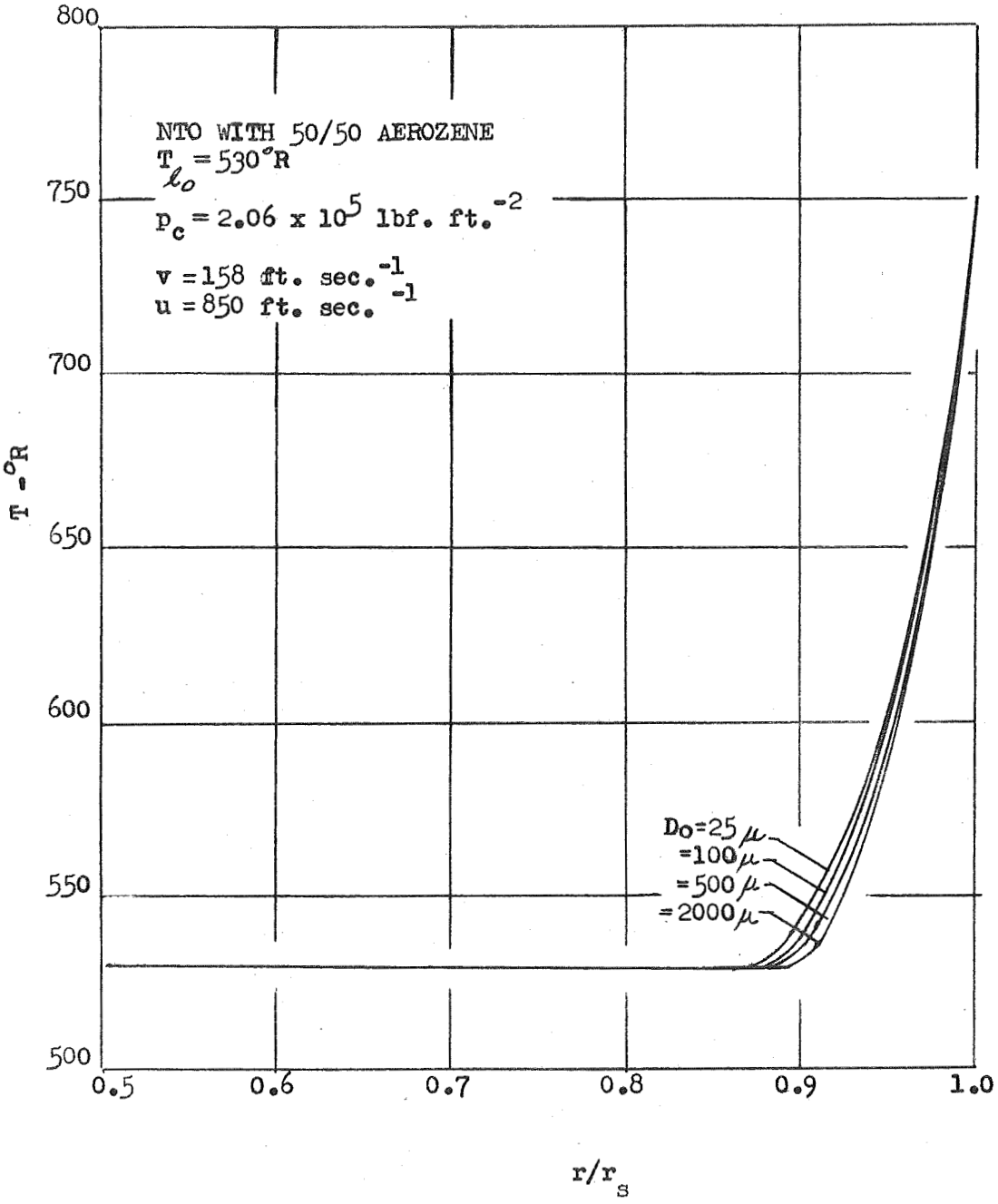

FIG. 4b. DROPLET TEMPERATURE DISTRIBUTION FOR VARIATION IN INITIAL DROPLET RADIUS, AT A TIME OF 10^{-4} SECOND, NTO WITH 50/50 AEROZINE

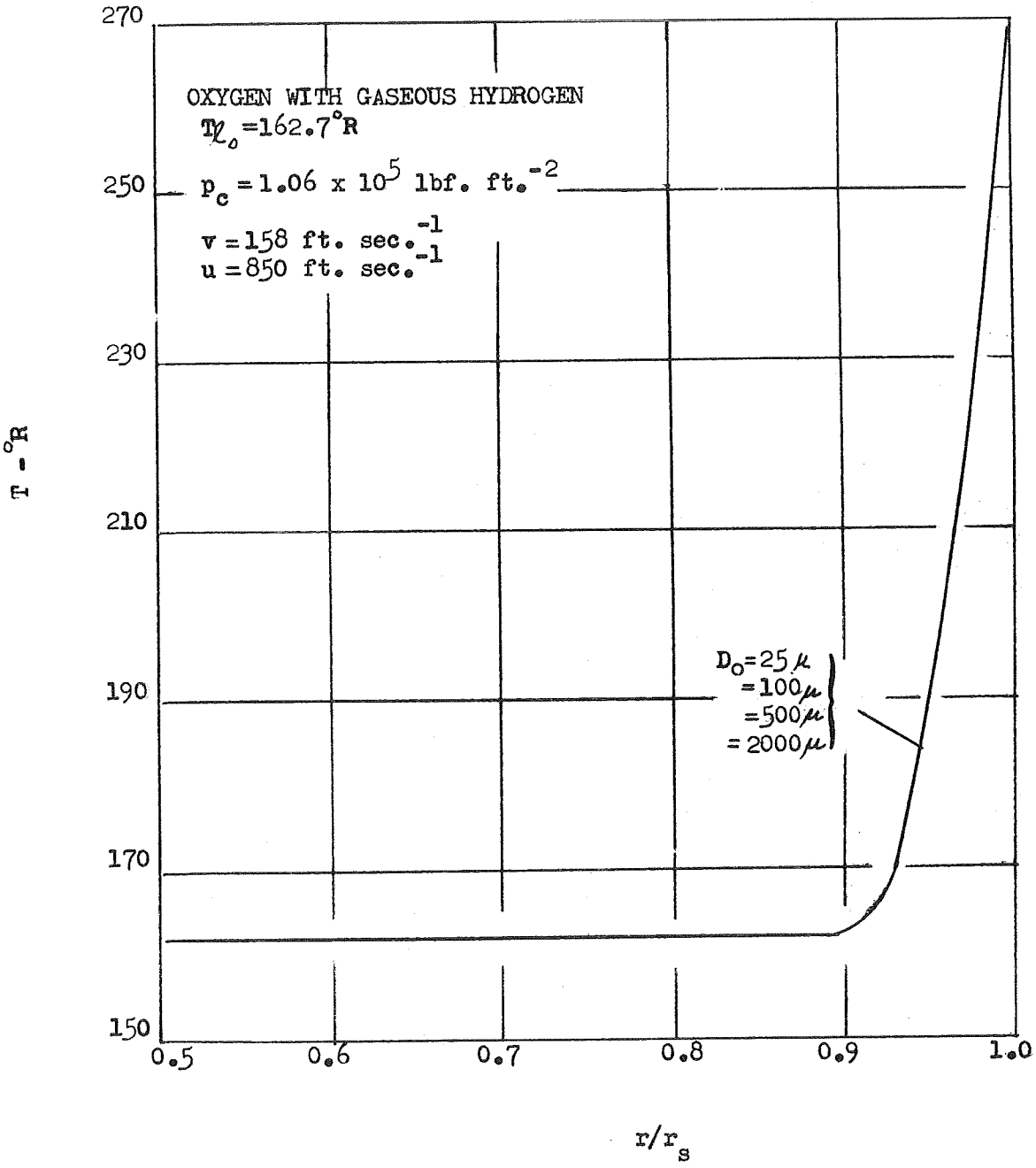

FIG. 4c. DROPLET TEMPERATURE DISTRIBUTION FOR VARIATION IN INITIAL DROPLET RADIUS, AT A TIME OF 10^{-4} SECOND, OXYGEN WITH GASEOUS HYDROGEN

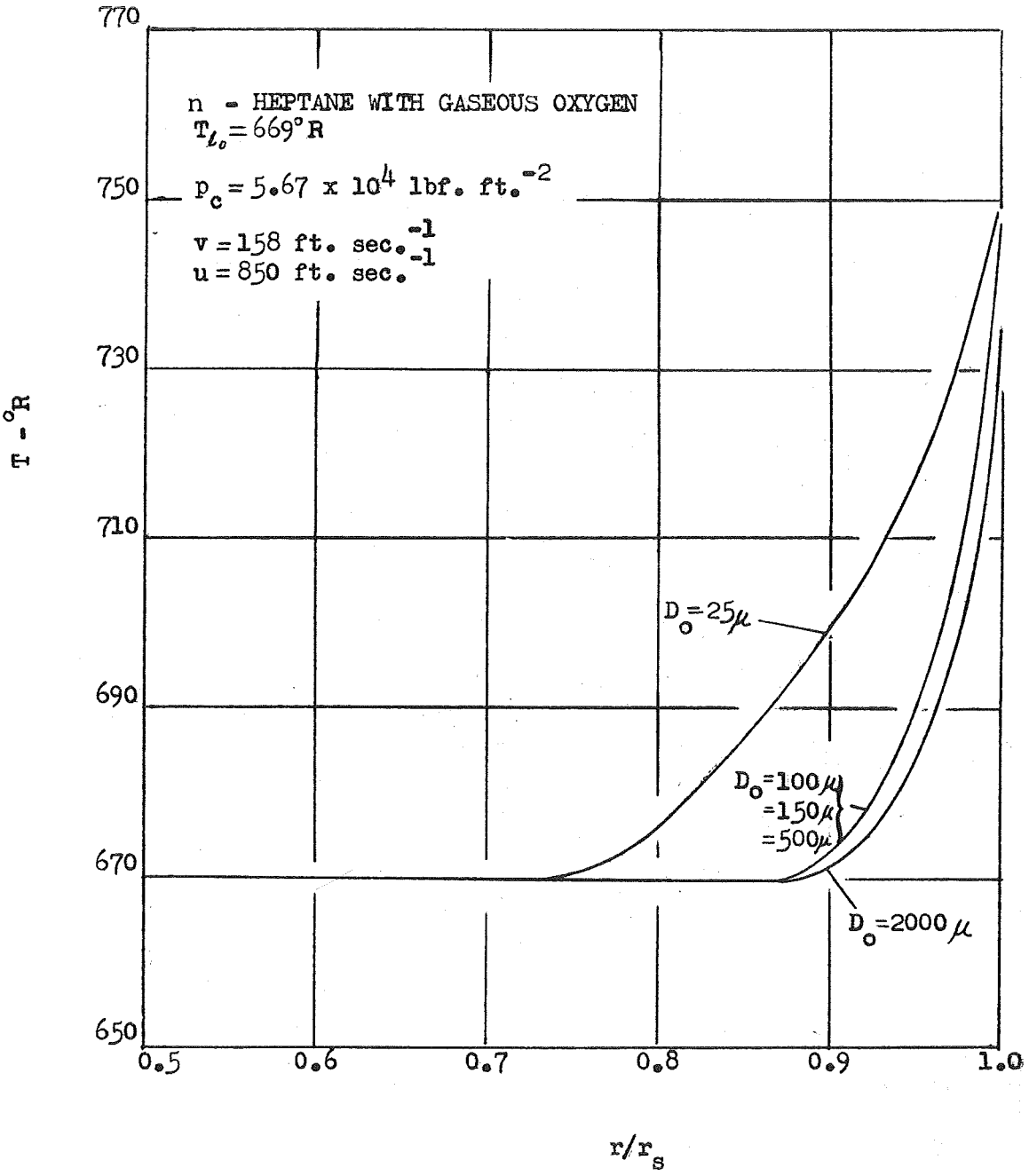

FIG. 4d/ DROPLET TEMPERATURE DISTRIBUTION FOR VARIATION IN INITIAL DROPLET RADIUS, AT A TIME OF 10^{-4} SECOND, n-HEPTANE WITH GASEOUS OXYGEN

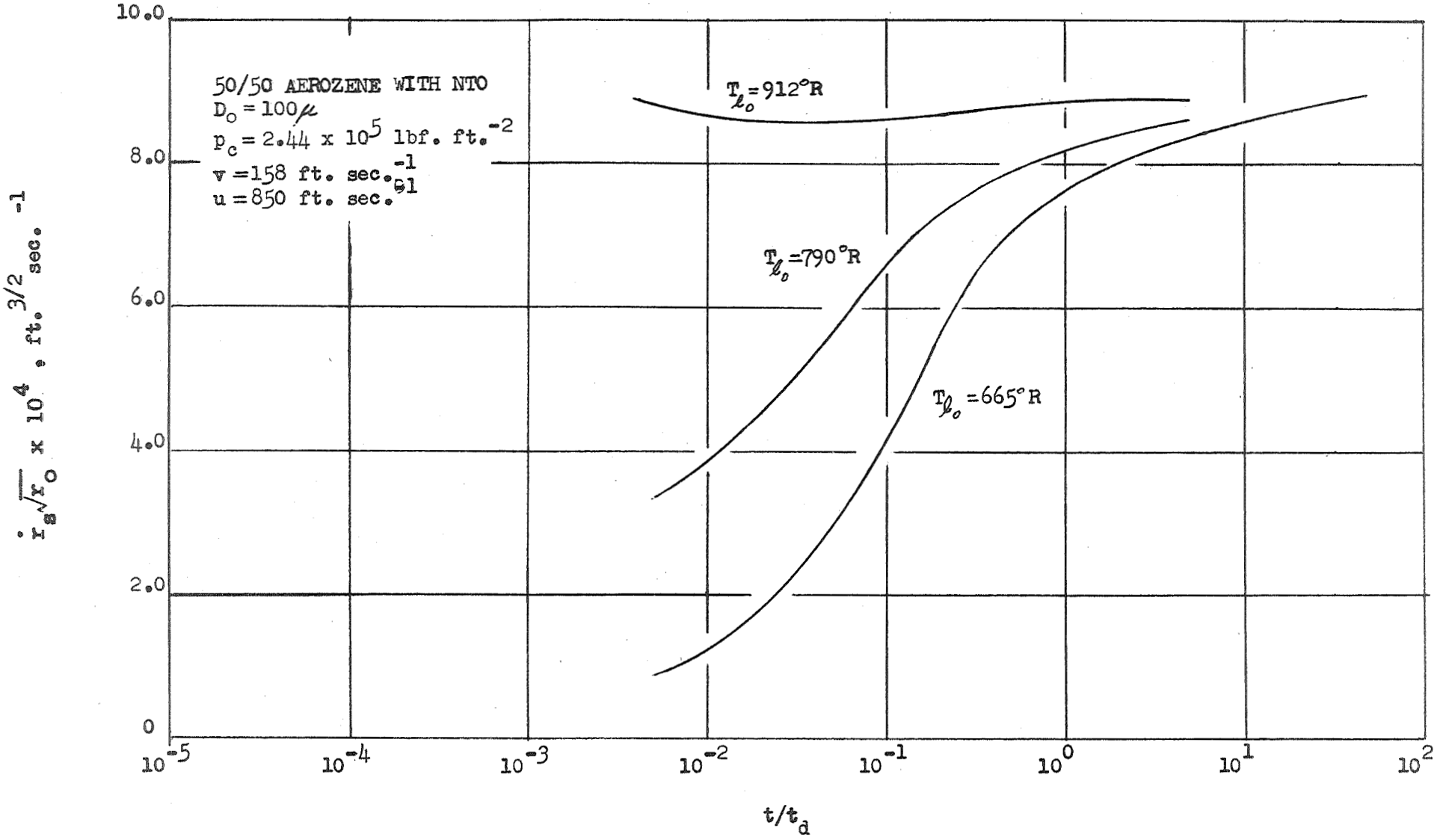

FIG. 5a . SURFACE REGRESSION RATE VS. TIME FOR VARIATION IN INITIAL DROPLET TEMPERATURE, 50/50 AEROZINE WITH NTO

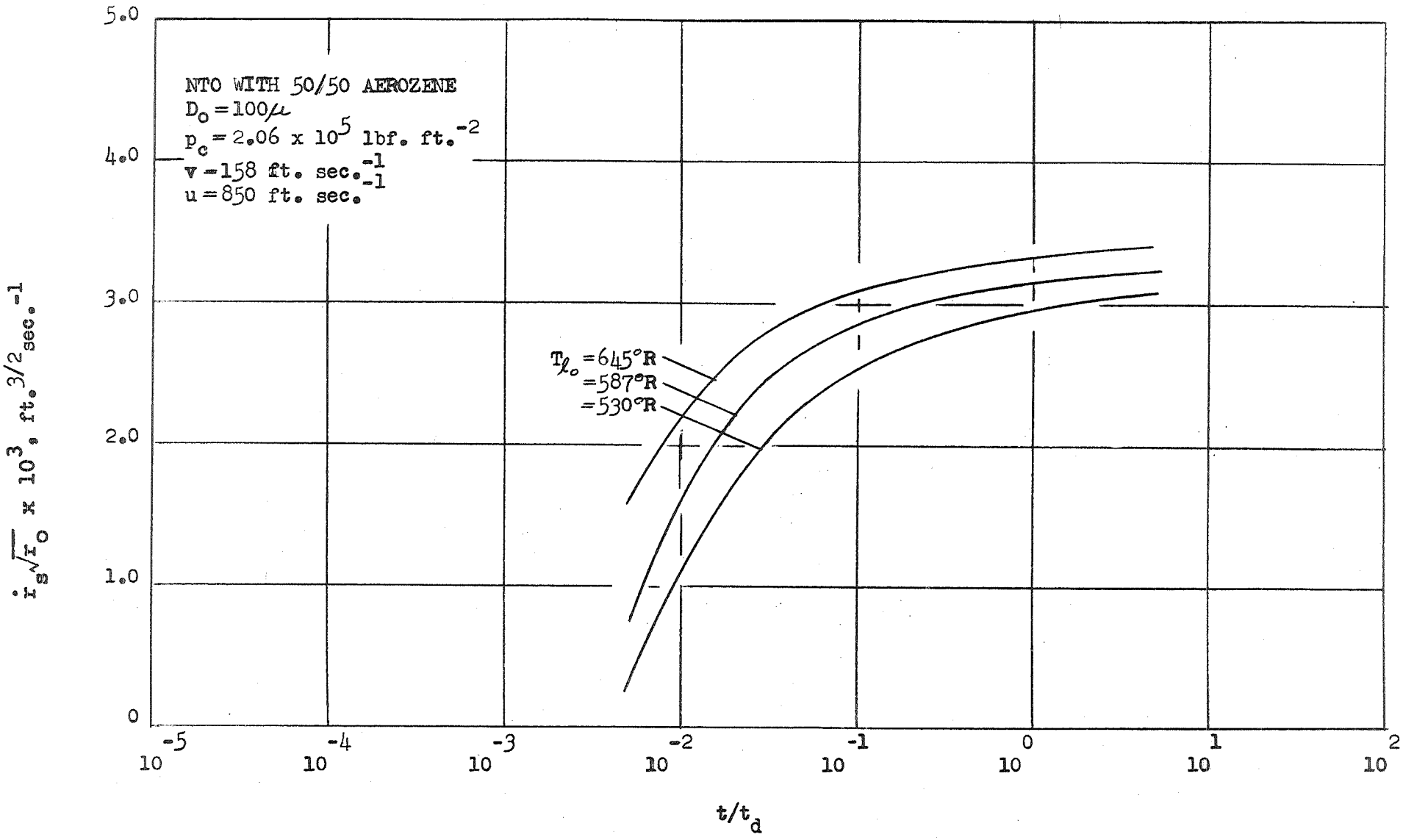

FIG. 5b. SURFACE REGRESSION RATE VS. TIME FOR VARIATION IN INITIAL DROPLET TEMPERATURE, NTO WITH 50/50 AEROZINE

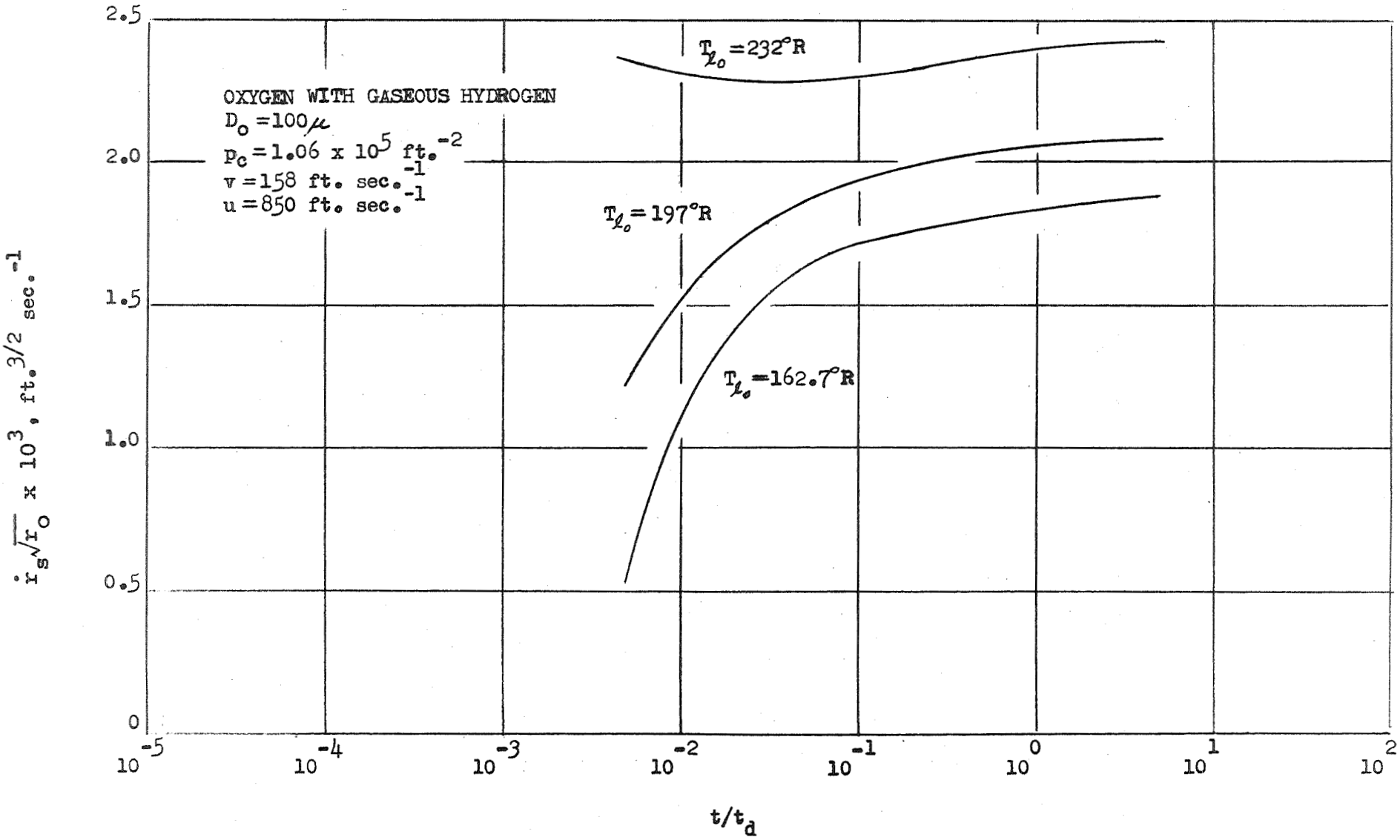

FIG. 5c. SURFACE REGRESSION RATE VS. TIME FOR VARIATION IN INITIAL DROPLET TEMPERATURE, OXYGEN WITH GASEOUS HYDROGEN

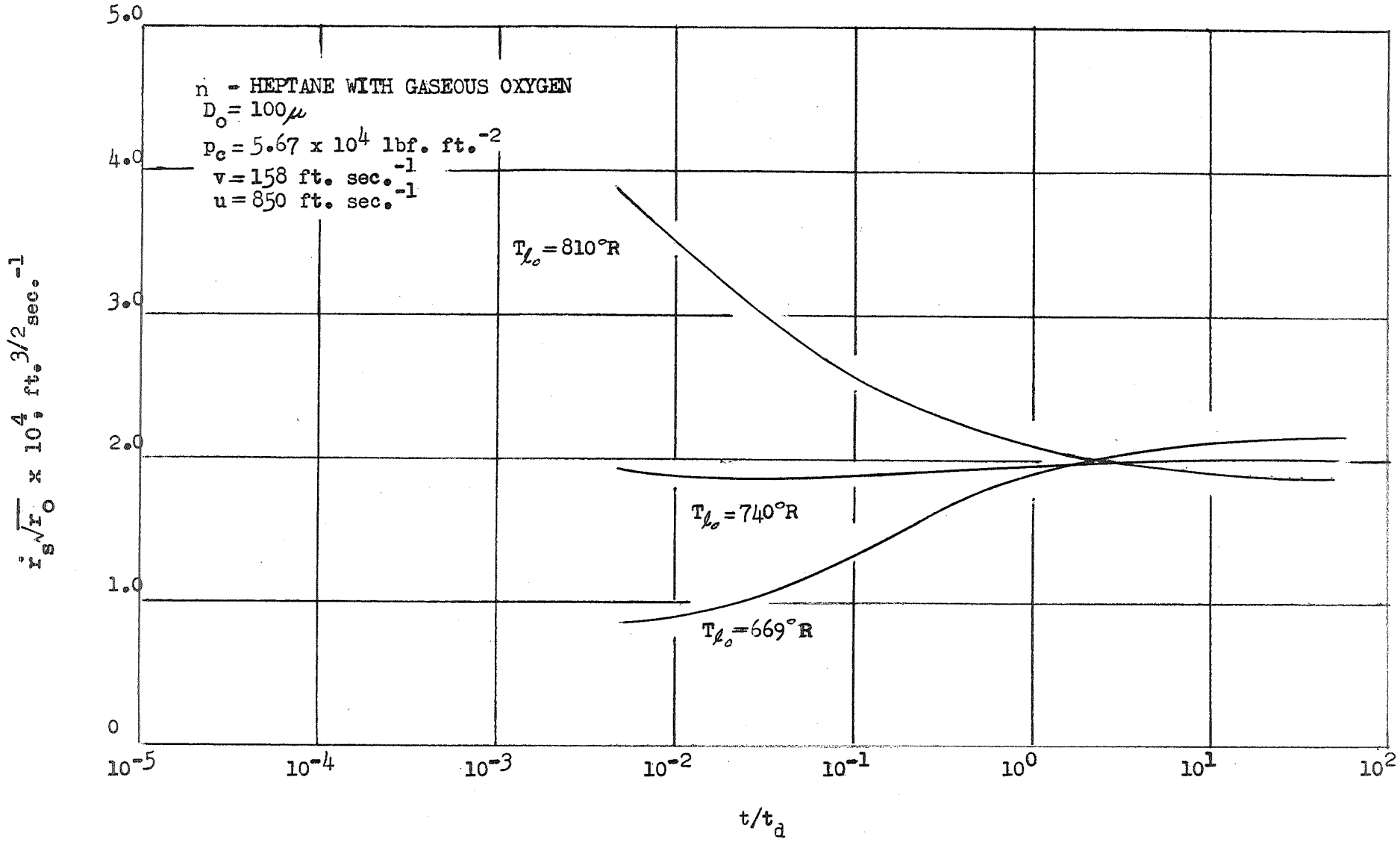

FIG. 5 d. SURFACE REGRESSION RATE VS. TIME FOR VARIATION IN INITIAL DROPLET TEMPERATURE, n-HEPTANE WITH GASEOUS OXYGEN

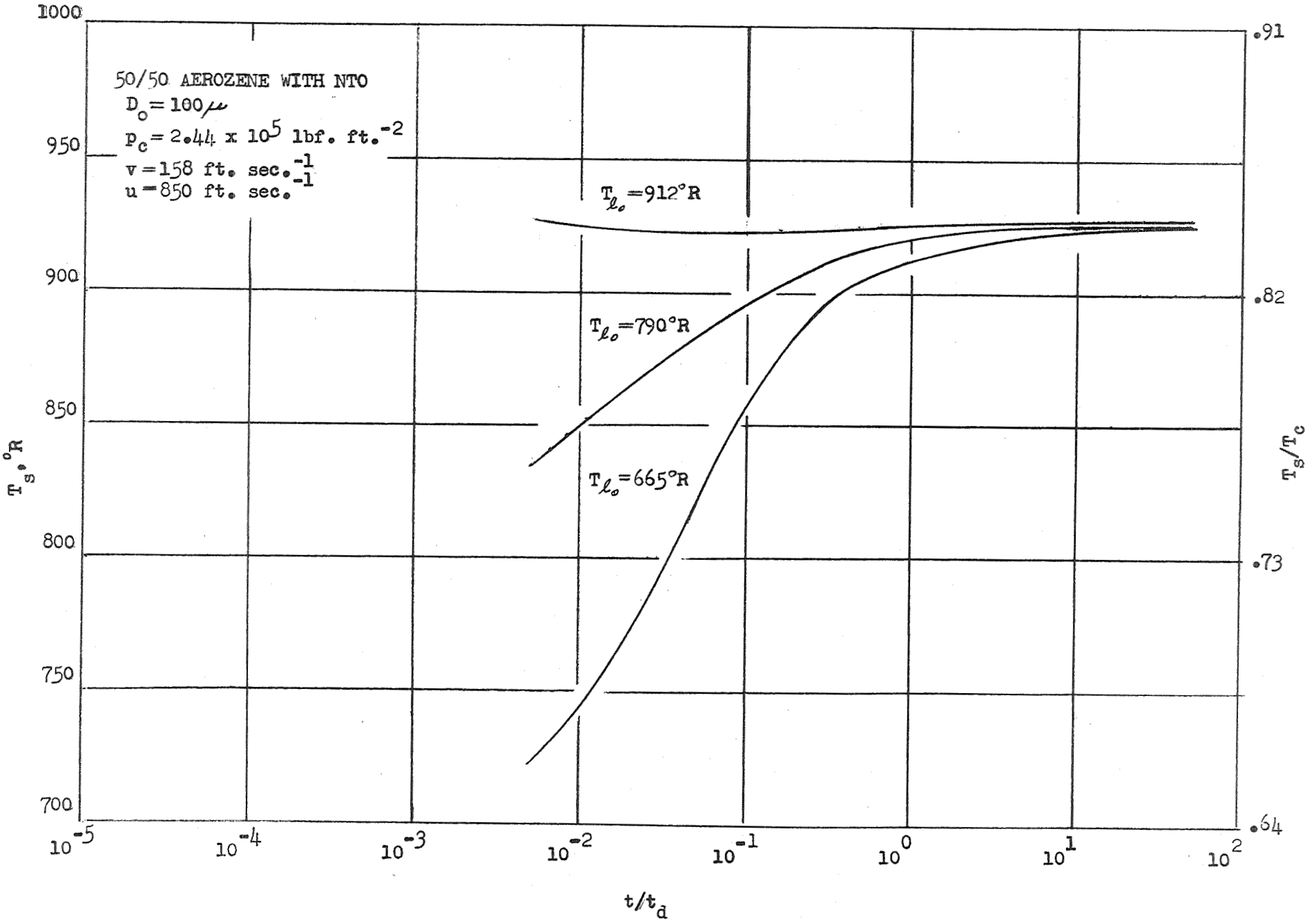

FIG. 6a. SURFACE TEMPERATURE VS. TIME FOR VARIATION IN INITIAL DROPLET TEMPERATURE, 50/50 AEROZINE WITH NTO

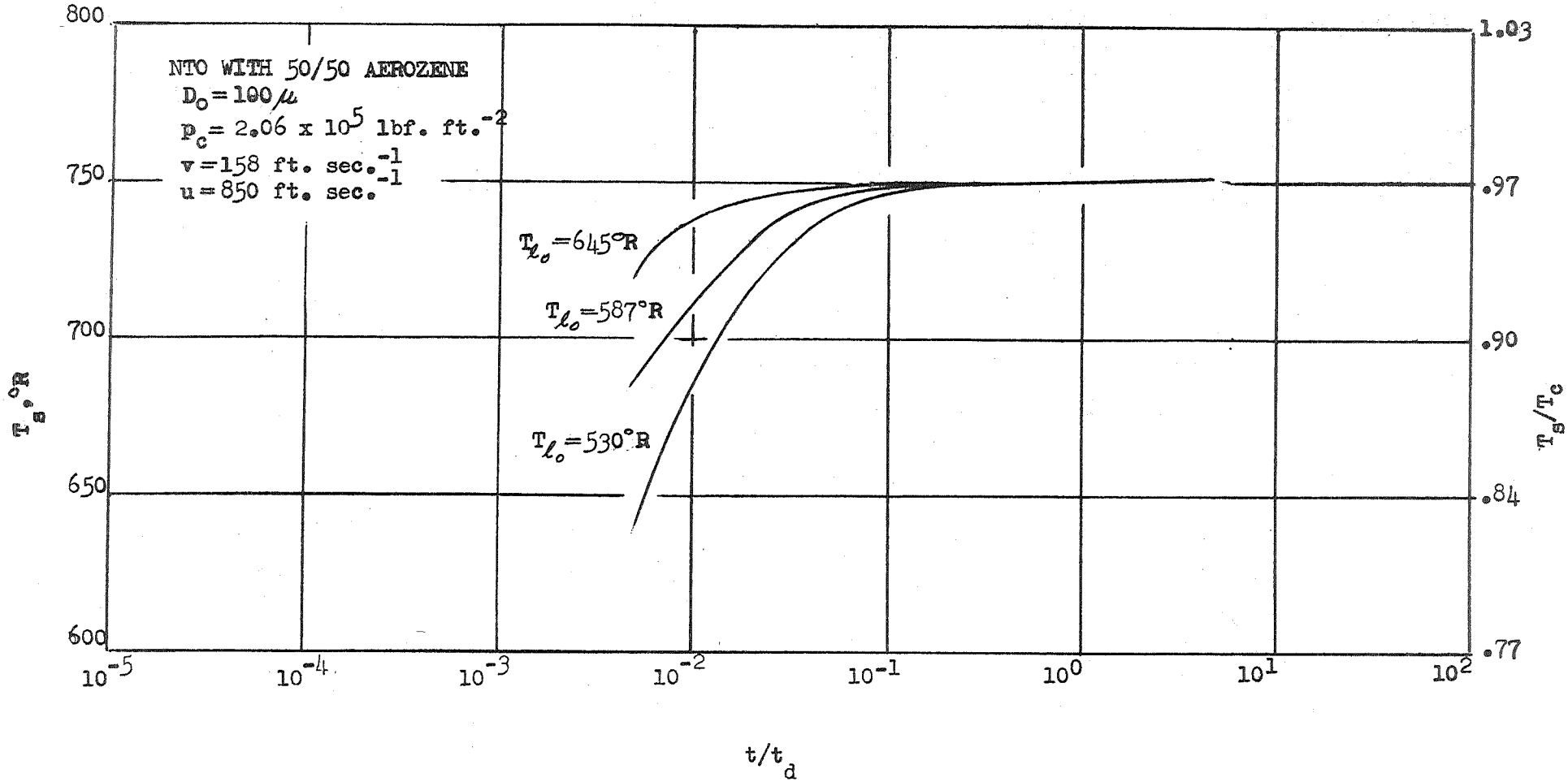

FIG. 6b. SURFACE TEMPERATURE VS. TIME FOR VARIATION IN INITIAL DROPLET TEMPERATURE, NTO WITH 50/50 AEROZINE

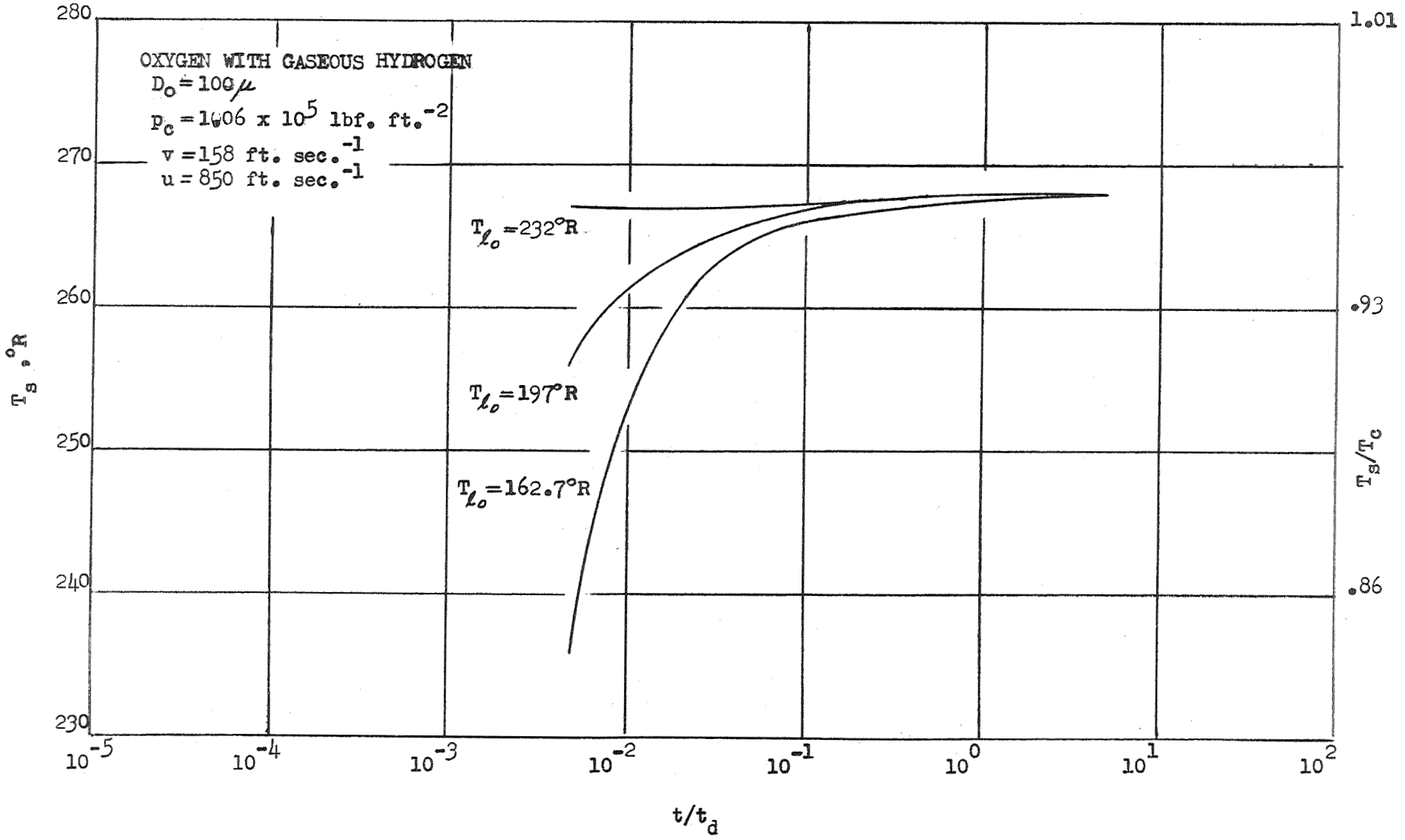

FIG. 6c. SURFACE TEMPERATURE VS. TIME FOR VARIATION IN INITIAL DROPLET TEMPERATURE, OXYGEN WITH GASEOUS HYDROGEN

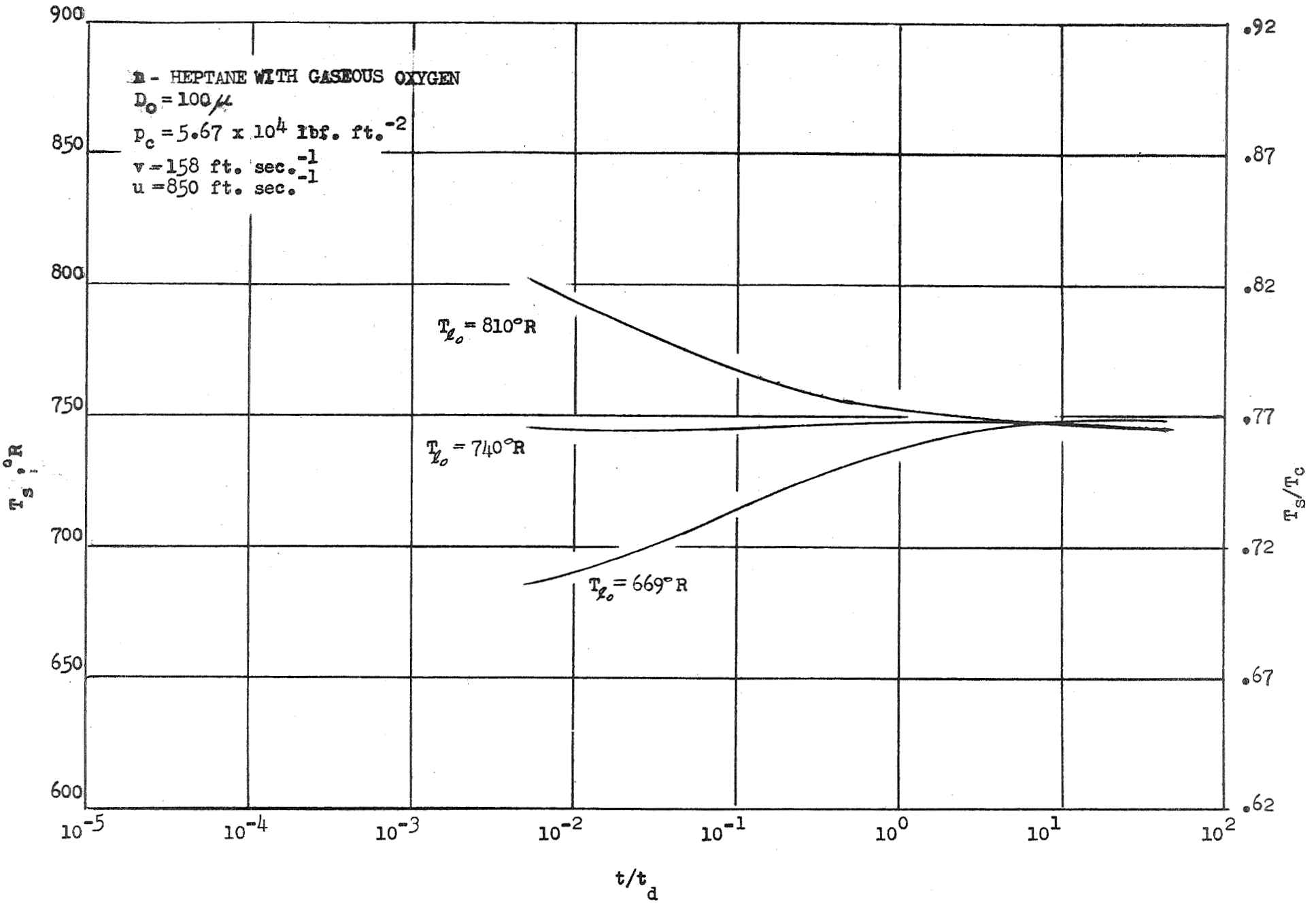

FIG. 6d. SURFACE TEMPERATURE VS. TIME FOR VARIATION IN INITIAL DROPLET TEMPERATURE, n-HEPTANE WITH GASEOUS OXYGEN

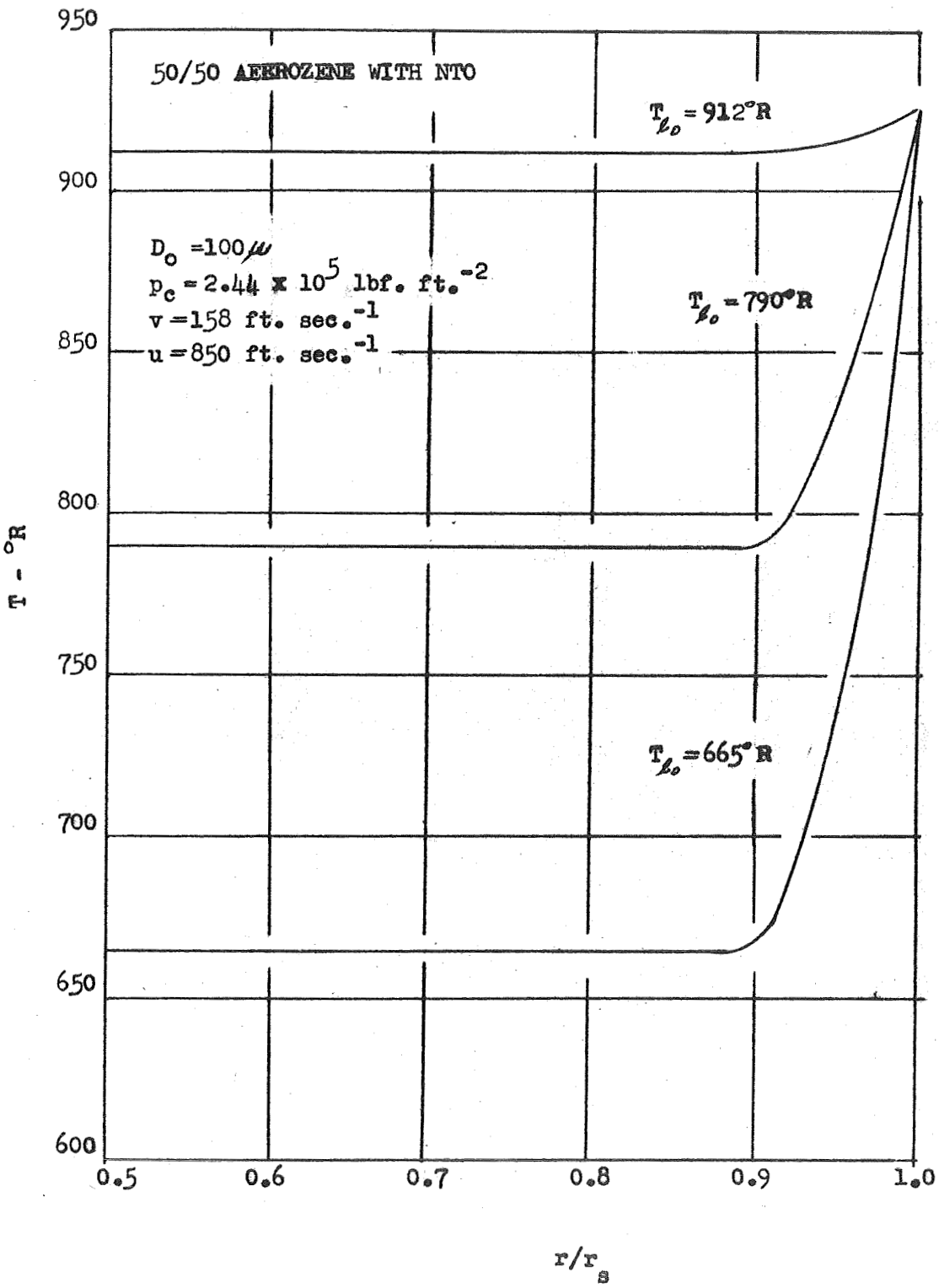

FIG. 7a. DROPLET TEMPERATURE DISTRIBUTION FOR VARIATION IN INITIAL DROPLET TEMPERATURE, AT A TIME OF 10^{-4} SECOND, 50/50 AEROZINE WITH NTO

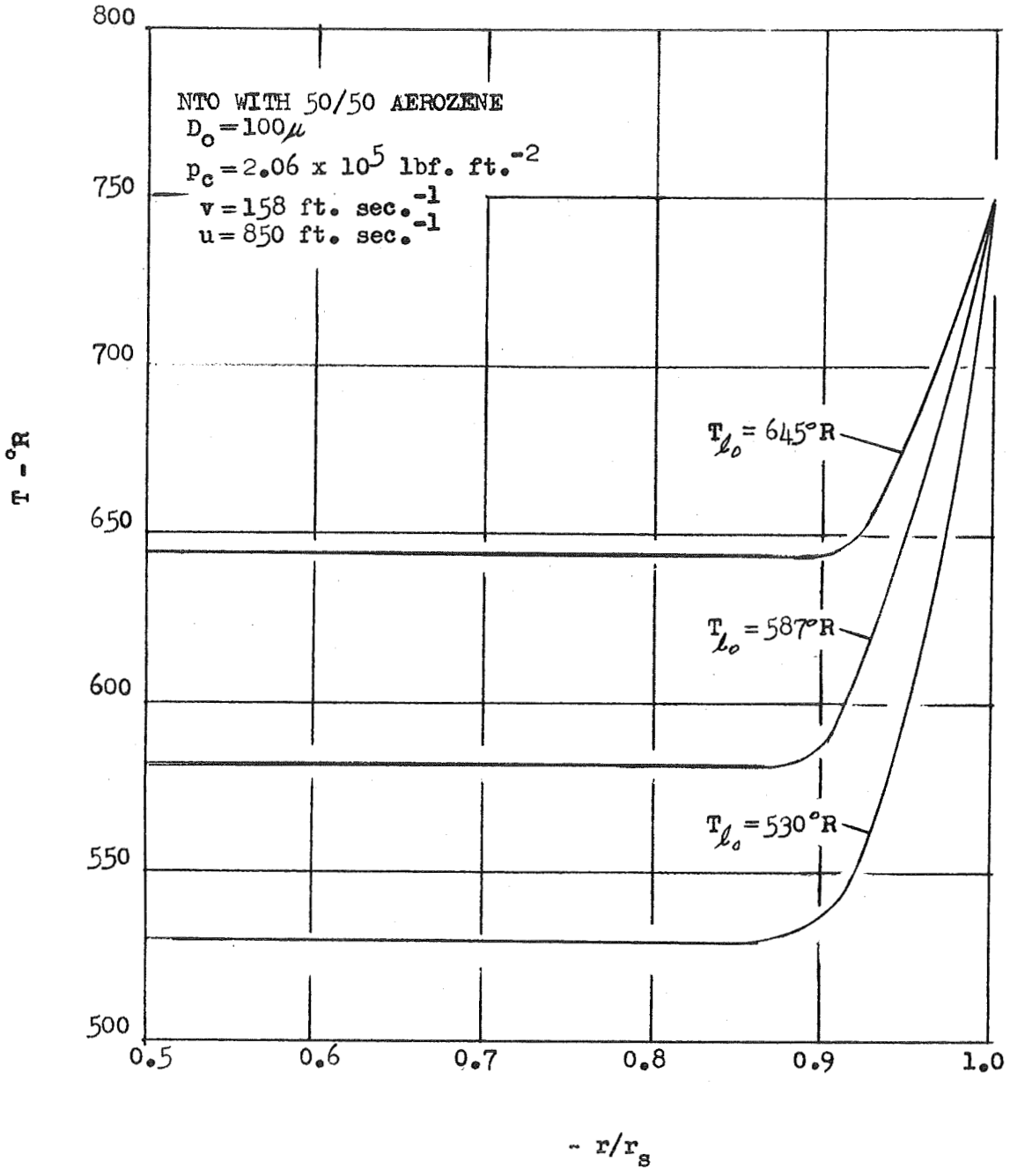

FIG. 7b. DROPLET TEMPERATURE DISTRIBUTION FOR VARIATION IN INITIAL DROPLET TEMPERATURE, AT A TIME OF 10^{-4} SECOND, NTO WITH 50/50 AEROZINE

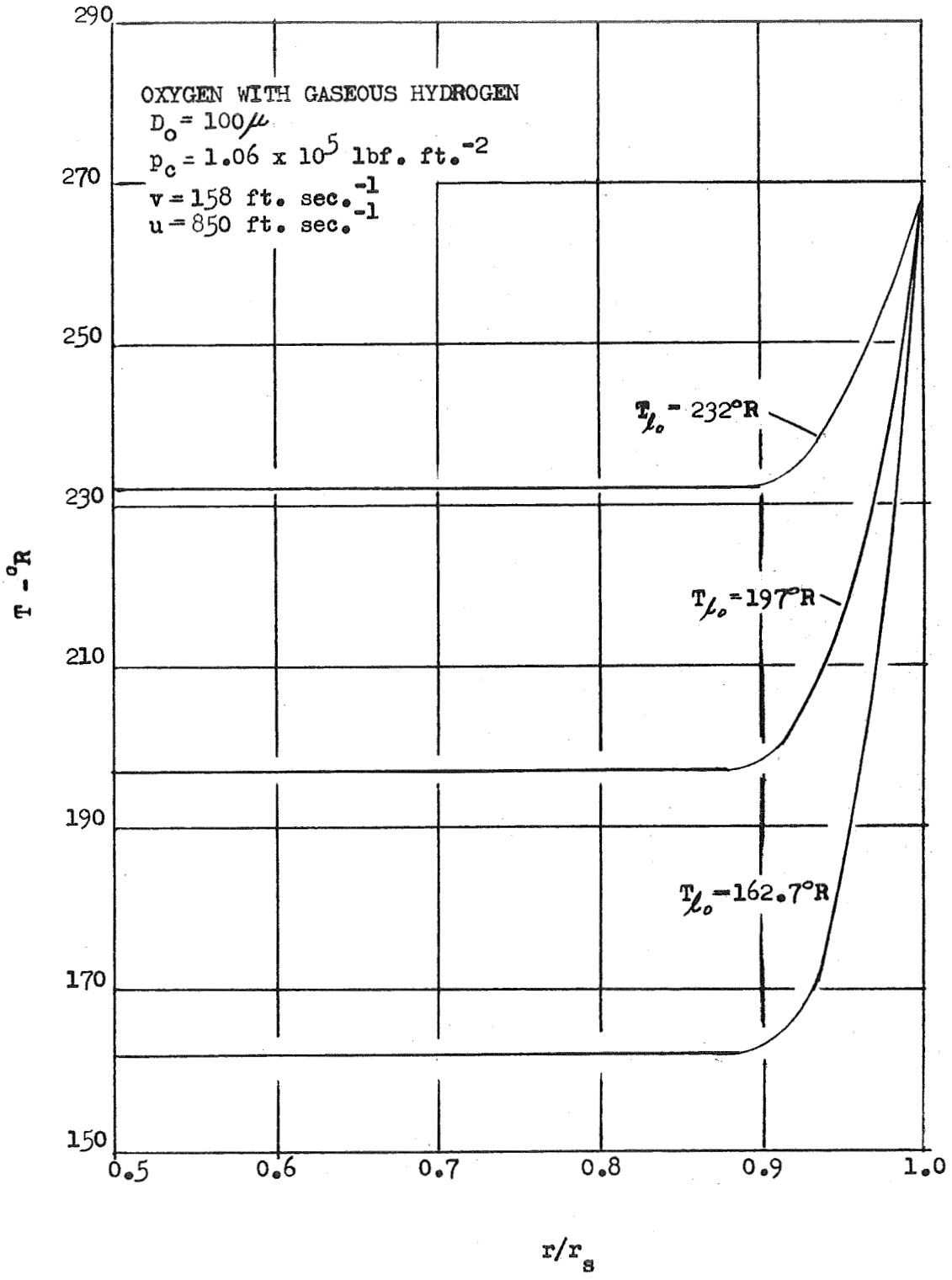

FIG. 7c. DROPLET TEMPERATURE DISTRIBUTION FOR VARIATION IN INITIAL DROPLET TEMPERATURE, AT A TIME OF 10^{-4} SECOND, OXYGEN WITH GASEOUS HYDROGEN

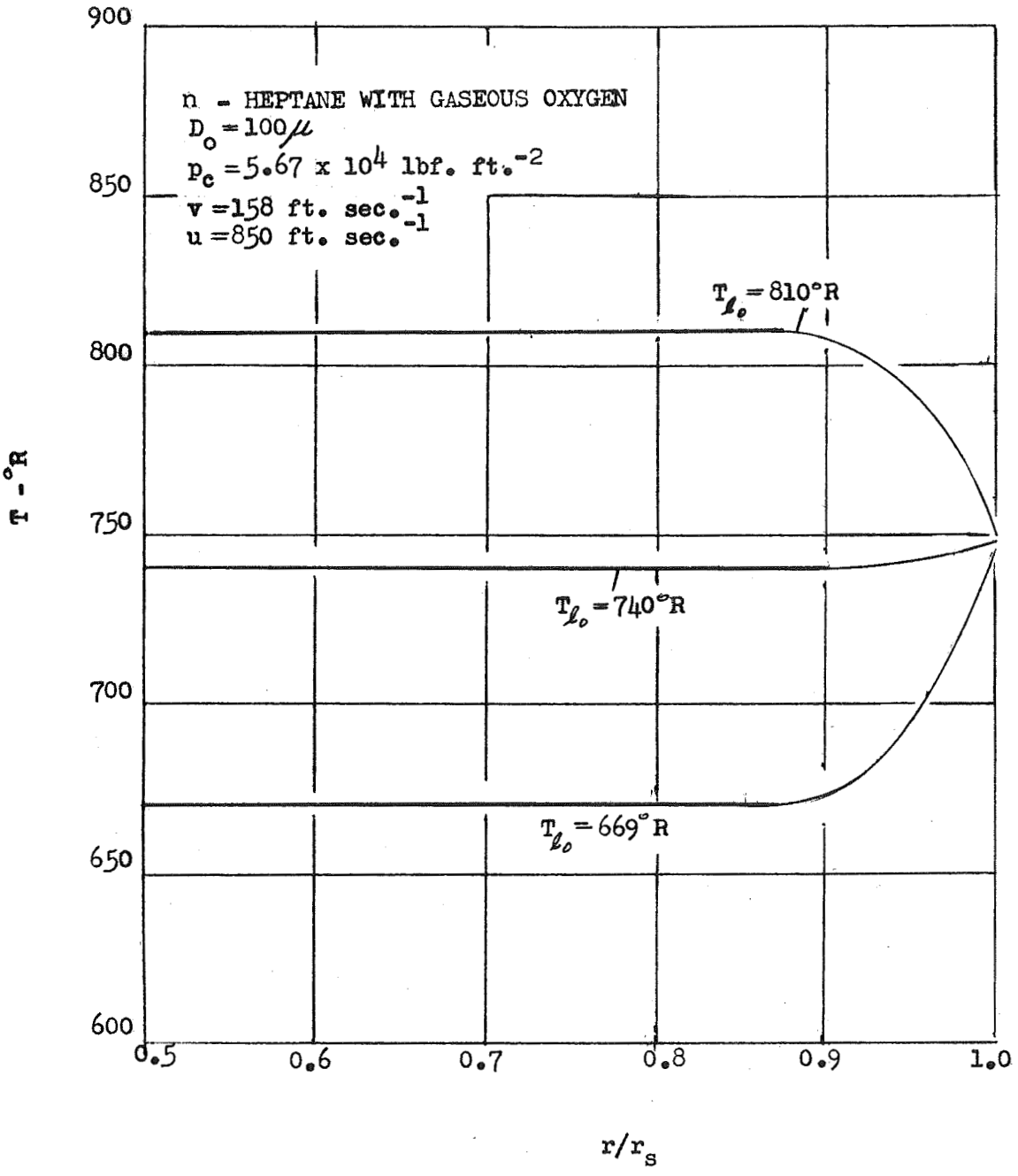

FIG. 7d. DROPLET TEMPERATURE DISTRIBUTION FOR VARIATION IN INITIAL DROPLET TEMPERATURE, AT A TIME OF 10^{-4} SECOND, n-HEPTANE WITH GASEOUS OXYGEN

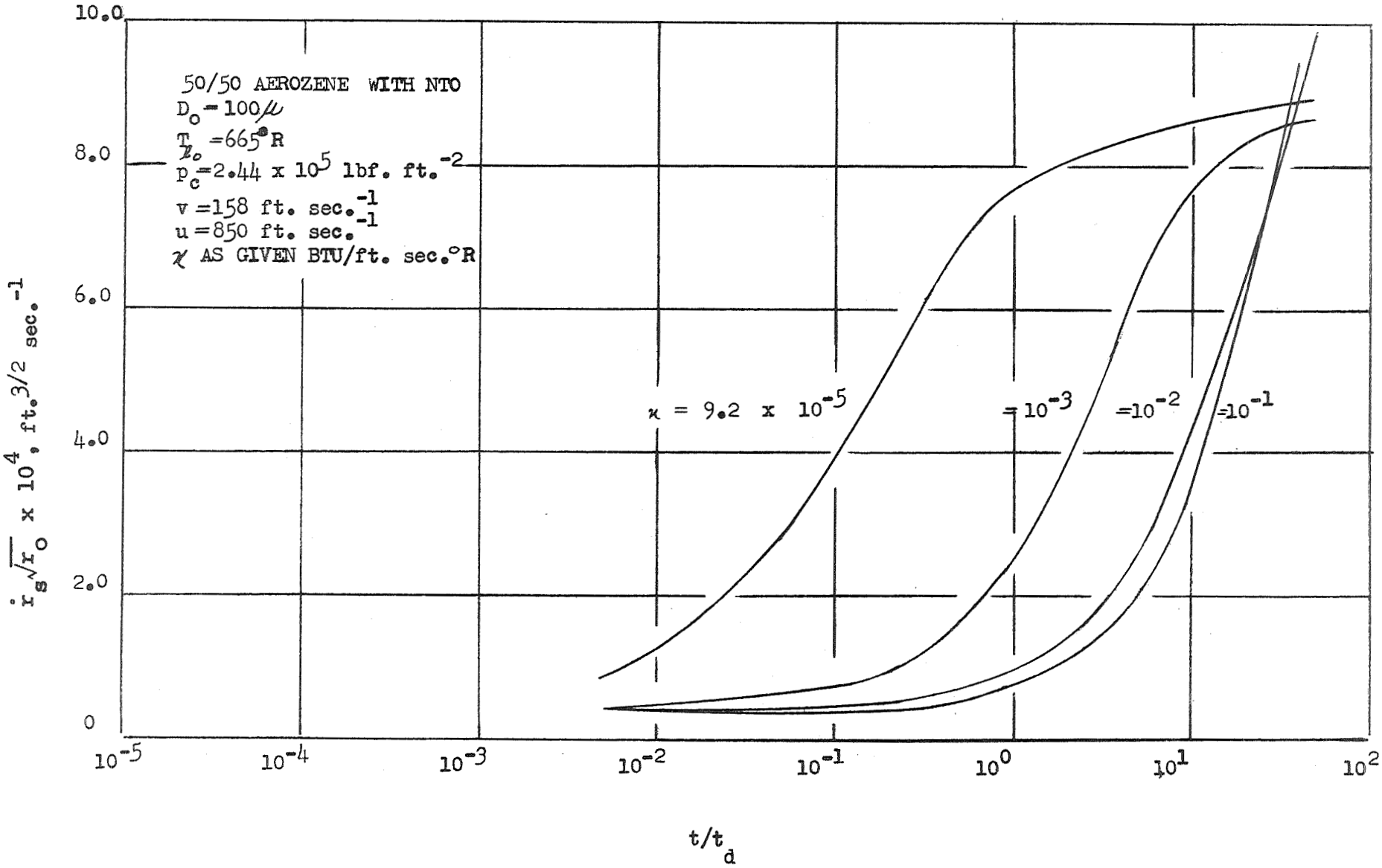

FIG. 8a. SURFACE REGRESSION RATE VS. TIME FOR VARIATION IN PROPELLANT THERMAL CONDUCTIVITY, 50/50 AEROZINE WITH NTO

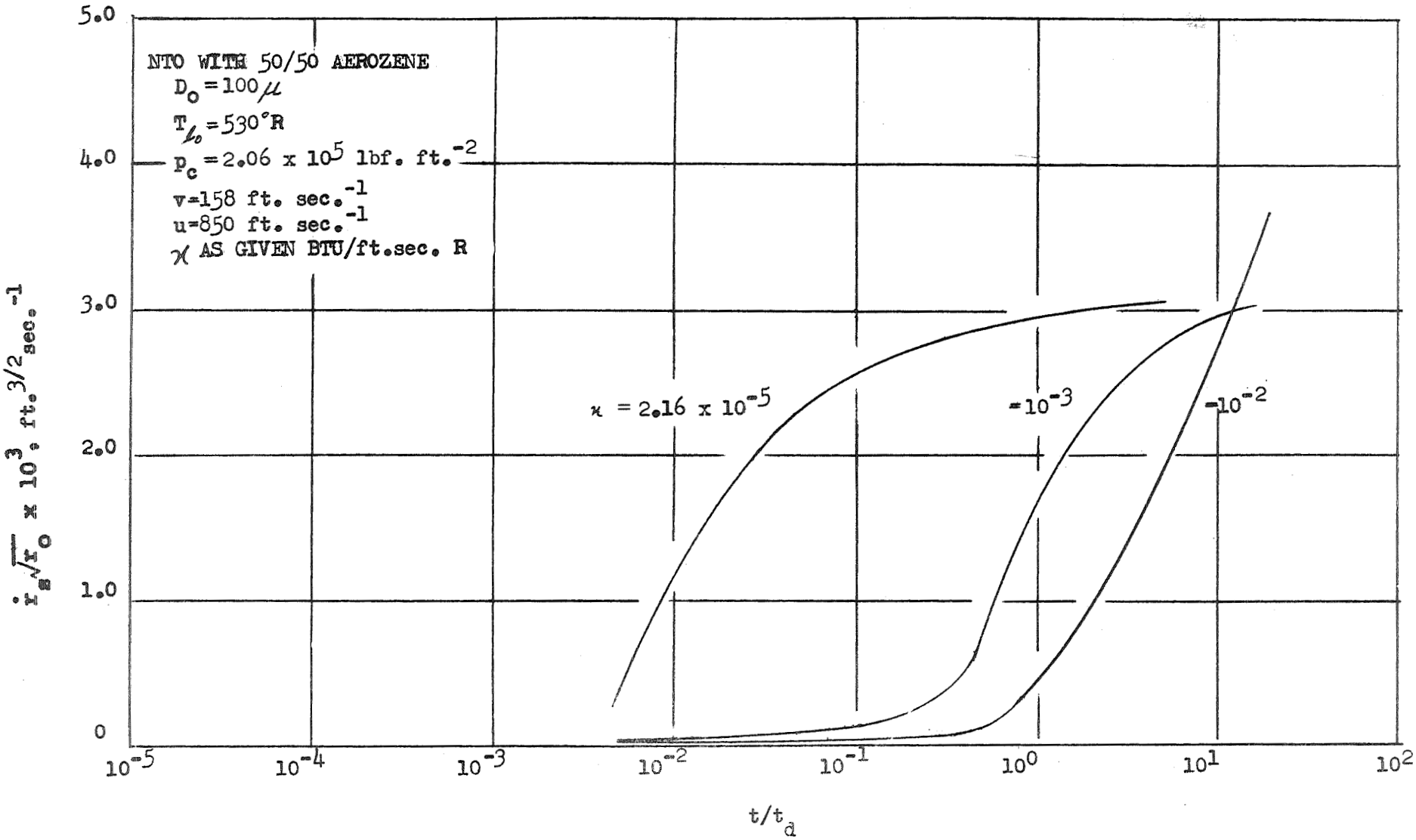

FIG. 8b. SURFACE REGRESSION RATE VS. TIME FOR VARIATION IN PROPELLANT THERMAL CONDUCTIVITY, NTO WITH 50/50 AEROZINE

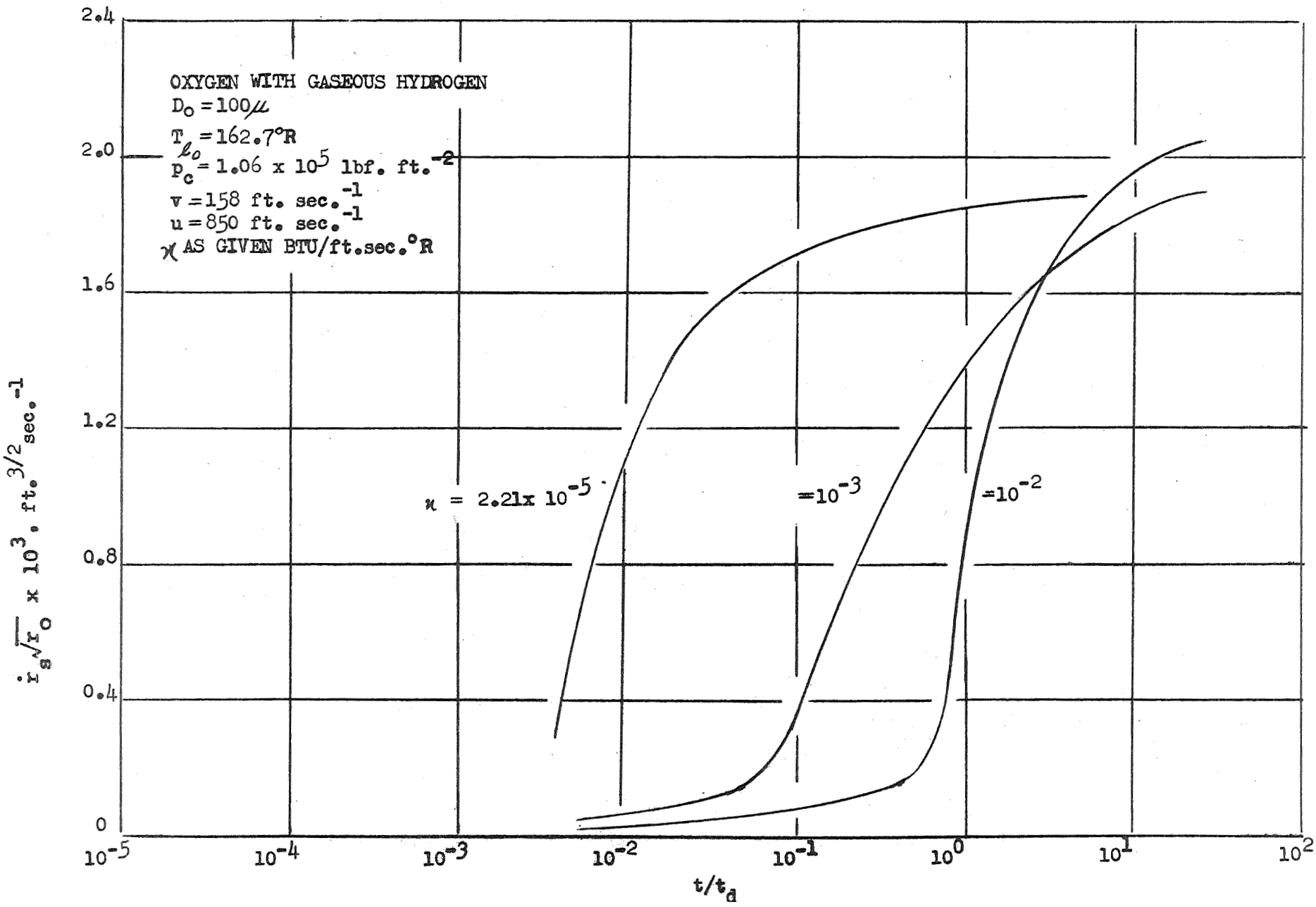

FIG. 8c. SURFACE REGRESSION RATE VS. TIME FOR VARIATION IN PROPELLANT THERMAL CONDUCTIVITY, OXYGEN WITH GASEOUS HYDROGEN

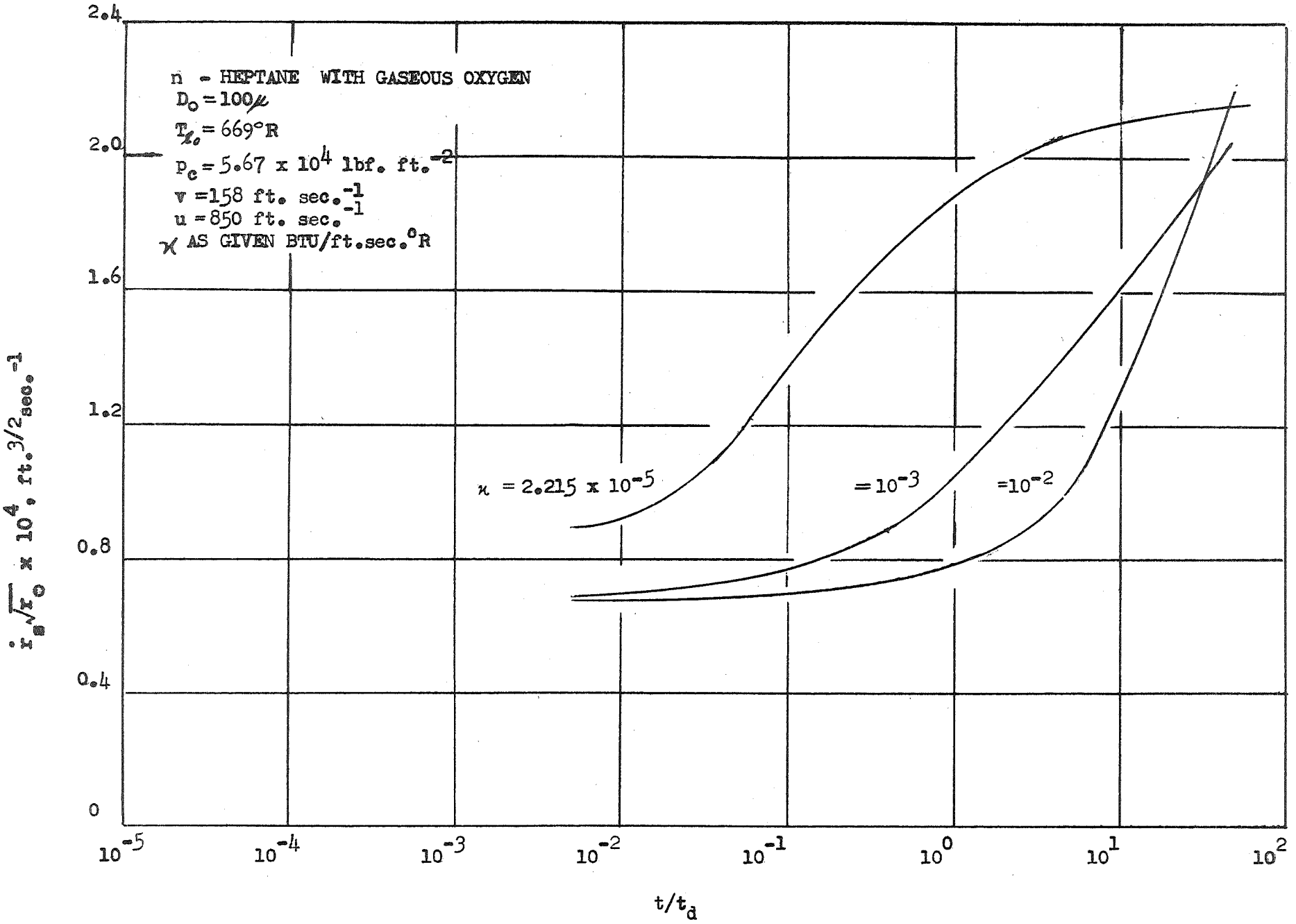

FIG. 8d. SURFACE REGRESSION RATE VS. TIME FOR VARIATION IN PROPELLANT THERMAL CONDUCTIVITY, n-HEPTANE WITH GASEOUS OXYGEN

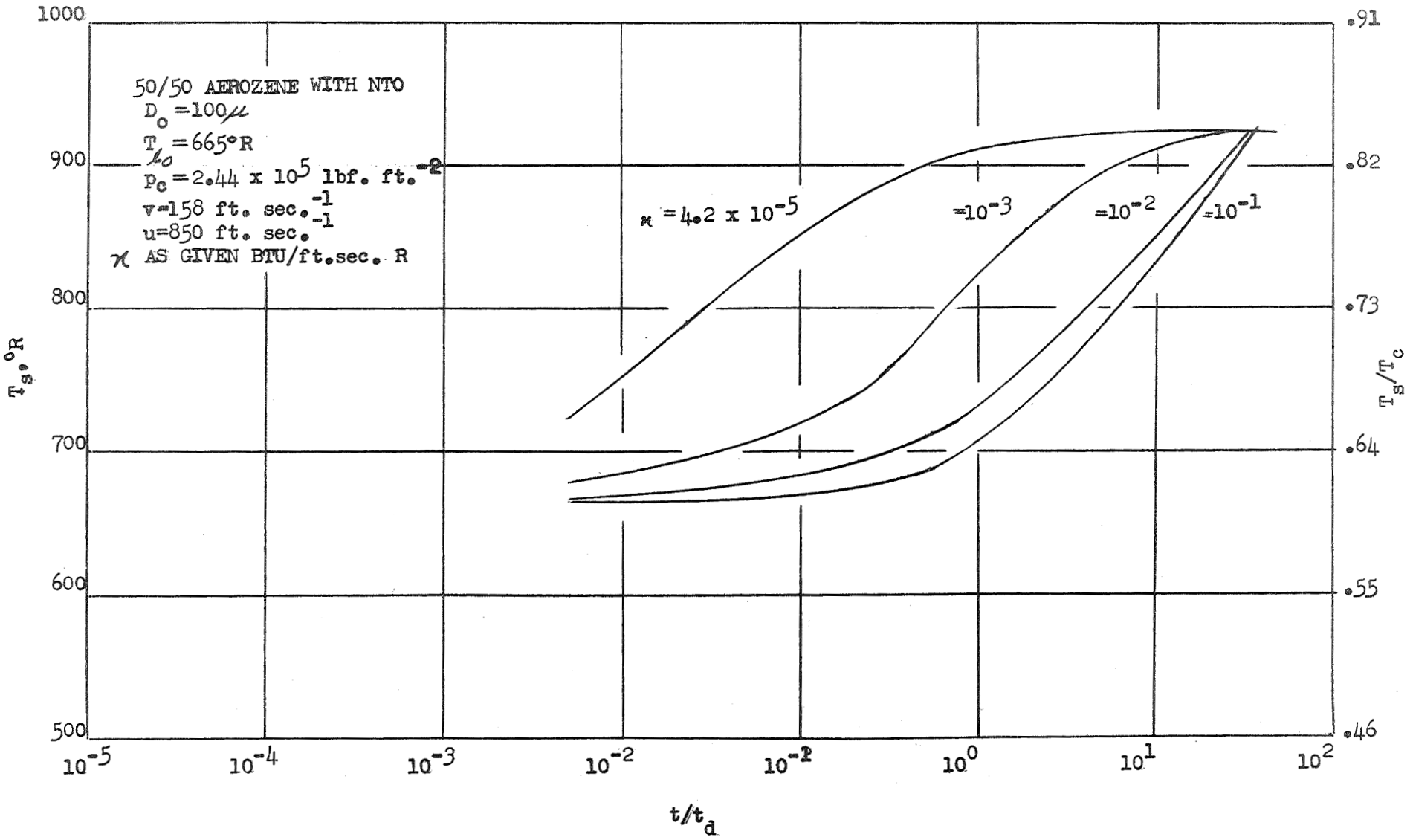

FIG. 9a. SURFACE TEMPERATURE VS. TIME, 50/50 AEROZINE WITH NTO

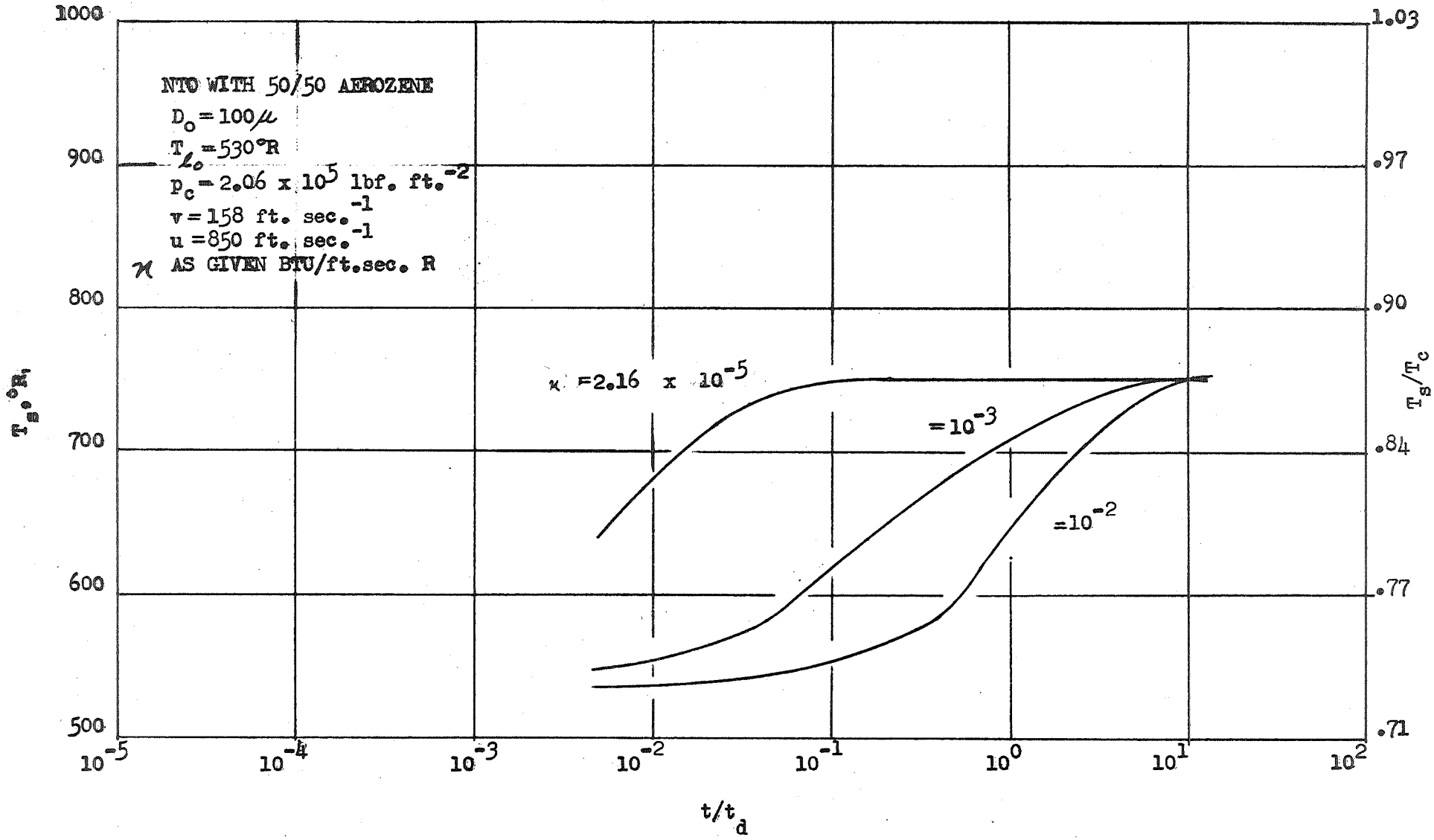

FIG. 9b. SURFACE TEMPERATURE VS. TIME, NTO WITH 50/50 AEROZINE

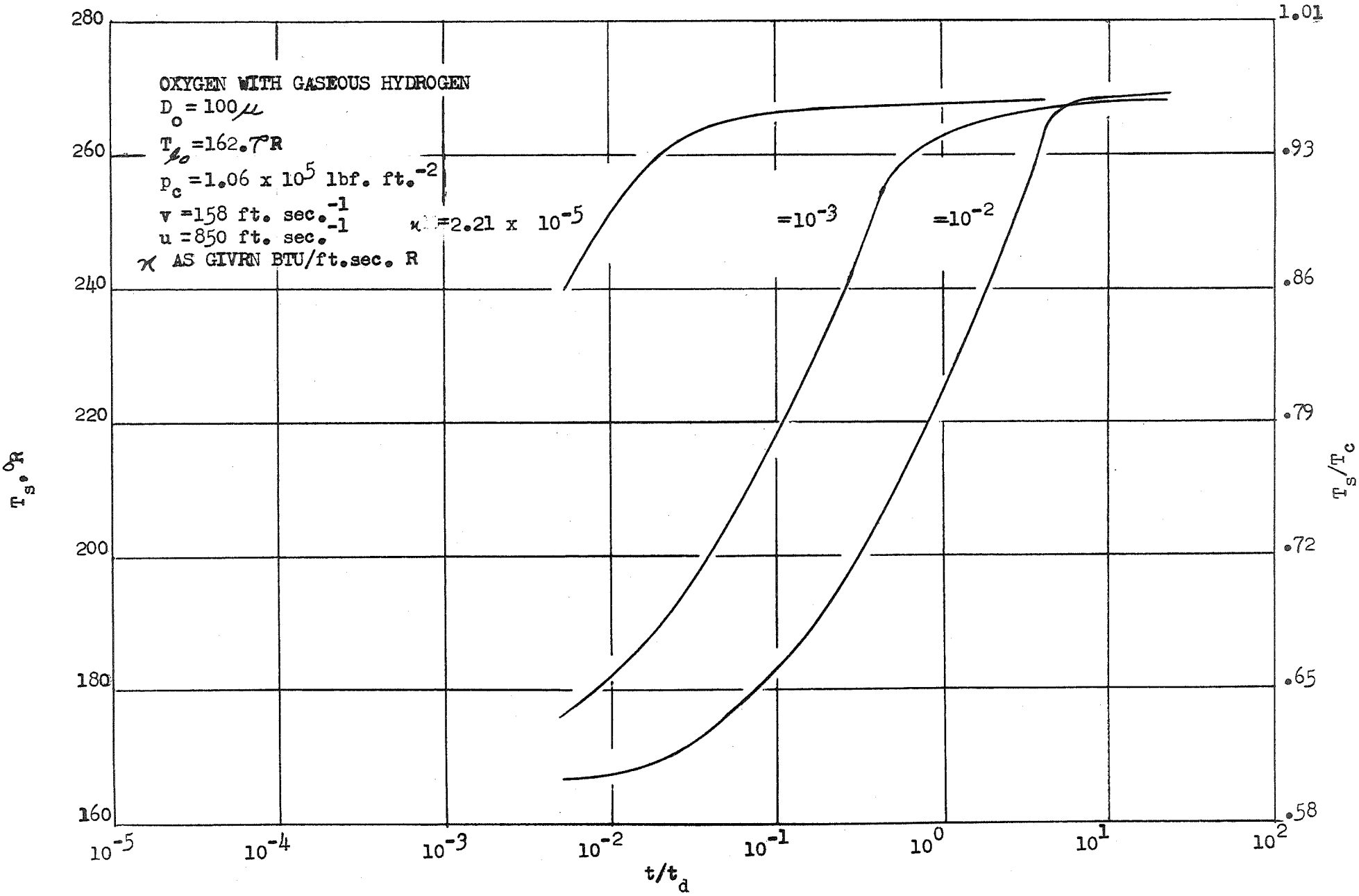

FIG. 9c. SURFACE TEMPERATURE VS. TIME, OXYGEN WITH GASEOUS HYDROGEN

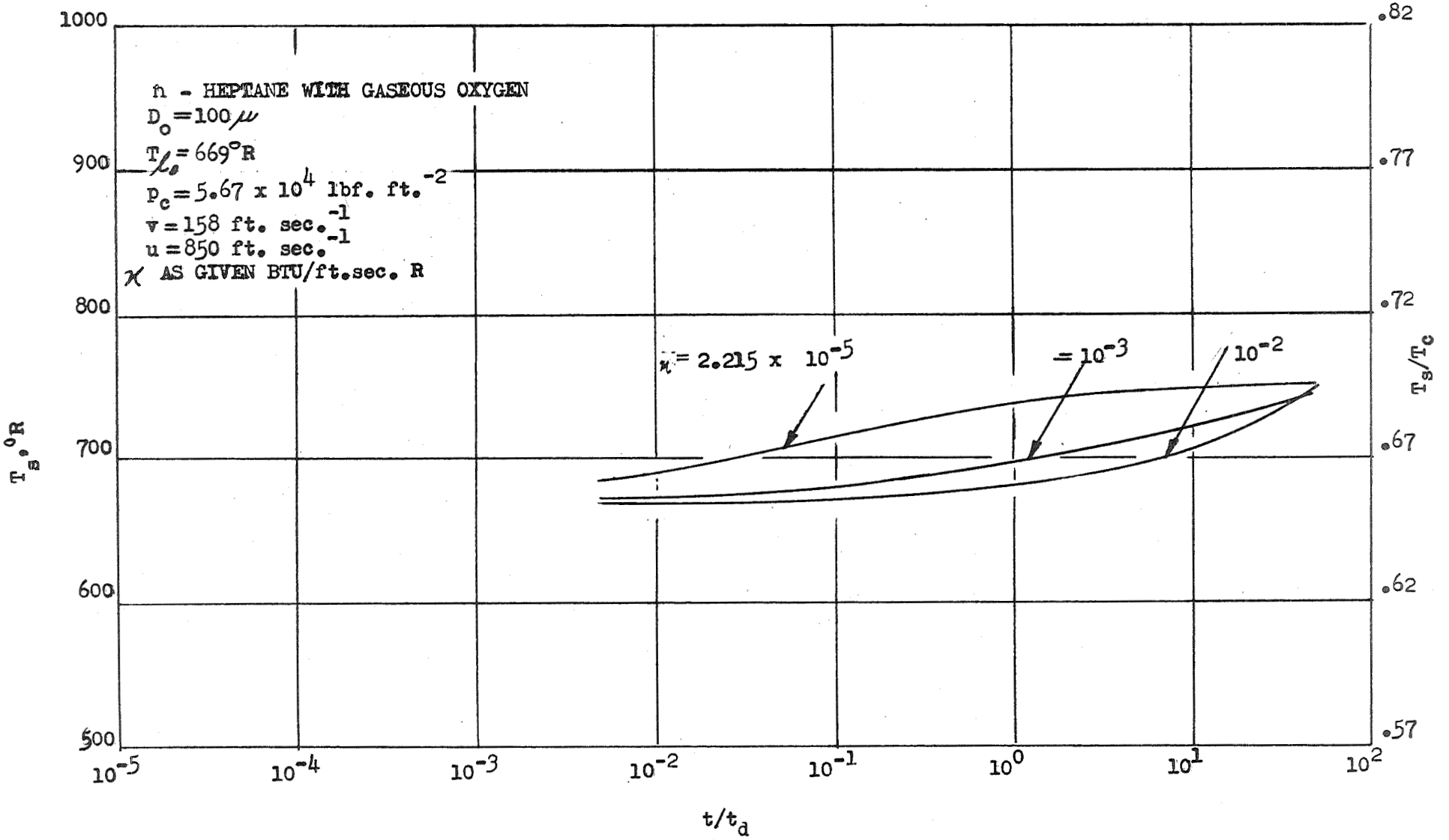

FIG. 9d. SURFACE TEMPERATURE VS. TIME, n-HEPTANE WITH GASEOUS OXYGEN

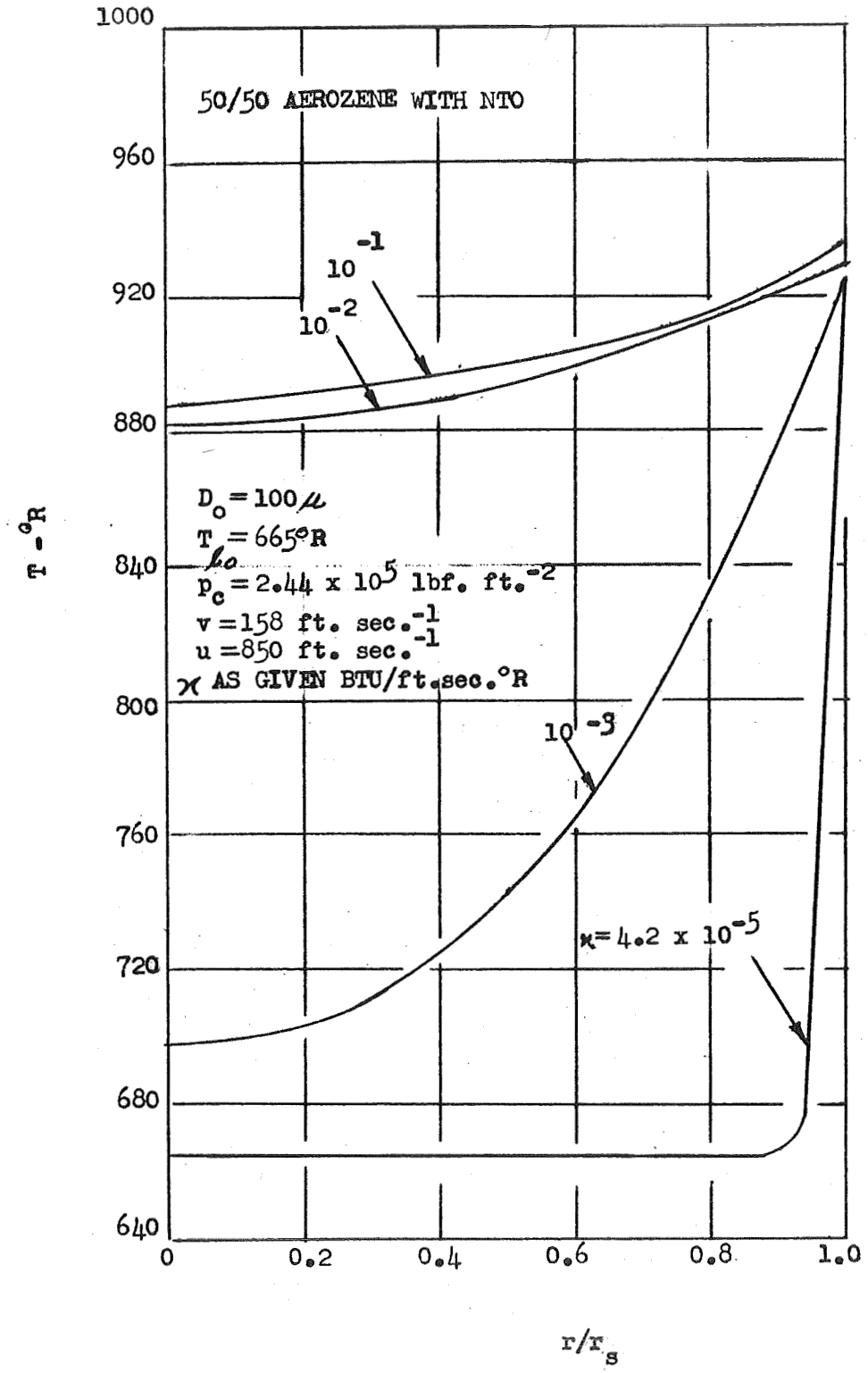

FIG. 10a. DROPLET TEMPERATURE DISTRIBUTION, AT TEN PERCENT DROPLET MASS EVAPORATION, 50/50 AEROZINE WITH NTO

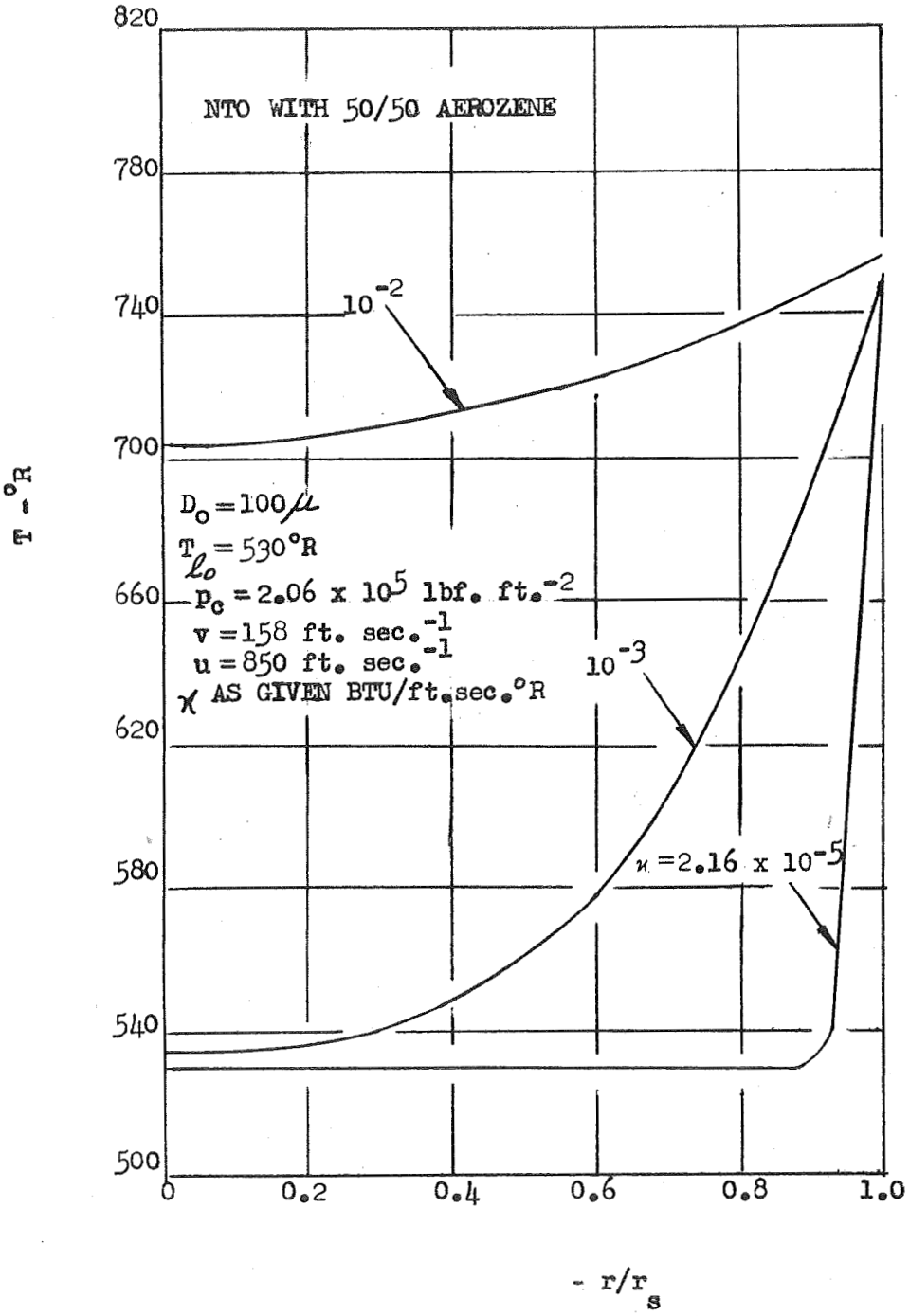

FIG. 10b. DROPLET TEMPERATURE DISTRIBUTION, AT TEN PERCENT DROPLET MASS EVAPORATION, NTO WITH 50/50 AEROZINE

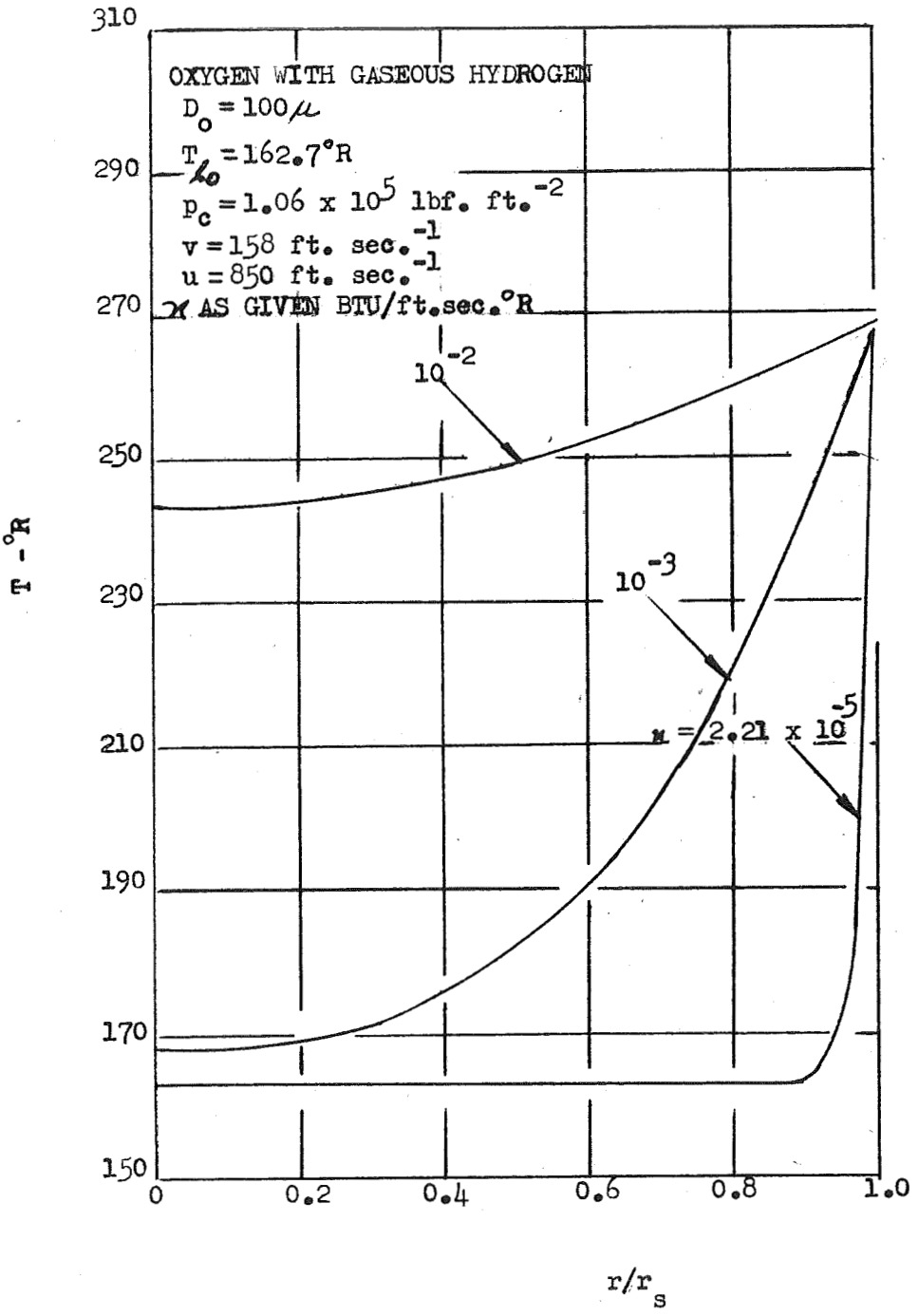

FIG. 10c. DROPLET TEMPERATURE DISTRIBUTION, AT TEN PERCENT DROPLET MASS EVAPORATION, OXYGEN WITH GASEOUS HYDROGEN

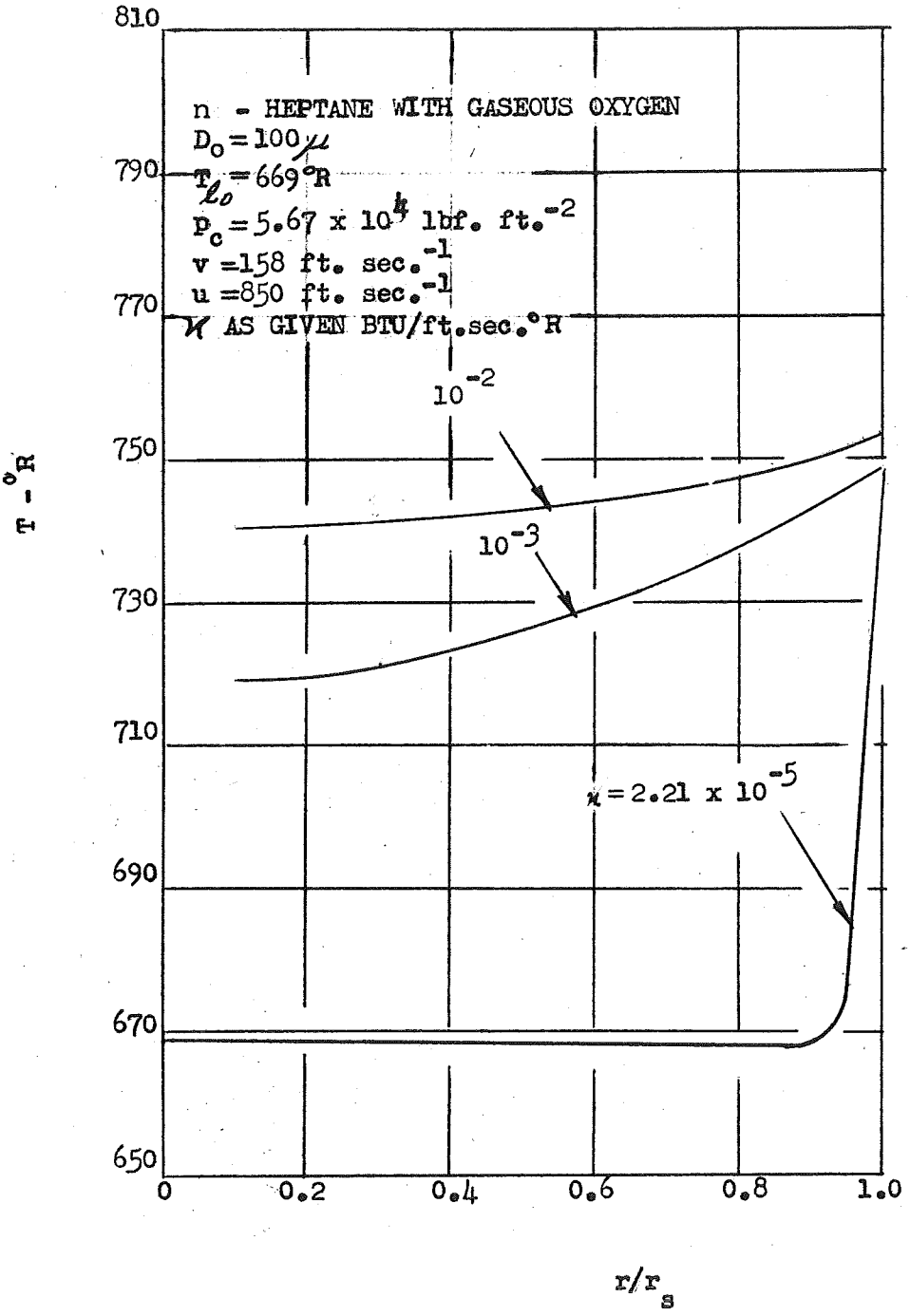

FIG. 10d. DROPLET TEMPERATURE DISTRIBUTION, AT TEN PERCENT DROPLET MASS EVAPORATION, n-HEPTANE WITH GASEOUS OXYGEN

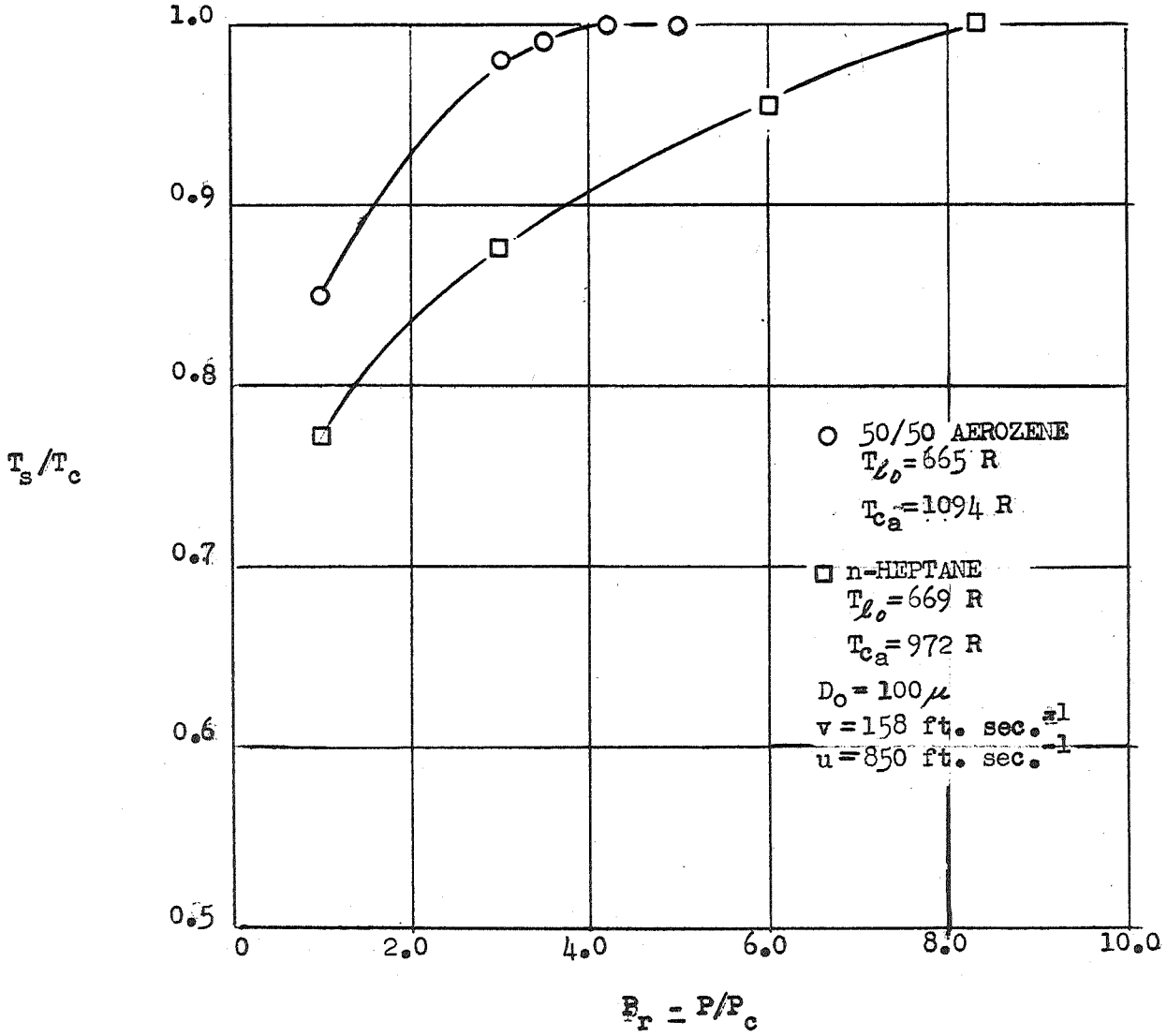

FIG. 11a. DROPLET SURFACE TEMPERATURE VS. ENVIRONMENTAL GAS PRESSURE, n-HEPTANE WITH GASEOUS OXYGEN, 50/50 AEROZINE WITH NTO

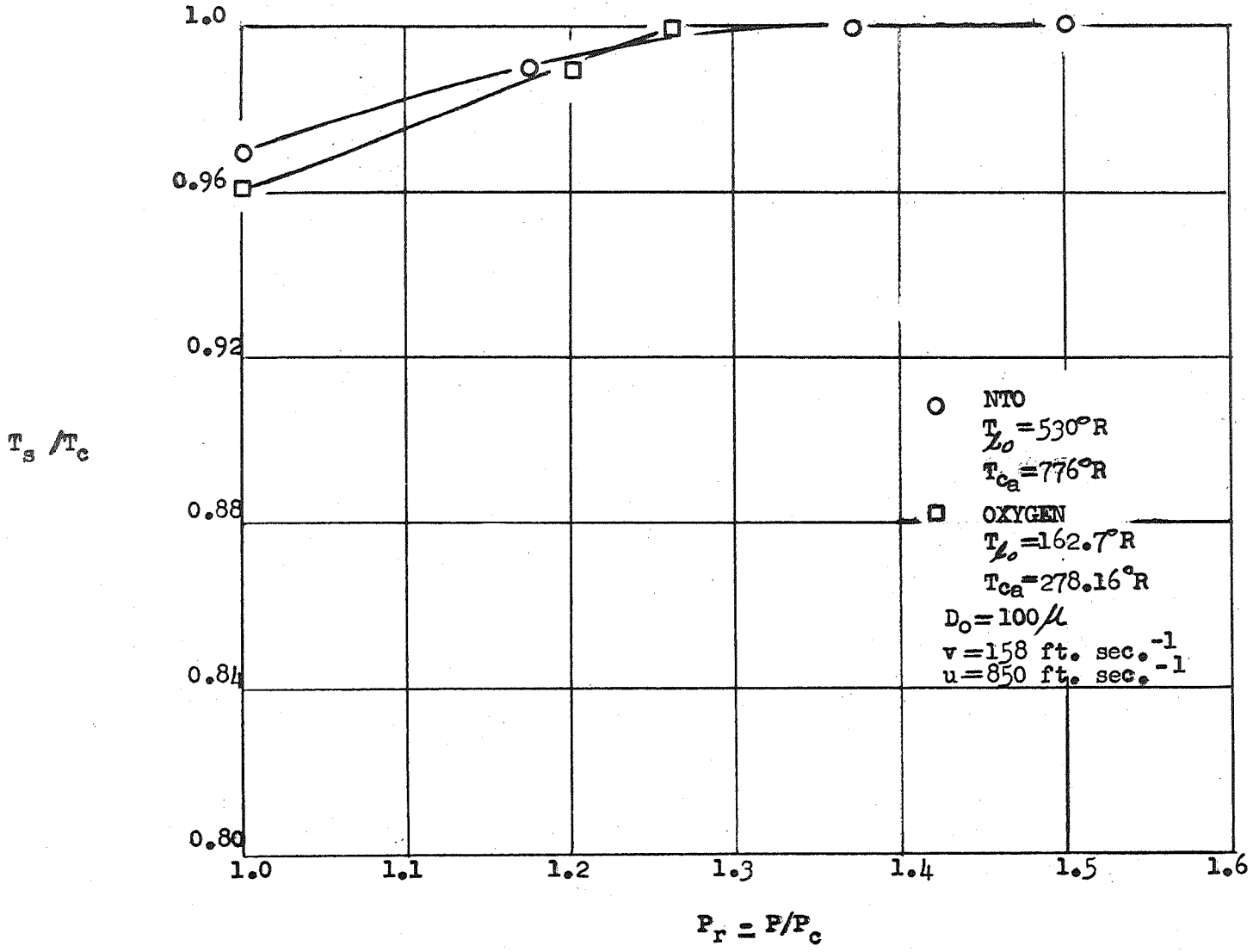

FIG. 11b. DROPLET SURFACE TEMPERATURE VS. ENVIRONMENTAL GAS PRESSURE, NTO WITH 50/50 AEROZINE, OXYGEN WITH GASEOUS HYDROGEN

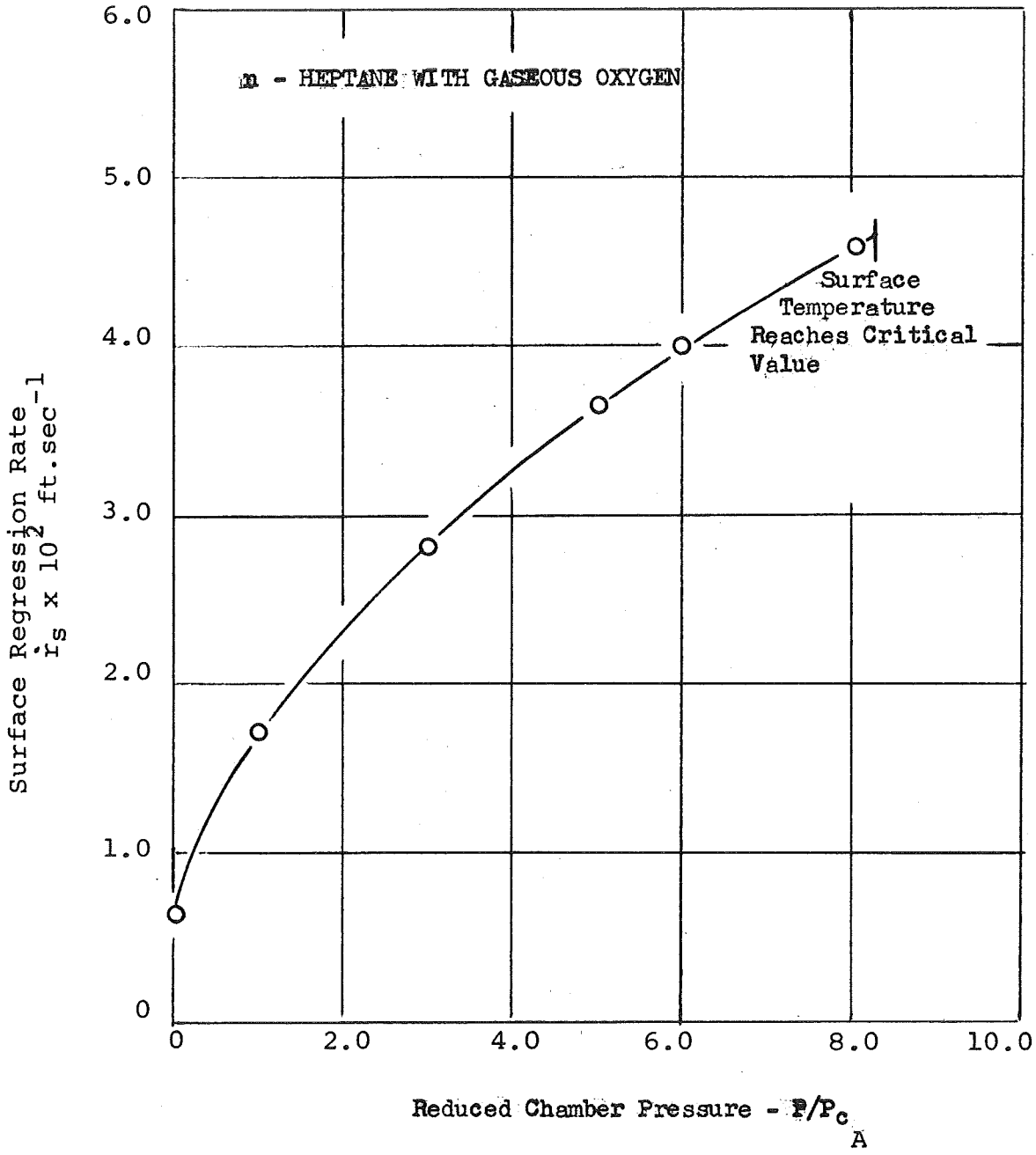

FIG. 12 SURFACE REGRESSION RATE AT SUPERCRITICAL PRESSURES FOR n-HEPTANE

1970 DISTRIBUTION

Dr. R.J. Priem MS 500-204
NASA Lewis Research Center
21000 Brookpark Road
Cleveland, Ohio 44135 (2)

Norman T. Musial
NASA Lewis Research Center
21000 Brookpark Road
Cleveland, Ohio 44135

Library (2)
NASA Lewis Research Center
21000 Brookpark Road
Cleveland, Ohio 44135

Report Control Office
NASA Lewis Research Center
21000 Brookpark Road
Cleveland, Ohio 44135

NASA Representative (6)
NASA Scientific and Technical
Information Facility
P.O. Box 33
College Park, Maryland 20740

V. Agosta
Brooklyn Polytechnic Institute
Long Island Graduate Center
Route 110
Farmingdale, New York 11735

B.P. Breen
Dynamic Science, a Division of
Marshall Industries
1900 Walker Avenue
Monrovia, California 91016

Thomas J. Chew
AFRPL (RPPZ)
Edwards, California 93523

T.W. Christian
Chemical Propulsion Information
Agency
8621 Georgia Avenue
Silver Spring, Maryland 20910

R.M. Clayton
Jet Propulsion Laboratory
Calif. Institute of Technology
4800 Oak Grove Drive
Pasadena, California 91103

E.W. Conrad MS 500-204
NASA Lewis Research Center
21000 Brookpark Road
Cleveland, Ohio 44135

Dr. E.K. Dabora
University of Connecticut
Aerospace Department
Storrs, Connecticut 06268

O.W. Dykema
Aerospace Corp.
P.O. Box 95085
Los Angeles, California 90045

G.W. Elverum
TRW Systems
1 Space Park
Redondo Beach, Calif. 90278

R. Edse
Ohio State University
Dept. of Aeronautical and
Astronautical Engineering
Columbus, Ohio 43210

G.M. Faeth
The Pennsylvania State Univ.
Mechanical Engineering Dept.
207 Mechanical Engineering Blvd.
University Park, Pa. 16802

G. D. Garrison
Pratt and Witney Aircraft
Florida Research & Development Ctr.
P.O. Box 2691
West Palm Beach, Fla. 33402

M. Gerstein
Dept. Mech. Engr.
Univ. of Southern California
University Park
Los Angeles, Calif. 90007

I. Glassman
Princeton University
James Forrestal Research Ctr.
P.O. Box 710
Princeton, N.J. 08540

Richard W. Haffner
Air Force Office of Scientific
Research
1400 Wilson Blvd.
Arlington, Virginia 22209

D. Harrje
Princeton University
James Forrestal Research Center
P.O. Box 710
Princeton, New Jersey 08540

T. Inouye Code 4581
U.S. Naval Weapons Center
China Lake, Calif. 93555

R.D. Jackel, 429
Office of Naval Research
Navy Department
Washington, D.C. 20360

R. B. Lawhead
Rocketdyne
A Division of North American
Aviation
6633 Canoga Avenue
Canoga Park, Calif. 91304

R.S. Levine, Code RPL
NASA Headquarters
6th and Independence Ave., S.W.
Washington, D.C. 20546

Ted Male MS 500-209
NASA Lewis Research Center
21000 Brookpark Road
Cleveland, Ohio 44135

J.M. McBride
Aerojet-General Corp.
P.O. Box 15847
Sacramento, Calif. 95809

P.D. McCormack
Dartmouth University
Hanover, New Hampshire 03755

C.E. Mitchell
Colorado State University
Fort Collins, Colorado 80521

P.S. Myers
University of Wisconsin
Mechanical Engineering Dept.
1513 University Ave.
Madison, Wisconsin 53705

J.A. Nestlerode
Rocketdyne
A Division of North American
Aviation
6633 Canoga Avenue
Canoga Park, Calif. 91304

J.A. Nicholls
University of Michigan
Aerospace Engineering
Ann Arbor, Michigan 48104

James C. O'Hara
Tulane University
Dept. of Mechanical Engr.
New Orleans, La. 70118

A.K. Oppenheim
University of California
Dept. of Aeronautical Sciences
6161 Etcheverry Hall
Berkeley, Calif. 94720

J.R. Osborn
Purdue University
School of Mechanical Engr.
Lafayette, Indiana 47907

Dr. K. Ragland
University of Wisconsin
Mechanical Engineering Dept.
Madison, Wisconsin 53705

Dr. A.A. Ranger
Purdue University
School of Aeronautics, Astronautics
and Engineering Sciences
Lafayette, Indiana 47907

F.H. Reardon
Sacramento State College
School of Engineering
6000 J Street
Sacramento, Calif. 95819

B.A. Reese
Purdue University
School of Mechanical Engr.
Lafayette, Indiana 47907

R.J. Richmond R-Pand VE-PA
NASA George C. Marshall Space
Flight Center
Huntsville, Alabama 35812

J.H. Rupe
Jet Propulsion Laboratory
Calif. Institute of Technology
4800 Oak Grove Drive
Pasadena, Calif. 91103

Dr. R.F. Sawyer
Univ. of California
Mechanical Engineering, Thermal
Systems
Berkeley, California 94720

K. Scheller
ARL(ARC)
Wright-Patterson AFB
Dayton, Ohio 45433

Roger A. Strehlow
University of Illinois
Aeronautical Engineering Dept.
Urbana, Illinois 61801

J.G. Thibadaux
NASA Manned Spacecraft Center
Houston, Texas 77058

T.P. Torda
Illinois Institute of Technology
Room 200 M.H.
3300 S. Federal Street
Chicago, Ill. 60616

T.Y. Toong
Massachusetts Inst. of Technology
Dept. of Mechanical Engr.
Cambridge, Mass. 02139

Richard Weiss
AFRPL
Edwards, Calif. 93523

W.W. Wharton AMSMI-RKL
U.S. Army Missile Command
Redstone Arsenal, Ala. 35808

F.A. Williams
University of California
Aerospace Engineering Dept.
P.O. Box 109
La Jolla, Calif. 92038

L.M. Wood
Bell Aerosystems Company
P.O. Box 1
Mail Zone J-81
Buffalo, New York 14205

B.T. Zinn
Georgia Institute of Technology
Aerospace School
Atlanta, Georgia 30332

Library
Goddard Space Flight Ctr. (NASA)
Greenbelt, Maryland 20771

Library
NASA John F. Kennedy Space Ctr.
Cocoa Beach, Florida 32931

Library
NASA Langley Research Center
Langley Station
Hampton, Virginia 23365

Library
NASA Manned Spacecraft Center
Houston, Texas 77001

Library
NASA George C. Marshall Space
Flight Center
Huntsville, Ala. 35812

Library
Jet Propulsion Laboratory
4800 Oak Grove Drive
Pasadena, Calif. 91103

Library
NASA Flight Research Center
P.O. Box 273
Edwards, Calif. 93523

Library
NASA Ames Research Center
Moffett Field, Calif. 94035

TISIA
Defense Documentation Center
Cameron Station
Building 5
5010 Duke Street
Alexandria, Virginia 22314

Office of Asst. Dir. (Chem. Tech.)
Office of the Director of Defense
Research & Engineering
Washington, D.C. 20301

D.E. Mock
Advanced Research Projects Agency
Washington, D.C. 20525

Dr. H.K. Doetsch
Arnold Engineering Development Ctr.
Air Force Systems Command
Tullahoma, Tenn. 37389

Library
Air Force Rocket Propulsion
Laboratory (RPR)
Edwards, Calif. 93523

Library
Air Force Rocket Propulsion
Laboratory (RPM)
Edwards, Calif. 93523

Library
Bureau of Naval Weapons
Department of the Navy
Washington, D.C.

Library
Director (Code 6180)
U.S. Naval Research Laboratory
Washington, D.C. 20390

APRP (Library)
Air Force Aero Propulsion Lab.
Research & Technology Division
Air Force Systems Command
United States Air Force
Wright-Patterson AFB, Ohio 45433

Technical Information Dept.
Aeronutronic Div. of Philco Ford
Corp.
Ford Road
Newport Beach, Calif. 92663

Library-Documents
Aerospace Corporation
2400 E. El Segundo Blvd.
Los Angeles, Calif. 90045

Library
Bell Aerosystems, Inc.
Box 1
Buffalo, New York 14205

Report Library, Room 6A
Battelle Memorial Institute
505 King Avenue
Columbus, Ohio 43201

D. Suichu
General Electric Company
Flight Propulsion Lab. Dept.
Cincinnati, Ohio 45215

Library
Ling-Temco-Vought Corp.
P.O. Box 5907
Dallas, Texas 75222

Marquardt Corporation
16555 Saticoy Street
Box 2013 - South Annes
Van Nuys, Calif. 91409

P.F. Winternitz
New York University
University Heights
New York, New York 10453

I. Forsten
Picatinny Arsenal
Dover, New Jersey 07801

R. Stiff
Propulsion Division
Aerojet-General Corp.
P.O. Box 15847
Sacramento, Calif. 95803

Library, Dept. 596-306
Rocketdyne Div. of Rockwell
North American Rockwell Inc.
6633 Canoga Ave.
Canoga Park, Calif. 91304

Library
Stanford Research Institute
333 Ravenswood Ave.
Menlo Park, Calif. 94025

Library
Susquehanna Corporation
Atlantic Research Division
Shirley Highway & Edsall Road
Alexandria, Virginia 22314

STL Tech. Lib. Doc. Acquisitions
TRW Systems Group
1 Space Park
Redondo Beach, Calif. 90278

Dr. David Altman
United Aircraft Corp.
United Technology Center
P.O. Box 358
Sunnyvale, Calif. 94088

Library
United Aircraft Corp.
Pratt & Whitney Division
Florida Research & Development
Center
P.O. Box 2691
West Palm Beach, Fla. 33402